PET imaging of targets and targeted anticancer therapies to shed light on personalized treatment strategies

Mammatas, Lemonitsa Hillegonda

2021

document version
Publisher's PDF, also known as Version of record

PET imaging of targets and targeted anticancer therapies to shed light on personalized treatment strategies

Lemonitsa H. Mammatas

PET imaging of targets and targeted anticancer therapies to shed light on personalized treatment strategies – Lemonitsa H. Mammatas

ISBN/EAN: 978-94-6419-190-5

Cover design by Hans Droog
Layout and design by Birgit Vredenburg, persoonlijkproefschrift.nl
Printing: Gildeprint Enschede, gildeprint.nl

Printing of this thesis was financially supported by Uitgeverij Jaap, Pfizer and Chipsoft.

VRIJE UNIVERSITEIT

PET imaging of targets and targeted anticancer therapies to shed light on personalized treatment strategies

ACADEMISCH PROEFSCHRIFT

ter verkrijging van de graad Doctor,
aan de Vrije Universiteit Amsterdam,
op gezag van de rector magnificus
prof.dr. V. Subramaniam,
in het openbaar te verdedigen
ten overstaan van de promotiecommissie
van de Faculteit der Geneeskunde
op dinsdag 25 mei 2021 om 11.45 uur
in de aula van de universiteit,
De Boelelaan 1105

door
Lemonitsa Hillegonda Mammatas
geboren te Amsterdam

promotoren:	prof.dr. H.M.W. Verheul prof.dr. A.A. Lammertsma
copromotoren:	dr. C.W. Menke-van der Houven van Oordt prof.dr. E. Boven

Voor alle patiënten die dit onderzoek mogelijk hebben gemaakt
en hun dierbaren.

‘Nothing in life is to be feared, it is only to be understood.
Now is the time to understand more, so that we may fear less.’

Marie Curie

Contents

Preface and outline of the thesis

Background

Cancer is the most important cause of death and morbidity in Europe after cardiovascular diseases and has major impact on patients, families and society. Each year, more than 3 million new patients are diagnosed with cancer and 1.7 million deaths occur as a result of this disease.[1] Multiple therapeutic advances have been made the last decade, including the development of new targeted anticancer therapies. Targeted anticancer therapies are defined as 'drugs or other substances that block the growth and spread of cancer by interfering with specific molecules ("targets") that are involved in the growth, progression, and spread of cancer'.[2] In contrast to traditional cytotoxic chemotherapy, which is incorporated in rapidly growing cells without selectivity for cancer cells versus normal healthy cells, targeted anticancer therapies take benefit of differences in malignant versus non-malignant cells, such as (over)expression or mutations in tumor driving molecules.[2] The oldest form is endocrine therapy, which blocks the hormone-receptor interaction in hormone driven tumors.[2,3] Rapid progress in our knowledge on cancer at molecular levels has led to an expansion of targeted anticancer drugs approved for use in daily clinical practice. Drugs that block specific intracellular signaling pathways (such as the EGFR inhibitor erlotinib), modulate the function of genes (e.g. the BCR-ABL fusion protein inhibitor imatinib), or inhibit angiogenesis in the surrounding tumor microenvironment (like the VEGF inhibitor bevacizumab) are only a few examples.[4]

Remarkable enough, only half of the currently approved targeted anticancer therapies have predictive biomarkers available, while prediction of response or nonresponse is essential for all treated patients.[5] In patients with breast cancer for example, the expression of hormone receptors, HER2 receptor amplification and recently mutations in PIC_3CA are a prerequisite to support the use of endocrine therapy, HER2-blocking drugs or $PI_3K\alpha$-specific inhibitors, respectively.[6-8] However, even if biomarkers are available to support therapeutic decisions, these all have their limitations. Biomarkers are still mainly collected from tumor tissue with invasive biopsies, which are not always feasible or safe due to the location of the tumor, nor patient friendly.[9] In addition, it has been reported that the expression of biomarkers can change over time between different tumor lesions within one patient and as a result a single tumor biopsy may give inadequate information for an individualized treatment plan.[10-12] Therefore, it is important to develop new methods for response prediction and treatment optimization strategies in oncology.

Positron Emission Tomography (PET) is an imaging technique that allows visualization and quantification of the distribution of molecules labeled with positron-emitting isotopes.[13] PET imaging has the advantage of being a non-invasive technique that can provide information on the different tumor lesions within a patient. For targeted therapies, PET can provide insight in target expression throughout the body or whether or not a radiolabeled drug reaches its target sites.[14-17] Therefore, PET is an interesting technique to aid in the prediction and monitoring of targeted therapy effects.

Several promising PET techniques are emerging to visualize targets and targeted therapies in oncology, including hormone receptor imaging and imaging with radiolabeled drugs such as small molecule protein kinase inhibitors (e.g. [^{11}C]erlotinib, [^{11}C]afatinib and [^{11}C]lapatinib PET), and monoclonal antibodies (e.g. [^{89}Zr]trastuzumab, [^{89}Zr]rituximab and [^{89}Zr]atezolizumab PET).[14,15,17-20] Eventually, these techniques could lead to personalized treatment strategies. The amount of tracer uptake in tumors may be predictive for treatment effects, guide the choice of therapy and provide insight in the optimal treatment dosage for a patient.[21]

Regarding the optimal treatment dosage of targeted anticancer therapies, further optimization is urgently needed in order to fully exploit their potential antitumor activity. Dose optimization strategies currently under investigation include drug monitoring to achieve a target plasma concentration of a drug, and alternative dosing schedules such as high-dose pulsatile/intermittent dosing of targeted drugs previously given in daily continuous schedules. For several small molecule protein kinase inhibitors, such as sunitinib, erlotinib and lapatinib, there is accumulating evidence that high-dose pulsatile schedules may improve antitumor effects or overcome resistance based on higher tumor accumulation and/or enhanced inhibition of drug targets.[22-24] In addition, in multiple phase I studies, PET imaging is incorporated in the study design to determine the optimal drug dose until full target occupancy is reached.[25-28] Therefore, evaluation of the potential and limitations of PET imaging techniques is necessary to enable optimal use of targeted anticancer therapies in daily clinical practice.

Outline of the thesis

The aim of this thesis was to explore the value of different PET imaging techniques visualizing targets and targeted anticancer therapies for future treatment tailoring.

As a general introduction, *chapter 1* provides an overview of the available literature on molecular imaging with PET for the improvement of personalized cancer care.

Part I of this thesis focusses on visualizing targets: estrogen receptor (ER) and androgen receptor (AR) imaging in patients with breast cancer. Approximately 75% of the patients with breast cancer have an ER-positive tumor. The success rate of endocrine therapy relies heavily on the ER expression of the tumor.[8] Recently, also AR expression emerged as a possible target of therapy, because it is present in 70–80% of the patients with breast cancer.[29] In *chapter 2*, [^{18}F]fluoroestradiol ([^{18}F]FES) PET and [^{18}F]fluorodihydrotestosterone ([^{18}F]FDHT) PET are evaluated to assess whether uptake correlates with the levels of ER and AR expression in simultaneous biopsied metastases. *In chapter 3,* the interobserver variability in visual and quantitative assessment of [^{18}F]FES and [^{18}F]FDHT PET are determined, because reliable, observer-independent evaluation is necessary for application of these new techniques in clinical practice.

Part II concerns strategies to optimize treatment with the targeted anticancer drug sorafenib, a small molecule protein kinase inhibitor. Sorafenib has activity against multiple targets involved in the growth, angiogenesis and spread of cancer including C-RAF, B-RAF, mutant B-RAF, vascular endothelial growth factor receptors 1, 2 and 3, platelet-derived growth factor receptor β, FMS-like tyrosine kinase 3, c-Kit protein and RET receptor tyrosine kinase.[30] Sorafenib has been approved for treatment of locally advanced and metastatic hepatocellular carcinoma, renal cell carcinoma and iodine-refractory differentiated thyroid carcinoma at a standard fixed dose of 400 mg twice daily in a continuous schedule.[31-33] Currently, no biomarkers are available to predict response to sorafenib in an individual patient. *In chapter 4,* we examine whether [^{11}C]sorafenib PET and [^{15}O]H_2O perfusion PET have the potential to predict the treatment efficacy of sorafenib. *In chapter 5*, the results of a phase I exposure escalation study are presented investigating an alternative high-dose, pulsatile schedule of sorafenib using drug monitoring in attempt to improve the efficacy of sorafenib.

Finally, *chapter 6* summarizes the main results of this thesis, accompanied by a discussion and future perspectives. A Dutch summary of this dissertation is given in the *Appendix*.

Literature

1. World Health Organization: Cancer, 2020, http://www.euro.who.int/en/health-topics/noncommunicable-diseases/cancer/cancer, visited 1-1-2020.
2. National Cancer Institute: Targeted Cancer Therapies, 2020, https://www.cancer.gov/about-cancer/treatment/types/targeted-therapies/targeted-therapies-fact-sheet#what-types-of-targeted-therapies-are-available, visited 1-1-2020
3. Faivre S, Djelloul S, Raymond E: New paradigms in anticancer therapy: targeting multiple signaling pathways with kinase inhibitors. Semin Oncol 33:407-20, 2006
4. Li J, Chen F, Cona MM, et al: A review on various targeted anticancer therapies. Target Oncol 7:69-85, 2012
5. Kurnit KC, Dumbrava EEI, Litzenburger B, et al: Precision Oncology Decision Support: Current Approaches and Strategies for the Future. Clin Cancer Res 24:2719-2731, 2018
6. Borley A, Mercer T, Morgan M, et al: Impact of HER2 copy number in IHC2+/FISH-amplified breast cancer on outcome of adjuvant trastuzumab treatment in a large UK cancer network. Br J Cancer 110:2139-43, 2014
7. Andre F, Ciruelos E, Rubovszky G, et al: Alpelisib for PIK3CA-Mutated, Hormone Receptor-Positive Advanced Breast Cancer. N Engl J Med 380:1929-1940, 2019
8. Blamey RW, Hornmark-Stenstam B, Ball G, et al: ONCOPOOL - a European database for 16,944 cases of breast cancer. Eur J Cancer 46:56-71, 2010
9. Youk JH, Kim EK, Kim MJ, et al: Missed breast cancers at US-guided core needle biopsy: how to reduce them. Radiographics 27:79-94, 2007
10. Amir E, Miller N, Geddie W, et al: Prospective study evaluating the impact of tissue confirmation of metastatic disease in patients with breast cancer. J Clin Oncol 30:587-92, 2012
11. Heinzerling L, Baiter M, Kuhnapfel S, et al: Mutation landscape in melanoma patients clinical implications of heterogeneity of BRAF mutations. Br J Cancer 109:2833-41, 2013
12. Jeantet M, Tougeron D, Tachon G, et al: High Intra- and Inter-Tumoral Heterogeneity of RAS Mutations in Colorectal Cancer. Int J Mol Sci 17, 2016
13. Townsend DW, Carney JP, Yap JT, et al: PET/CT today and tomorrow. J Nucl Med 45 Suppl 1:4S-14S, 2004
14. Bensch F, Brouwers AH, Lub-de Hooge MN, et al: (89)Zr-trastuzumab PET supports clinical decision making in breast cancer patients, when HER2 status cannot be determined by standard work up. Eur J Nucl Med Mol Imaging 45:2300-2306, 2018
15. Bahce I, Smit EF, Lubberink M, et al: Development of [(11)C]erlotinib positron emission tomography for in vivo evaluation of EGF receptor mutational status. Clin Cancer Res 19:183-93, 2013
16. Varrone A, Varnas K, Jucaite A, et al: A PET study in healthy subjects of brain exposure of (11)C-labelled osimertinib - A drug intended for treatment of brain metastases in non-small cell lung cancer. J Cereb Blood Flow Metab:271678X19843776, 2019
17. Bensch F, van der Veen EL, Lub-de Hooge MN, et al: (89)Zr-atezolizumab imaging as a non-invasive approach to assess clinical response to PD-L1 blockade in cancer. Nat Med 24:1852-1858, 2018

18. van de Stadt E, Yaqub M, Poot A, et al: Can [18F] afatinib PET/CT be used in identifying NSCLC patients with different EGFR mutational status: tracer quantification and assessment of tumor uptake. Journal of Nuclear Medicine 60:522-522, 2019
19. Saleem A, Searle GE, Kenny LM, et al: Lapatinib access into normal brain and brain metastases in patients with Her-2 overexpressing breast cancer. EJNMMI Res 5:30, 2015
20. Jauw YW, Zijlstra JM, de Jong D, et al: Performance of 89Zr-Labeled-Rituximab-PET as an Imaging Biomarker to Assess CD20 Targeting: A Pilot Study in Patients with Relapsed/Refractory Diffuse Large B Cell Lymphoma. PLoS One 12:e0169828, 2017
21. Mammatas LH, Verheul HM, Hendrikse NH, et al: Molecular imaging of targeted therapies with positron emission tomography: the visualization of personalized cancer care. Cell Oncol (Dordr) 38:49-64, 2015
22. Milton DT, Azzoli CG, Heelan RT, et al: A phase I/II study of weekly high-dose erlotinib in previously treated patients with nonsmall cell lung cancer. Cancer 107:1034-41, 2006
23. Zhu Y, Du Y, Liu H, et al: Study of efficacy and safety of pulsatile administration of high-dose gefitinib or erlotinib for advanced non-small cell lung cancer patients with secondary drug resistance: A single center, single arm, phase II clinical trial. Thorac Cancer 7:663-669, 2016
24. Chien AJ, Munster PN, Melisko ME, et al: Phase I dose-escalation study of 5-day intermittent oral lapatinib therapy in patients with human epidermal growth factor receptor 2-overexpressing breast cancer. J Clin Oncol 32:1472-9, 2014
25. Wang YB, Ayres KL, Goldman DA, et al: F-18-Fluoroestradiol PET/CT Measurement of Estrogen Receptor Suppression during a Phase I Trial of the Novel Estrogen Receptor-Targeted Therapeutic GDC-0810: Using an Imaging Biomarker to Guide Drug Dosage in Subsequent Trials. Clinical Cancer Research 23:3053-3060, 2017
26. Menke-van der Houven van Oordt CW, McGeoch A, Bergstrom M, et al: Immuno-PET Imaging to Assess Target Engagement: Experience from (89)Zr-Anti-HER3 mAb (GSK2849330) in Patients with Solid Tumors. J Nucl Med 60:902-909, 2019
27. Bensch F, Lamberts LE, Smeenk MM, et al: (89)Zr-Lumretuzumab PET Imaging before and during HER3 Antibody Lumretuzumab Treatment in Patients with Solid Tumors. Clin Cancer Res 23:6128-6137, 2017
28. Lockhart AC, Liu Y, Dehdashti F, et al: Phase 1 Evaluation of [(64)Cu]DOTA-Patritumab to Assess Dosimetry, Apparent Receptor Occupancy, and Safety in Subjects with Advanced Solid Tumors. Mol Imaging Biol 18:446-53, 2016
29. Collins LC, Cole KS, Marotti JD, et al: Androgen receptor expression in breast cancer in relation to molecular phenotype: results from the Nurses' Health Study. Mod Pathol 24:924-31, 2011
30. Wilhelm SM, Adnane L, Newell P, et al: Preclinical overview of sorafenib, a multikinase inhibitor that targets both Raf and VEGF and PDGF receptor tyrosine kinase signaling. Mol Cancer Ther 7:3129-40, 2008
31. Escudier B, Eisen T, Stadler WM, et al: Sorafenib for treatment of renal cell carcinoma: Final efficacy and safety results of the phase III treatment approaches in renal cancer global evaluation trial. J Clin Oncol 27:3312-8, 2009
32. Llovet JM, Ricci S, Mazzaferro V, et al: Sorafenib in advanced hepatocellular carcinoma. N Engl J Med 359:378-90, 2008

33. Brose MS, Nutting CM, Jarzab B, et al: Sorafenib in radioactive iodine-refractory, locally advanced or metastatic differentiated thyroid cancer: a randomised, double-blind, phase 3 trial. Lancet 384:319-28, 2014

CHAPTER 1

Molecular imaging of targeted therapies with positron emission tomography: *the visualization of personalized cancer care*

Lemonitsa H. Mammatas, Henk M. W. Verheul, N. Harry Hendrikse, Maqsood Yaqub, Adriaan A. Lammertsma, C. Willemien Menke-van der Houven van Oordt

Published in: Cellular Oncology. 2015;38:49–64

Abstract

Molecular imaging has been defined as the visualization, characterization and measurement of biological processes at the molecular and cellular level in humans and other living systems. In oncology it enables to visualize (part of) the functional behaviour of tumour cells, in contrast to anatomical imaging that focuses on the size and location of malignant lesions. Available molecular imaging techniques include single photon emission computed tomography (SPECT), positron emission tomography (PET) and optical imaging. In PET, a radiotracer consisting of a positron emitting radionuclide attached to the biologically active molecule of interest is administrated to the patient. Several approaches have been undertaken to use PET for the improvement of personalized cancer care. For example, a variety of radiolabelled ligands have been investigated for intratumour target identification and radiolabelled drugs have been developed for direct visualization of the biodistribution in vivo, including intratumour therapy uptake. First indications of the clinical value of PET for target identification and response prediction in oncology have been reported. This new imaging approach is rapidly developing, but uniformity of scanning processes, standardized methods for outcome evaluation and implementation in daily clinical practice are still in progress. In this review we discuss the available literature on molecular imaging with PET for personalized targeted treatment strategies. In conclusion, molecular imaging with radiolabelled targeted anticancer drugs has great potential for the improvement of personalized cancer care. The non-invasive quantification of drug accumulation in tumours and normal tissues provides understanding of the biodistribution in relation to therapeutic and toxic effects.

1. Introduction

In the last decade the U.S. Food and Drug Administration approved more than 50 new targeted agents interfering with the underlying biology of the disease, especially for the treatment of solid and haematological malignancies [1]. In general, these drugs are only effective in a subgroup of patients, but upon treatment all patients are exposed to potential toxicity. Therefore, selection of patients for treatment with a targeted drug is important to improve cancer care. Several methods, including gene and protein profiling are in development and a few successes of treatment selection have reached daily clinical practice, e.g. BRAF mutation in patients with melanoma [2]. However, for many targeted agents no predictive biomarkers are available. Molecular imaging may provide an attractive alternative method for treatment selection. In this review we discuss the development of molecular imaging for personalized treatment strategies.

2. General principles of molecular imaging

Molecular imaging has been defined as the visualization, characterization and measurement of biological processes at the molecular and cellular level in humans and other living systems [3]. In oncology it permits the visualization of (part of) the functional behaviour of tumour cells, as opposed to anatomical imaging that focuses on the size and location of malignancies.

The development of several molecular imaging techniques has greatly advanced this field, including single photon emission computed tomography (SPECT), positron emission tomography (PET) and optical imaging. In PET a radiotracer consisting of a positron emitting radionuclide attached to the biologically active molecule of interest is administrated to the patient. As the radionuclide decays a positron is emitted in the body, which then annihilates with a nearby electron. This results in the production of two gamma-ray photons with energies of 511 keV that are ejected in opposite directions (Fig. 1). The PET scanner senses this pair of high-energy photons with crystal detectors placed in a ring around the patient. Thereby their source along the line of coincidence can be identified, enabling a three-dimensional reconstruction of the tracer concentration within the body [4]. The positron emitting radionuclides are produced in a cyclotron by bombarding target material with accelerated protons or deuterons. Each radionuclide will decay according to its own half-life (Table 1). Radiolabelled ligands and radiolabelled drugs require significant biological evaluation before use in clinical trials is possible. This includes the determination of both affinity and selectivity for target proteins as well as metabolic stability of the tracer. Furthermore, several quality assessments

are necessary before each administration, such as radiochemical purity, tracer integrity and apyrogenicity [5].

Figure 1. In PET the radiotracer emits a positron that annihilates with a nearby electron. This results in the production of *two gamma ray photons* with energies of 511 keV that are sensed with crystal detectors placed in a ring around the patient. Thereby, a three-dimensional reconstruction of the tracer concentration within the body can be made

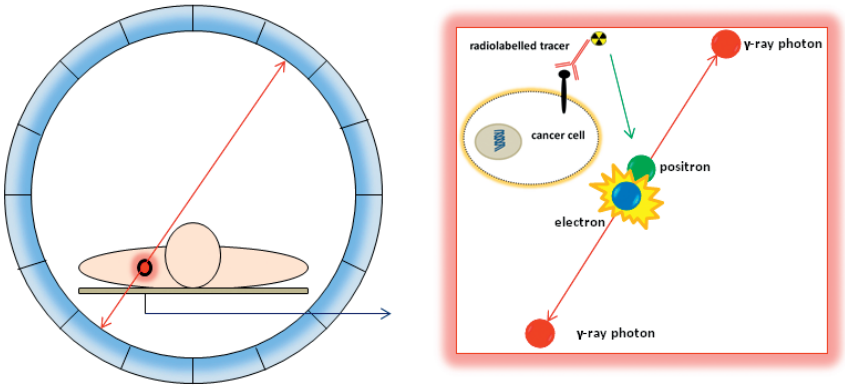

PET has a superior sensitivity and spatial resolution compared with SPECT, in which the radionuclide only emits one single gamma ray photon that has to be detected by a gammacamara rotating around a patient [6]. In addition, the tissue penetration depth of PET is much higher compared with optical imaging, in which emitted light from a fluorescence or bioluminescence tracer is detected only up to several centimetres distance from the source [7]. Due to the higher sensitivity and superior spatial resolution, as well as the possibility to combine PET with CT yielding detailed anatomical information, PET has emerged as the preferred technique for clinical applications [8].

3. Radiolabelled ligands

3.1 Radioligands for imaging of cellular processes

In the clinical setting, PET has been most extensively used with the tracer [^{18}F]-fluorodeoxyglucose ([^{18}F]FDG), which makes it possible to measure glucose metabolism in cells. Due to the high rate of glycolysis in cancer cells, [^{18}F]FDG PET is successfully used for detection and staging of malignancies and is being evaluated in the clinic as a method for response monitoring of for example oesophageal cancer, non-small cell lung cancer (NSCLC) and malignant lymphoma. In these malignancies it increased the sensitivity of CT-evaluation significantly, but its clinical impact is still under evaluation [9–11]. The most

important limitation of this tracer is the relatively low specificity since any process that leads to increased glucose metabolism, such as inflammation, may lead to increased [^{18}F]FDG uptake [12]. Other tracers reflecting proliferation of tumour cells, tumour perfusion, apoptosis and hypoxia, have also been developed to image cellular processes important for prognosis, treatment decisions and response evaluation [13–16]. For example, [^{15}O]H_2O PET was shown to be a valuable tool for the measurement of tissue and tumour perfusion, with good reproducibility [14]. At this moment however, most of these tracers need further validation before clinical use is possible. In addition, more drug specific tracers have been developed.

Table 1. Commonly used PET radionuclides

Radionuclide	Half-life	Decay modes	Maximum positron energy
Carbon-11	20,4 min	100 % positron emission	0,96 MeV
Nitrogen-13	10,0 min	100 % positron emission	1,20 MeV
Oxygen-15	2,0 min	100 % positron emission	1,74 MeV
Fluorine-18	109,8 min	97 % positron emission and 3 % electron capture	0,63 MeV
Copper-64	12,7 h	19 % positron emission, 41 % electron capture and 40 % β^- decay	0,65 MeV
Bromine-76	16,1 h	57 % positron emission and 43 % electron capture	3,40 MeV
Yttrium-86	14,7 h	34 % positron emission and 78 % electron capture	3,10 MeV
Zirconium-89	78,4 h	25 % positron emission and 75 % electron capture	0,90 MeV
Iodine-124	4,2 days	25 % positron emission and 75 % electron capture	3,16 MeV

3.2 Radioligands for imaging of hormone receptors

Hormone receptors are important targets for anticancer therapies, particularly for patients with breast and prostate cancer. Radiolabelled ligands have been developed to image these target receptors and include 16α-[^{18}F]-fluoro-17β-oestradiol ([^{18}F]FES) for oestrogen receptors, 21-[^{18}F]fluoro-16 alphaethyl-19-norprogesterone ([^{18}F]FENP) for progesterone receptors and 16β-[^{18}F]fluoro-5α-dihydrotestosterone ([^{18}F]FDHT) for androgen receptors [17–19]. Of these, [^{18}F]FES has been most extensively studied.

[^{18}F]FES is an analogue of oestradiol with similar binding characteristics [20]. Several studies investigated the sensitivity and specificity of [^{18}F]FES PET

compared to the ER expression in tumour biopsies. An overall sensitivity of 84 % (95 % CI 73–91 %) and specificity of 98 % (95 % CI 90–100 %) are promising [21]. Its potential clinical value is discussed further on.

In contrast, imaging of the progesterone receptor (PR) is more difficult. The use of [^{18}F]-FENP as a progesterone analogue in breast cancer was disappointing, which may be attributed to low receptor affinity and rapid metabolism [18, 22]. Further investigations with new PR radioligands are ongoing [23].

Evaluation of the androgen receptor (AR) using [^{18}F]FDHT is also feasible [19]. [^{18}F]FDHT PET detected 78 % of the lesions established with conventional imaging methods in patients with metastasized prostate cancer [24]. After 1 day of treatment with the AR antagonist flutamide [^{18}F]FDHT uptake decreased > 50 % indicating target site occupancy [19]. Expression levels of AR are known to be heterogeneous in prostate cancer [25] and [^{18}F]FDHT may be able to quantify those levels before and during treatment which may improve response prediction and early response monitoring.

3.3 Radioligands for imaging of receptor tyrosine kinases

Inhibitors of receptor tyrosine kinases have been clinically approved for various malignancies. Because, in general, only a subgroup of patients will respond to these agents, different radiolabelled ligands have been developed for imaging receptor tyrosine kinases with PET to be potentially used for treatment selection. These include tracers made from natural ligands or their analogues, antibody fragments, affibodies and nanobodies [26–31].

Epidermal growth factor (EGF), the natural ligand of the epidermal growth factor receptor (EGFR), has been developed as a tracer, but its use was limited by rapid internalization and degradation after receptor binding and by high liver uptake [26]. Another drawback was uncertain binding activity associated with random radiolabelling of EGF. Based on EGF other compounds have been developed to improve image quality such as Cys-tagged EGF (cEGF). It provides site specific binding for labelling with N-[2-(4-[^{18}F]fluorobenzamido)ethyl]maleimide to form the radioligand [^{18}F]FBEM-cEGF, which retained the characteristics of the parent compound [27].

Antibody fragments have the advantage of a longer half-life than the natural ligand, though a much shorter half-life than the complete antibody. Antibody fragments facilitate repetitive PET scans in a short period of time. Also, their smaller size may theoretically result in better transport from

blood to tissue and a higher tumour-to-background ratio [32]. Antibody fragments of the anti-HER2 antibody trastuzumab were labelled with ^{68}Ga and allowed good sequential imaging of HER2 expression [28].

Affibodies are a type of scaffold proteins in which the framework of 58 amino acids is constant (the scaffold Z-domain), while amino acids in the binding site are individualized to the receptor of choice and optimized with a higher receptor affinity [33]. The EGFR based affibodies [^{64}Cu]ZEGFR:1907 and [^{18}F]ZEGFR:1907 showed high and rapid tumour accumulation in animal studies. Tumours were well visualized 1 to 3 h after injection [29, 30]. In contrast, optimal visualization of EGFR-positive tumours with the labelled anti-EGFR-antibody [^{64}Cu]cetuximab or [^{89}Zr]cetuximab was achieved later at 24–72 h post injection [34, 35].

Finally, nanobodies are the smallest antigen binding fragments and consist of a single monomeric variable domain. The first nanobodies were derived from heavy-chain only antibodies found in species of Camelidae [36]. [^{68}Ga]2Rs15dHis6 is a nanobody directed against the HER2 receptor. Intense tracer uptake was shown in HER2 expressing xenografts in comparison with nonexpressing tumours. No significant uptake in other tissues was shown, except for the kidneys [31]. Nanobodies bind to different epitopes of the tyrosine kinase receptor than monoclonal antibodies. Therefore, these may in the future be combined with therapy to directly study the effects on receptor expression [36]. Although these analogues of receptor ligands are promising imaging tracers, use of the original drug as a radiotracer offers the potential of direct insight in its biodistribution, including tumour uptake, in relation to treatment effects.

4. Radiolabelled drugs

4.1 Technical aspects

The high sensitivity of PET in combination with the high specific activity (i.e. the radioactivity per unit mass) of a radiolabelled drug make it possible to visualize extremely small amounts of the drug in the body, at concentrations in the lower femtomole range (10–15 mol) for which only a microdose of radiolabelled drug has to be administrated [37, 38]. Microdosing PET permits studying the kinetic behaviour of a drug without saturation of transporters and targets as well as avoiding toxic effects as long as such a low dose behaves identical to a therapeutic dose [39].

The development of clinically meaningful radiolabelled targeted drugs is a complex process requiring several considerations. First, attachment of the radionuclide should not alter the chemical structure of the drug, because

this may disturb its biochemical properties interfering with the functionality of the drug. In addition, the attachment has to be stable and the in vivo generation of radiolabelled metabolites as well as their affinity for the target of the drug should be known [40]. Second, the choice of radionuclide depends on expected pharmacokinetics of the drug. The half-life of the radionuclide should be compatible with the time it takes for the drug to achieve an optimal tumour-to-nontumour ratio. For small molecules a short-lived tracer will be appropriate. However, in case of a radionuclide with a short half-life, such as ^{11}C, onsite production using a cyclotron is required. Long-lived tracers, such as antibodies labelled with ^{89}Zr, can be distributed over a larger distance making central synthesis for different hospitals possible. Third, the kinetic behaviour of the radiolabelled drug has to be determined with respect to optimal dose and ideal timing for PET imaging. Finally, the tumour uptake of a microdose should correlate with that of the therapeutic dose of the drug.

4.2 Radiolabelled monoclonal antibodies

Monoclonal antibodies have a large size of ~150 kDa. This large size makes it possible to use a bifunctional chelating agent for radionuclide binding. These chelators have two binding sites: one metal binding site for chelation to the radionuclide and one chemically reactive group for binding to the drug. Examples of frequently used chelators are diethylenetriamine pentaacetic acid (DTPA), 1,4,7,10-tetraazacylcododecane-N,N',N'',N'''-tetraacetic acid (DOTA) and desferrioxamine. Important factors to choose an appropriate chelator include charge, matching cavity size of the chelator compared to the ionic radius of the radionuclide as well as type and number of binding groups. In addition, the conjunction of the chelator to the monoclonal antibody should lead to a stable binding without altered immune reactivity [41].

The size of monoclonal antibodies results in slow distribution and target binding, which is dependent on diffusion and extravasation to the extracellular space. Due to these slow kinetics PET scans need to be performed several days after injection of the tracer. In addition, clearance is slow and this results in long biological half-lifes. For instance, the biological $t_{½}$ of cetuximab is 70–100 h and therefore long-lived positron emitters such as ^{89}Zr ($t_{½}$ 78,4 h) are suitable for radiolabelling this drug [35]. Several monoclonal antibodies will be internalized after receptor binding [42]. This should be considered in the choice of the radionuclide. ^{76}Br and ^{124}I are rapidly degraded upon internalization and cleared from the target cells. In contrast, ^{64}Cu, ^{86}Y and ^{89}Zr are trapped intracellularly in lysosomes upon internalisation. These accumulated radionuclides result in better visualization of drug targeting [43].

4.3 Radiolabelled tyrosine kinase inhibitors and hormone receptor antagonists
Tyrosine kinase inhibitors (TKIs) and hormone receptor antagonists are molecules < 1 kDa. Both bind to their respective target receptors inhibiting signal transduction into the cell. The small structures of these drugs in combination with their lipophilicities provide an easy passage through the cell membrane.

To preserve the exact characteristics of these small molecule drugs in vivo, radionuclides are built in, rather than attached to the molecular structure. For TKIs often ^{11}C is used to replace a cold carbon atom, such as in [^{11}C]erlotinib and [^{11}C]sorafenib [44, 45]. In principle all molecules can be labelled by replacing a carbon atom with ^{11}C and the radiation dose is much lower than for longer lived radionuclides. However, ^{11}C has a short half-life ($t_{½}$ 20,4 min). This requires rapid tracer synthesis and direct PET imaging. In addition, the radiolabelled TKI should have a relatively fast tissue distribution to match the half-life of ^{11}C for adequate visualization. The half-life of ^{18}F is longer ($t_{½}$ 109,8 min) and can sometimes be used if a cold fluorine atom is available in the molecular structure, like in [^{18}F]gefitinib [46]. ^{18}F has also been used to label tamoxifen and fulvestrant by adding a fluorine atom to the molecular structure. It was successful for tamoxifen, but the addition of ^{18}F at the 16 α-position of fulvestrant dramatically decreased the binding affinity for the oestrogen receptor making it unsuitable for in vivo use [47, 48].

In contrast to the monoclonal antibodies that are metabolically fairly stable in the circulation, TKIs and hormone receptor antagonists may form radioactive metabolites which cannot be distinguished from the original drug during PET imaging. Direct measurements of the original drug and radiolabelled metabolites in blood samples taken during imaging are necessary for all new radiolabelled drugs, in order to accurately quantify drug biodistribution with PET. In addition, different positions of the radionuclide in the molecular structure of the drug should be considered, as this may influence the formation of radioactive metabolites.

5. Biodistribution of drugs

5.1 Biodistribution
Molecular imaging of radiolabelled drugs with PET provides direct insight into the biodistribution of the drug over time in tumours and normal tissues, which is preferably investigated with a dynamic scan, rather than a static scan. A dynamic scan generates continuous images in a selected period of time. However, as a consequence it is limited to the relatively small field of view of the scanner, which is up to 25 cm. In contrast, a static scan visualizes the whole

body by moving the scanner bed over multiple positions, but it only captures one moment in time [49].

A region of interest (ROI) can be drawn onto the acquired dynamic PET images in which the radioactivity is measured over time resulting in a time-activity curve (TAC). Kinetic modelling can be applied to describe the tissue uptake of a drug within the ROI over time. A directly measured blood curve is used as an input function and the output function is the TAC of the tissue of interest corrected for the intravascular background contribution to the signal. With computer modelling an appropriate compartment model is then chosen to accurately describe the kinetic behaviour of the drug over time. The most frequently applied compartment models are the single tissue model, the reversible two tissue model and the irreversible two tissue model (Fig. 2) [50–52]. With an appropriate compartment model several parameters of interest can be derived, such as the total volume of distribution (VT), the binding potential (BPND) for the receptor or, if irreversible binding is the case, the net rate of drug accumulation (Ki) [50, 53].

This type of kinetic analysis is not possible with monoclonal antibodies, since a dynamic PET is not feasible due to the long biological half-lifes of up to several weeks. As an alternative, serial static scans are made in a period of 1–2 weeks from which TACs are derived. The biodistribution of monoclonal antibodies has been described using a single tissue compartment model with K1 reflecting extravasation and k2 washout of the large molecules [54]. However, limitations are the lack of time points as in practice a maximum of 4–6 static scans can be performed. In addition, for monoclonal antibodies it is frequently required to co-administer unlabelled antibody for saturation of 'sink' tissue, i.e. normal tissue in which the relatively low tracer dose sequestrates, which may interfere with the accurate quantification of binding to target sites.

Figure 2 (right). Kinetic modelling with radiolabelled drugs. **a**. The plasma TAC is used as an input function derived from the blood sampler. **b**. The tumour TAC is used as an output function measured with PET. **c**. In the single tissue model the drug concentration in a certain tissue (C_{tissue}) depends on the drug concentration in the plasma (C_{plasma}), the drug transport from plasma to tissue (K_1) and the drug transport from tissue to plasma (k_2). **d**. In the two tissue model the radiolabelled drug concentrations are divided over two tissue compartments: a free and a bound fraction. In this model the kinetics of the radiolabelled drug not only depend on C_{plasma}, K_1 and k_2, but also on k_3 and k_4 that describe exchange between the free and bound tissue fraction, respectively. **e**. In the irreversible two tissue model k_4 is 0

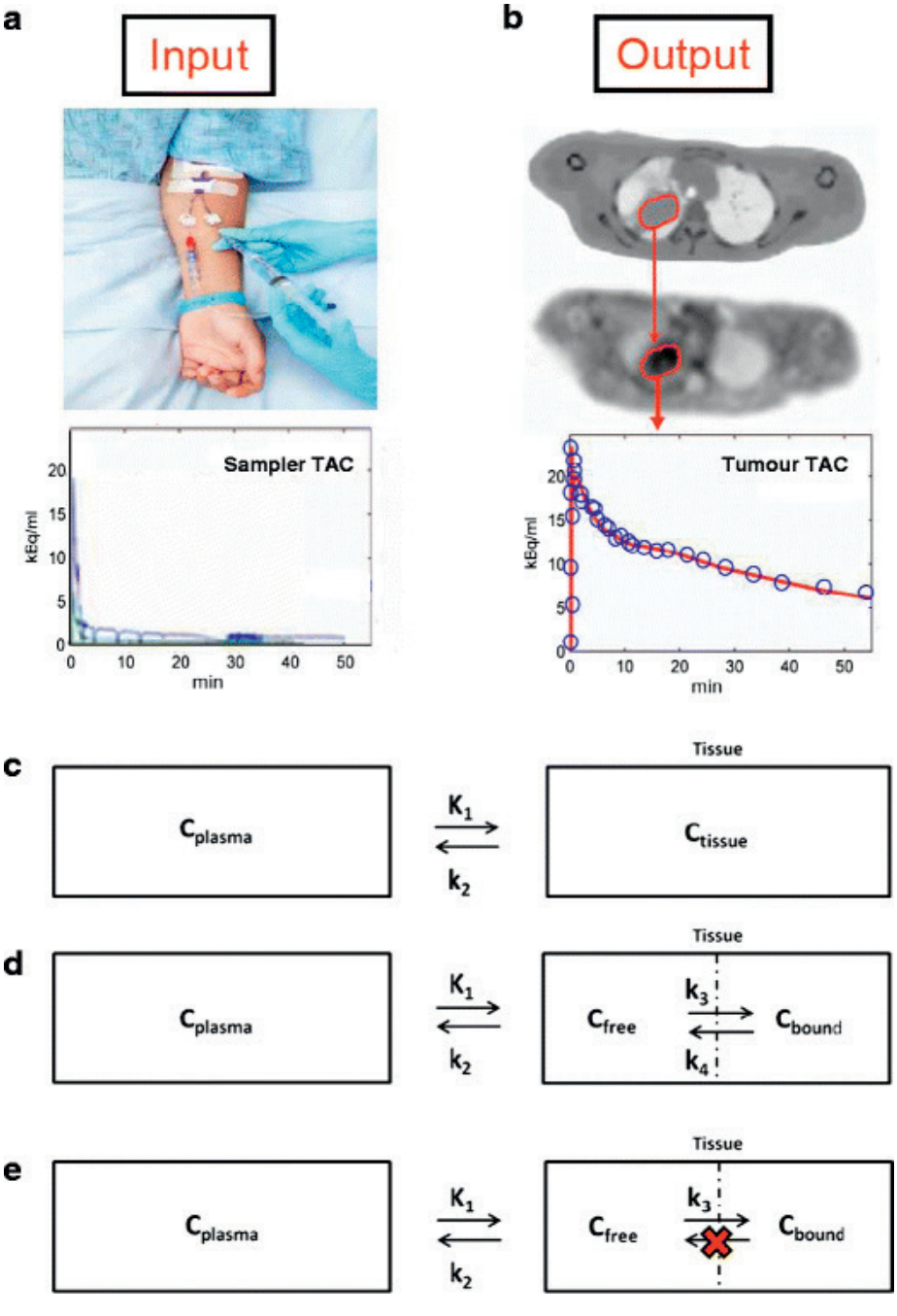
a
Input
Sampler TAC
kEq/ml
min
b
Output
Tumour TAC
kEq/ml
min
c
Tissue
C_{plasma}
K_1
k_2
C_{tissue}
d
Tissue
C_{plasma}
K_1
k_2
C_{free}
k_3
k_4
C_{bound}
e
Tissue
C_{plasma}
K_1
k_2
C_{free}
k_3
C_{bound}

Once an appropriate compartment model is determined, it can be used as a 'gold standard' for the validation of simplified outcome measures to facilitate clinical use. The simplest tool for identifying tracer uptake is of course visual inspection: is there tumour targeting or not? For comparison of results however, simplified standardized quantification methods such as the standardized uptake value (SUV) have been investigated. The SUV is the tracer uptake within a ROI, measured at a certain time after administration and normalized to the injected dose and to a factor accounting for body mass (e.g. body weight, body surface area or lean body weight). The accumulation of a radiolabelled drug within a ROI may be reported as SUV_{mean}, SUV_{max} or SUV_{peak}. SUV_{mean} is the average SUV of all voxels within a ROI, SUV_{max} is the highest voxel within a ROI and SUV_{peak} is the average SUV in a small defined area surrounding the voxel with the highest activity. Each method has its own benefits, but an unequivocal outcome measure is important for comparison of patients [55]. Using methods such as the SUV, a threshold may be defined that correlates with treatment response or toxicity in normal tissues. In addition, changes in SUV after treatment may be useful for early response evaluation. However, the SUV needs to be validated as in some instances different results are obtained when compared with the gold standard, i.e. full kinetic analysis [56]. Finally, one static Pet at a single optimal time point has to be selected from the TAC data to make it feasible for daily clinical practice.

5.2 Pharmacokinetic and pharmacodynamic insight with molecular imaging

The insight in drug behaviour has led to the incorporation of microdosing PET in early clinical drug development [57]. PET can help to select an appropriate starting dose in clinical trials by identifying the lowest dose needed for intratumoral target occupancy in a small number of patients. In these dose finding studies reduced radioactivity in the ROI after an increasing amount of unlabelled drug indirectly implies target site occupancy [37]. On the contrary, an extra unlabelled drug dose may also induce tracer uptake in the ROI, thereby suggesting saturation of sink tissue. The accumulation of radiolabelled drugs will depend on the affinity of the drug for its target in the tumour in combination with (nonspecific) binding in other tissues and pharmacokinetics.

In addition, the biodistribution of a new drug may provide some insight in its efficacy. For example, it has been demonstrated in brain tumours that PET can non-invasively determine the capacity of a drug to cross the blood–brain barrier [58]. Prediction of toxicity at sites of drug accumulation, such as the heart and bone marrow, is another potential advantage of molecular imaging.

Table 2. Radiolabelled targeted anticancer therapies for molecular imaging with PET

Drug class	Radiolabelled drug	Targets	Tumour uptake	Personalized treatment strategies
HR[a] antagonists	[^{18}F]fulvestrant	ER	Not feasible [47]	n.a.[b]
	[^{18}F]tamoxifen	ER	In animals [48, 105] and in humans [74]	Potential for response prediction in humans [74]
Tyrosine kinase inhibitors	[^{11}C]erlotinib	EGFR	In animals [44, 106] and in humans [56, 76]	Potential for response prediction in humans [56]
	[^{11}C]gefitinib	EGFR	In animals [107]	n.a.
	[^{18}F]gefitinib	EGFR	In animals [46, 108]	n.a.
	[^{11}C]imatinib [109]	BCR-ABL, c-KIT, PDGFR	n.a.	n.a.
	[^{18}F]lapatinib [110]	EGFR, HER2	n.a.	n.a.
	[^{11}C]sorafenib	VEGFR, PDGFR, B-RAF, C-RAF, FLT3, c-KIT, RET	In animals [45, 111]	n.a.
	[^{18}F]sunitinib [112]	VEGFR, PDGFR, FLT3, c-KIT, RET	n.a.	n.a.
	[^{11}C]vandetanib [113]	VEGFR, RET, EGFR	n.a.	n.a.

Drug class	Radiolabelled drug	Targets	Tumour uptake	Personalized treatment strategies
Monoclonal antibodies	[^{64}Cu]bevacizumab	VEGF	In animals [83, 114]	Potential for early response evaluation in animals [83]
	[^{86}Y]bevacizumab	VEGF	In animals [115]	n.a.
	[^{89}Zr]bevacizumab	VEGF	In animals [82, 84, 88, 116] and in humans [69, 85]	Potential for early response evaluation in animals [82, 84] and humans [85] Potential for drug combining strategies in animals [88]
	[^{64}Cu]cetuximab	EGFR	In animals [34, 79, 117–120]	Potential for early response evaluation in animals [79]
	[^{86}Y]cetuximab	EGFR	In animals [121, 122]	n.a.
	[^{89}Zr]cetuximab	EGFR	In animals [123] and in humans [68]	n.a.
	[^{89}Zr]ibritumomab tiuxetan	CD20	In animals [97] and in humans [98]	Potential for dose titration in humans [98]
	[^{64}Cu]panitumumab	EGFR	In animals [124]	n.a.
	[^{86}Y]panitumumab	EGFR	In animals [122, 125]	n.a.
	[^{89}Zr]panitumumab	EGFR	In animals [126–128]	n.a.
	[^{64}Cu]rituximab	CD20	In animals [129]	n.a.
	[^{89}Zr]rituximab	CD20	In animals [130]	n.a.
	[^{76}Br]trastuzumab [131]	HER2	n.a.	n.a.
	[^{64}Cu]trastuzumab	HER2	In animals [80] and in humans [65, 66]	Potential for early response evaluation in animals [80]
	[^{89}Zr]trastuzumab	HER2	In animals [77, 81, 88, 132, 133] and in humans [67]	Potential for early response evaluation in animals [77, 81] Potential for drug combining strategies in animals [88]

[a]Hormone receptor

[b]To our knowledge not available

It should be noted that most tracers are administered intravenously, while many targeted agents are available in oral form. Pharmacokinetics may differ between oral and intravenous variants of a drug due to factors as absorption and first pass effect. Although oral tracer administration can be considered, it is often cumbersome due to formulation issues and radiation exposure with the need for longer-lived isotopes as a result of the slow gastrointestinal absorption. In addition, a first-pass effect may lead to higher non-specific accumulation in the liver resulting in less image quality [59].

6. Response prediction

6.1 Tracer uptake in tumours

In order for anticancer agents to be effective, the fundamental hypothesis is that adequate concentrations of the drug have to reach the tumour and the target has to be biologically active in that particular tumour. PET with radiolabelled ligands provides insight in the presence of the target. In addition, PET with radiolabelled anticancer drugs provides insight in intratumoral drug accumulation as well as target expression (Table 2 shows an overview of targeted anticancer drugs used in daily clinical practice that have been investigated as PET tracers). Both approaches may potentially predict response.

6.1.1 Uptake of [^{18}F]FES

Several studies investigated the sensitivity and specificity of [^{18}F]FES PET compared to the ER expression in tumour biopsies. Overall, there was a correlation with a pooled sensitivity of 84 % (95 % CI 73-91 %) and a specificity of 98 % (95 % CI 90–100 %) [21]. Moreover, [^{18}F]FES uptake in the tumour lesions showed predictive value. Tumours of patients with response to endocrine therapy revealed significantly more uptake at baseline, with a mean uptake about two times higher, compared with non-responders [60, 61]. Quantitative thresholds for [^{18}F]FES uptake have been defined in small studies resulting in a negative predictive value of up to 88 % and a corresponding positive predictive value of 65 % [21]. A high negative predictive value is of importance to correctly exclude patients from endocrine therapy and select alternative therapies. On the other hand, [^{18}F]FES PET may also identify susceptibility for endocrine therapy in patients with an ER negative biopsy and yet concurrent lesions with [^{18}F]FES uptake. It is well known that ER discrepancy between primary breast cancer and its metastases can be found in up to 40 % of patients [62–64]. With [^{18}F]FES PET non-invasive evaluation of ER expression in all tumour localizations can be performed thus identifying patients who potentially benefit from hormonal therapy (Fig. 3). In the future it could be possible that heterogeneous [^{18}F]FES uptake may lead to multimodal treatment strategies combining endocrine therapy with local modalities (such as radiotherapy)

for [18F]FES negative lesions. In addition, the absence of [18F]FES uptake may guide the start of cytotoxic chemotherapy. In a Dutch multicentre trial, we are currently prospectively studying the value of [18F]FES PET for selection of the first line treatment in patients with metastatic breast cancer (clinical trials.gov; NCT01957332).

Figure 3. Oestrogen receptor-positive metastases on [18F]FES PET. Oestrogen receptor-positive bone, liver, and nodal metastases are visible. Physiological [18F]FES uptake can be seen in the liver, bile duct, intestinal tract, and bladder. [18F]FES = 16α-[18F]-fluoro-17β-oestradiol. Reprinted from The Lancet Oncology, volume 14, M. van Kruchten et al., PET imaging of oestrogen receptors in patients with breast cancer, e465-475, Copyright 2013, with permission from Elsevier [21]

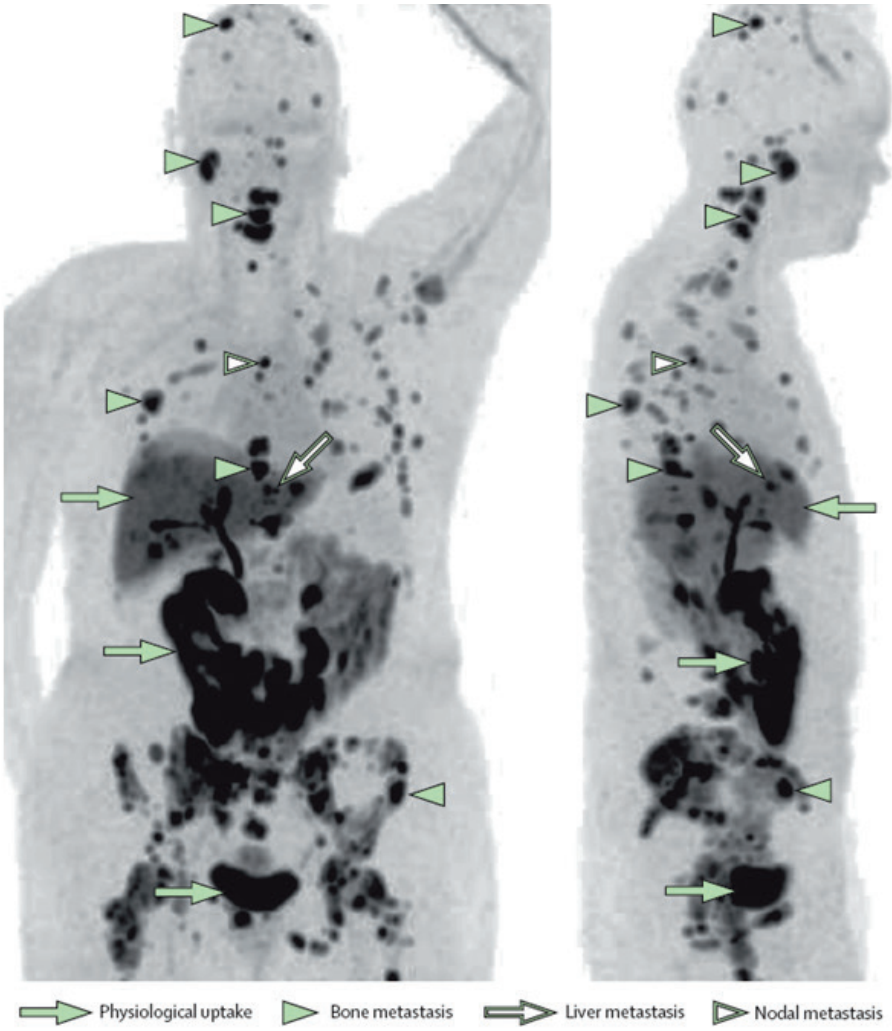

6.1.2 Uptake of radiolabelled monoclonal antibodies

The feasibility of radiolabelled trastuzumab for molecular imaging with static PET was demonstrated in three human studies. Two studies used [^{64}Cu]trastuzumab in a dose of ~130 MBq per 90 μg and ~450 MBq per 5 mg, respectively [65, 66]. PET scans were performed from 1 up to 48 h after injection and the best assessment of tumour uptake was 48 h after injection. Of the previously identified lesions with CT or MRI, 81–89 % showed uptake of [^{64}Cu]trastuzumab. In addition, new skeletal hot spots were detected which were too small to be identified on CT. The uptake in normal tissues was low, with exception of the heart wall, liver, spleen and kidneys. Combined infusion with 45 mg unlabelled trastuzumab increased the visualization of liver metastases presumably by saturation of the sink in normal liver tissue.

Trastuzumab has also been coupled to ^{89}Zr, which has a longer half-life compared with ^{64}Cu, to improve PET imaging as it is a relatively slow distributing agent. Indeed, the optimal imaging time point was 4–5 days after injection, with a lower blood pool activity and higher tumour uptake compared to earlier time points [67]. Similar to the results with [^{64}Cu]trastuzumab, the majority of lesions previously shown with conventional imaging methods were also identified with [^{89}Zr]trastuzumab PET and co-infusion of unlabelled trastuzumab improved detection of the lesions.

Recently, we performed a [^{89}Zr]cetuximab PET feasibility study in patients with KRAS wild type metastasized colorectal cancer prior to start of treatment with cetuximab. A dose of ~37 MBq per 10 mg [^{89}Zr]cetuximab was co-administrated with the first therapeutic dose cetuximab. The optimal visualization of non-hepatic tumour lesions was achieved 6 days after injection (Fig. 4). The SUV_{peak} in patients with tumour uptake ranged from 2.3 to 7.5. Due to high accumulation of cetuximab in healthy liver tissue, hepatic metastases could not be evaluated. Preliminary results in this feasibility study indicated that patients with tumour uptake have a higher chance of response [68].

The amount of uptake depends on expression/accessibility of the drug target, as well as binding characteristics such as receptor affinity and internalization. Most studies up to date assume a correlation between tracer uptake and therapeutic tumour concentrations, but factors like radiolabelled metabolites, dissociation of the label from the drug, as well competing unlabelled drug can interfere with the capacity of the PET scan to predict actual drug concentrations in the tumour tissue. Therefore, the quantitative correlation between radiolabelled drug uptake determined with PET and the actual drug targeting measured in tumour biopsies is required.

Figure 4. Representative [^{89}Zr]cetuximab PET images of a patient with metastasized colorectal cancer. **a**. The CT scan shows a pulmonary metastatic lesion in the left lower lobe. **b**. The [^{89}Zr]cetuximab PET scan made 1 day post injection (p.i.) shows high vascular uptake in for example the arcus aorta (A) and lung vessels (V), sequestration in liver (L) and spleen (S), as well as intestinal uptake (I) due to secretion of ^{89}Zr in feces. **c**. The [^{89}Zr]cetuximab PET scan made 3 days p.i. shows less vascular and splenic uptake and some tumour uptake in the pulmonary lesion. **d**. The [^{89}Zr]cetuximab PET scan made 6 days p.i. shows the best uptake in the pulmonary lesion as is indicated with the *color code*, with a SUV_{peak} of 3.0

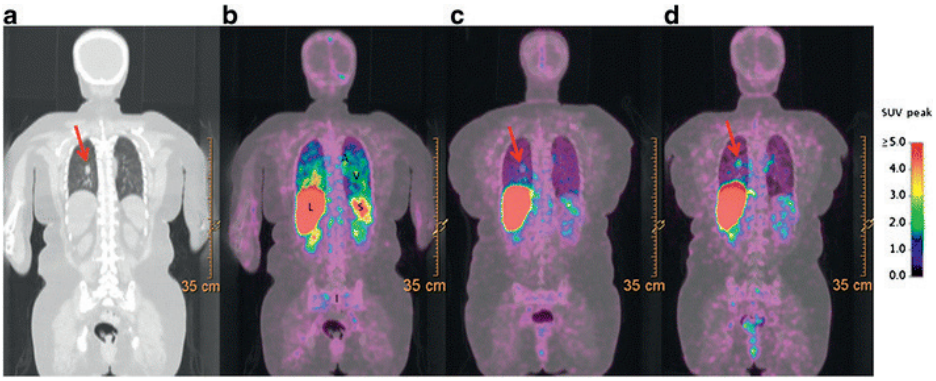

[^{89}Zr]bevacizumab, a radiolabelled monoclonal antibody against the circulating growth factor VEGF, has been studied in 23 patients with 26 resectable breast tumours before surgery [69]. Patients received ~37MBq per 5 mg [^{89}Zr]bevacizumab and a PET scan after 4 days showed a 3-fold higher SUV in tumours than in normal breast tissue in 25 out of 26 breast tumours. Expression of VEGF-A in breast tumours even exceeded that of normal breast tissue 10-20 fold, possibly due to the fact that tissue quantification also measured intracellular VEGF, whereas [^{89}Zr]bevacizumab only binds to extracellular VEGF.

These studies and other preliminary data indicate that for every new tracer the biodistribution has to be investigated and optimal conditions with respect to the amount of radiolabelled and unlabelled drug together with imaging time point have to be determined. At this moment, several studies have included analysis comparing drug uptake predicted with PET to target expression confirmed in tumour tissue. In addition, we are currently performing several trials comparing drug uptake predicted with PET with the actual drug concentrations measured in tumour biopsies, for radiolabelled monoclonal antibodies and TKIs (clinicaltrials.gov; NCT01691391 and NCT02111889). Thereby, the value of PET to predict therapeutic concentrations in the tumour will be established directly.

6.2 Tumour uptake predictive for response

One of the ultimate goals of PET imaging with radiolabelled targeted drugs is of course response prediction at the level of the patient as well as the separate tumour lesions. Several studies have shown association of tumour uptake and response. In the past, different chemotherapy agents have been labelled with PET tracers to study tumour uptake in relation to response prediction [70, 71]. Before start of therapy, [^{11}C]docetaxel PET revealed a significant correlation between tumour uptake and percentage decrease in longest tumour diameter in patients with NSCLC [72]. Similarly, in a small group of patients with metastasized colorectal cancer the SUV_{mean} of [^{18}F]5-FU PET prior to treatment with 5-FU was not only correlated with treatment response, but also with survival [73].

Regarding targeted therapy the predictive value of [^{18}F]tamoxifen PET was investigated in 10 patients with ER-positive breast cancer with 23 primary or metastatic lesions [74]. Three patients, each with a suspected lesion without [^{18}F]tamoxifen uptake, appeared to be truly negative for breast cancer based on tumour biopsies and clinical course. Six patients were evaluable for the response to tamoxifen. Three out of six patients with clinical benefit of tamoxifen had positive lesions on [^{18}F]tamoxifen PET. In contrast, two of the three patients with a poor outcome had negative lesions and one showed mixed uptake. However, high non-specific uptake in lungs, heart and liver have limited the further development of [^{18}F]tamoxifen as a tracer, in contrast to [^{18}F]FES.

A study in ten patients with NSCLC investigated the uptake of [^{11}C]erlotinib in relation to EGFR mutations such as exon 19 deletion and exon 21 point mutations, which are positively correlated with the antitumour activity of erlotinib [56]. Compared with wild type EGFR, these mutations result in a 2–3 fold higher TKI binding activity for both test and retest [^{11}C]erlotinib PET, p = 0,009 (Fig. 5). Tumour uptake in patients treated with erlotinib correlated well with treatment effect. Interestingly, one patient developed resistance to erlotinib shortly before the study. Although this patient demonstrated higher [^{11}C]erlotinib uptake than patients with wild type tumours, the uptake was the lowest of the mutated group. Eventually, this patient appeared to have a T790Mmutation in EGFR, which is known to cause resistance to erlotinib [75]. Another study in 13 patients with NSCLC reported uptake of [^{11}C]erlotinib in four out of 13 patients prior to start of treatment with erlotinib [76]. Three out of four patients with uptake had benefit of treatment with erlotinib, compared to two out of nine patients without uptake.

Figure 5. Representative [^{11}C]erlotinib PET images of two different patients with NSCLC. **a**. Patient with an EGFR exon 19 deletion, tumour in the right upper lobe (*black arrow*) and mediastinal lymph nodes (*black arrowhead*). **b**. Patient with wild-type EGFR, tumour located at the left hilum (*white arrow*). Patient a (with mean tumour V_T of 1.30) shows higher tumour uptake than patient b (with mean tumour V_T of 0.67) as indicated by the color code. The liver (#) shows physiologic uptake of metabolized and nonmetabolized [^{11}C]erlotinib. Notice artifacts caused by mediastinal blood vessels (*). Coronal images are shown of CT-fused parametric [^{11}C]erlotinib uptake (a1 and b1), CT (a2 and b2), and [^{18}F]FDG uptake (a3 and a3). High FDG uptake is seen in the heart (H). Reprinted from Clinical Cancer Research, volume 19, I. Bahce et al., Development of [11C]erlotinib positron emission tomography for in vivo evaluation of EGF receptor mutational status, 183–193, Copyright 2013, with permission from the American Association for Cancer Research (AACR) publishers [56]

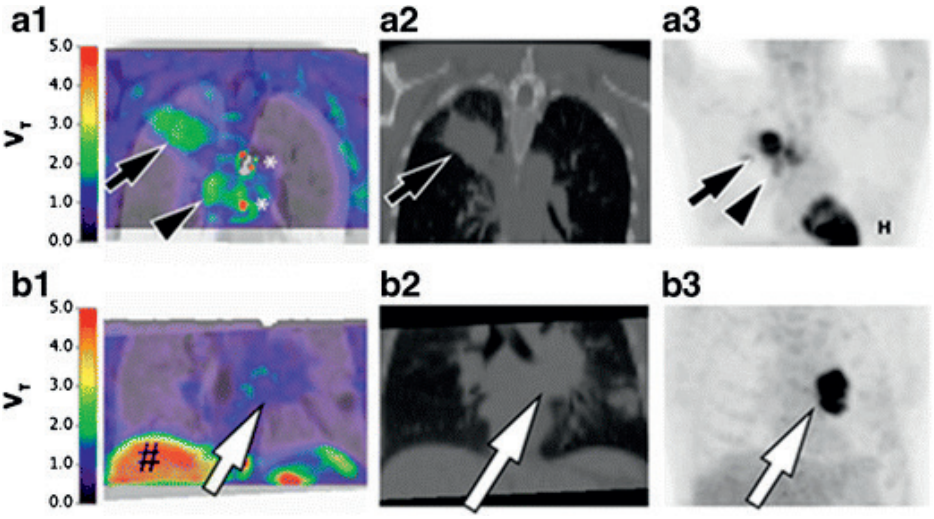

There are also ongoing studies regarding response prediction using radiolabelled therapeutic antibodies. For example, a study in patients with HER2-positive breast cancer evaluates the clinical utility of [^{89}Zr]trastuzumab for the identification of patients, who are unlikely to respond to TDM-1 (clinicaltrials.gov; NCT01565200). And yet another study investigates the clinical utility of [^{18}F]FES PET and [^{89}Zr]trastuzumab PET for the identification of patients with metastasized breast cancer who are likely to respond to first-line endocrine therapy and/or trastuzumab compared to standard treatment selection based on a tumour biopsy (clinicaltrials.gov; NCT01957332). These forthcoming studies will help to identify the possibilities and clinical utility of these types of imaging for treatment selection, response prediction and understanding tumour heterogeneity.

7. New clinical developments with PET

7.1 Early response evaluation with radiolabelled targeted drugs

Various animal studies have been performed to evaluate the early effects of targeted therapies on the expression of HER2, EGFR and VEGF together with vessel density using radiolabelled trastuzumab, cetuximab or bevacizumab PET, respectively (Table 2). Afatinib, an irreversible TKI of EGFR, HER2 and HER4, decreased [^{89}Zr]trastuzumab uptake > 80% after 1 week of treatment in HER2-positive NCI-N87 gastric cancer xenografted mice compared to mice injected with a control vehicle. Tumour biopsies showed HER2 downregulation and tumour size was reduced. In contrast, [^{18}F]FDG PET showed no differences in tumour uptake during treatment [77].

Another example is the effect of Heat Shock Protein 90 (Hsp90) inhibitors on EGFR, HER2 and VEGF expression. Hsp90 is a chaperone protein involved in the expression, conformation and activity of various oncological target proteins, including protein kinases and steroid hormone receptors. This novel group of anticancer drugs inhibits Hsp 90 at the ATP-binding site and they are currently being investigated in clinical trials [78]. In mice with various human tumour xenografts the Hsp90 inhibitors showed a 40–50 % decrease in tumour uptake of [^{64}Cu]cetuximab [79], [^{64}Cu]trastuzumab [80], [^{89}Zr]trastuzumab [81] as well as [^{89}Zr]bevacizumab [82] within 1 week of treatment compared to pre-treatment uptake and/or controls. This correlated well with the difference in EGFR, HER2 and VEGF expression and vessel density measured histologically, which was significantly decreased in the animals treated with the Hsp90 inhibitors. A simultaneously reduced proliferation rate was measured with Ki67 staining in mice with reduced PET uptake.

The early effect of everolimus on tumour vascularization was explored with radiolabelled bevacizumab in animal models. Everolimus, an inhibitor of mammalian target of rapamycin (mTOR), also inhibits the production of VEGF. It has shown clinical benefit in the treatment of patients with metastasized renal cell cancer and breast cancer. [^{64}Cu]bevacizumab or [^{89}Zr]bevacizumab PET was performed after treatment with everolimus in 786-O renal cancer and A2780luc+ ovarian cancer xenografted mice, respectively. Everolimus decreased the tumour uptake of radiolabelled bevacizumab about 50 % in comparison to mice treated with a control vehicle. This was in accordance with reduced VEGF-A levels, mean vascular density and tumour growth in mice treated with bevacizumab in contrast to controls [83,84].

Finally, one human study has been performed to study the effect of sunitinib and bevacizumab plus interferon on the uptake of [^{89}Zr]bevacizumab before and

during treatment in patients with metastatic renal cell carcinoma [85]. A total of 26 patients were included of which 22 patient were evaluable. Treatment with bevacizumab and interferon resulted in a significant, nearly 50 % drop in mean SUV_{max} of [^{89}Zr]bevacizumab uptake at 2 weeks with an additional 10 % decrease at 6 weeks. Whether these observations may correlate with early response remains to be evaluated in new clinical trials.

7.2 The value of PET for drug combination strategies

Besides response prediction and early response evaluation, molecular imaging provides insight in the interaction between anticancer therapies. It can take years to find effective drug combinations in clinical trials, as drug schedules have shown a profound effect on interaction between the different components. Only during clinical trials it became apparent that combining the anti-VEGF antibody bevacizumab with cetuximab or panitumumab reduced their efficacy significantly [86, 87]. Studying drug distribution with molecular imaging in combination treatment can provide a rationale to avoid possible detrimental drug combinations and select the potentially successful ones. The effect of bevacizumab on drug uptake in tumours has been investigated in animal as well human studies. Mice with SKOV-3 ovarian or OE19 oesophageal cancer xenografts were injected before treatment with [^{89}Zr]trastuzumab, [^{89}Zr]bevacizumab or [^{89}Zr]IgG on day zero [88]. On days 13, 16 and 19 the mice received 5 mg/kg unlabelled bevacizumab. A second tracer dose was injected on day 14 and PET was performed 1 and 6 days after each injection. Bevacizumab reduced the tumour uptake of all radiolabelled antibodies compared to baseline with a 40–50 % decrease in [^{89}Zr]trastuzumab, [^{89}Zr]bevacizumab and [^{89}Zr]IgG SUV_{mean}. The similar decrease in [^{89}Zr]IgG illustrates that the reduced antibody uptake is a general result of treatment with bevacizumab, possibly due to reduced leakage into the tumour tissue and diminished tumour perfusion.

Comparable results were obtained in human trials combining bevacizumab with cytotoxic chemotherapy. [^{18}F]5-fluorouracil PET showed a 20 % decrease in tumour uptake in patients with colorectal cancer after treatment with bevacizumab [89]. Another study in patients with NSCLC showed a significant decline in tumour [^{11}C]docetaxel uptake after the administration of bevacizumab. This decrease in [^{11}C]docetaxel uptake correlated with a reduction in tumour perfusion evaluated with [^{15}O]H_2O PET [90].

Other compounds can also interfere with blood flow and tumour uptake. Interferon-α was shown to increase tumour blood flow and tumour uptake of [^{18}F]5-FU in patients with various malignancies [91]. Pre-treatment with dexamethasone reduced tumour uptake of [^{11}C]docetaxel in patients with

NSCLC, possibly due to increased drug efflux activity by transporters, such as P-glycoprotein and breast cancer resistance protein [92, 93].

These studies illustrate the potential value of molecular imaging to design novel treatment combinations and dosage schedules as well as to understand and predict the combined efficacy and toxicity.

7.3 Dose titration

Traditionally, dose finding for anticancer agents in phase I trials has been directed to find the maximum tolerated dose assuming that the maximum dose will provide the maximum benefit. In contrast to cytotoxic chemotherapy, for many targeted anticancer agents dose limiting toxicity and a maximum tolerated dosage are not reached in phase I trials, e.g. for bevacizumab, trastuzumab and cetuximab [94-96]. Therefore, other criteria such as pharmacokinetics/dynamics as well as (in)activation of downstream targets are used to determine the optimal dose. For example, the dosage schedule of cetuximab is based on a plateau of clearance reached with increasing dosage and the associated nearly complete saturation of EGFRs [96]. Still, there is a large variation in through levels and AUC exposition between patients, suggesting pharmacokinetic differences between patients leading to potentially suboptimal therapeutic effects. Measurement of the intratumour concentrations of radiolabelled drugs with PET may help to predict the best dosage for an individual patient. Currently, we are recruiting patients to investigate image guided treatment optimization for patients with metastasized RAS wild type colorectal cancer with [^{89}Zr]cetuximab (clinicaltrials.gov; NCT01691391). Dosages of cetuximab will be adapted according to tumour uptake seen on the [^{89}Zr]cetuximab PET with the objective to improve clinical benefit in these patients.

Another example of potential dose titration with PET is radiation dosimetry for radioimmunotherapy. In general, a higher radiation dose is associated with more clinical benefit. However, toxicity of normal tissues must be prevented. ^{90}Yttrium emits high energy beta arrays suitable for radiation and bound to the anti-CD20 monoclonal antibody ibritumomab tiuxetan. [^{90}Y]ibritumomab tiuxetan is used as radioimmunotherapy in the treatment of relapsed or refractory non-Hodgkin lymphomas. Instead of a fixed dose/kg, individual dosing has been investigated using [^{89}Zr]ibritumomab tiuxetan to predict radiation dosimetry of [^{90}Y]ibritumomab tiuxetan [97]. In a human study, seven patients with relapsed B-cell non-Hodgkin lymphoma underwent PET 1, 72 and 144 h after the injection of 70 MBq [^{89}Zr]ibritumomab tiuxetan as well as 2 weeks later after injection of 15 or 30 MBq/kg [^{90}Y]ibritumomab tiuxetan [98]. Based on [^{89}Zr]ibritumomab tiuxetan PET the predicted doses correlated well with the absorbed organ doses (Pearson correlation coefficient r = 0,97) [94]. The dose-limiting organ with the

highest absorbed dose of [^{90}Y]ibritumomab tiuxetan was the liver, SUV_{mean} 3,2 ± 1,8 mGy/MBq. In comparison, tumour absorbed doses ranged from 8,6 to 28,6 mGy/MBq. Although it should be confirmed in a larger study, the SUV_{mean} of [^{89}Zr]ibritumomab tiuxetan in the liver at 72 or 144 h appears a good predictor for dose optimization with therapeutic [^{90}Y]ibritumomab tiuxetan.

8. Discussion and conclusions

With the growing amount of therapeutic options, the selection of the optimal treatment for an individual patient is increasingly important. Analysis of tumour material regarding pathological characteristics, mutational status and expression levels of target proteins is essential for treatment selection. However, repeated biopsies of multiple sites to characterize the individual metastases over time are limited by the accessibility of the lesions and the acceptable burden for the patient. 'Liquid biopsies' to investigate circulating tumour cells, circulating tumour DNA and other tumour related factors can support minimally invasive characterization of the evolving tumour. However, none of these techniques are able to appreciate tumour heterogeneity of all different lesions non-invasively within a single patient over time. Recent studies have suggested that intra- and intertumour heterogeneity for multiple different tumour types may be important [99, 100] in addition to changes in receptor expression and mutational status during the course of treatment [101]. PET using radiolabelled drugs or ligands identifying drug targets is a promising tool that may fill this gap, as it may be used to accurately quantify tumour heterogeneity and drug biodistribution over time non-invasively. We envision that molecular imaging may contribute to response prediction and early response evaluation of targeted drugs in patients with malignancies.

Integration of molecular imaging with PET in daily clinical practice has several challenges:

1. Uniformity of the scanning process and standardized methods for outcome evaluation are necessary for reproducibility and comparison of results. The main issue here is to determine the optimal trade-off between accuracy and simplicity. For [^{18}F]FDG scanning procedures have been harmonized [102] and recommendations have been made for standardization of response criteria [103].
2. There are potential confounding factors using PET. The question is whether the behaviour of a microdose of the radiolabelled drug is the same as that of a therapeutic dose. The microdose may not be enough to reach tumour sites because of a 'sink effect', i.e. the microdose binds to (non-specific) targets outside the tumour leaving not enough tracer for tumour accumulation,

which especially is a challenge for antibody-tracers. Addition of a cold dose of the drug may overcome this as has been shown for [^{89}Zr]trastuzumab [66].

3. A drug may also have a more general effect outside the tumour, for instance by activating immune cells like the monoclonal antibody ipilimumab, which binds to the cytotoxic T-lymphocyte associated antigen 4 and causes T-cell immune responses against tumours [104]. In this case, tumour uptake of the drug is not the issue.
4. Causes for false-positive results may include high background levels in tissues adjacent to the tumour and nonspecific vascular leakage due to abnormal tumour vasculature in the absence of adequate drug-target binding. False-negative uptake of the tracer may be caused by reduced vascular perfusion and tumour necrosis. These are typical problems using static measurements, with dynamic scans one can separate non-specific vascular leakage from specific uptake.

In conclusion, molecular imaging with radiolabelled targeted anticancer drugs has great potential for improvement of personalized cancer care. The non-invasive quantification of drug accumulation in tumour and normal tissues provides understanding of the biodistribution in relation to therapeutic and toxic effects. Although only a limited number of clinical studies with radiolabelled targeted anticancer drugs are available, the results indicate that there is value in response prediction, early response evaluation and optimization of dosing schedules. Larger studies are necessary to determine the exact role in daily clinical practice. Standardized methods regarding tracer production, PET procedures and outcome analysis are required to obtain meaningful results from these future trials in order to make individual treatment decisions for better patient outcome.

Acknowledgements
We sincerely thank Erik van Helden, Elske Gootjes and Otto Hoekstra for providing the [^{89}Zr]cetuximab PET images used in Fig. 4 as well as Geke Hospers and Idris Bahce for permission to reproduce Figs. 3 and 5, respectively.

Conflicts of interest
No potential conflicts of interest were disclosed.

References

1. U.S. Food and drug Administration, Hematology/oncology (cancer) approvals & safety notifications. (FDA 2013), http://www.fda.gov/drugs/informationondrugs/approveddrugs/ucm279174.htm. Accessed 2 January 2014.
2. K.T. Flaherty, I. Puzanov, K.B. Kim, et al., Inhibition of mutated, activated BRAF in metastatic melanoma. N Engl J Med. 363, 809-819 (2010).
3. D.A. Mankoff, A definition of molecular imaging. J Nucl Med. 48, 18N, 21N (2007).
4. P. Zanzonico, Positron emission tomography: a review of basic principles, scanner design and performance, and current systems. Semin Nucl Med. 34, 87-111(2004).
5. G.A. van Dongen, M. J. Vosjan. Immuno-positron emission tomography, shedding light on clinical antibody therapy. Cancer Biother Radiopharm. 25, 375-385 (2010).
6. A. Rahmim, H. Zaidi, PET versus SPECT: strengths, limitations and challenges. Nucl Med Commun. 29, 193-207 (2008).
7. R. Weissleder, M.K. Pittet, imaging in the era of molecular oncology. Nature 452, 580-589 (2008).
8. D.W. Townsend, PET/CT Today and Tomorrow. J Nucl Med. 45 suppl, 4S-14S (2004).
9. J.F. Bruzzi, S.G. Swisher, M.T. Truong, et al., Detection of interval distant metastases: clinical utility of integrated CT-PET imaging in patients with esophageal carcinoma after neoadjuvant therapy. Cancer. 109, 125-134 (2007).
10. G.A. Silvestri, M.K. Gould, M.L. Margolis, et al., Noninvasive staging of non-small cell lung cancer: ACCP evidenced-based clinical practice guidelines (2nd edition). Chest. 132, 178S-201S (2007).
11. M.E. Juweid, S. Stroobants, O.S. Hoekstra, et al., Use of positron emission tomography for response assessment of lymphoma: consensus of the imaging subcommittee of international harmonization project in lymphoma. J Clin Oncol. 25, 571-578 (2007).
12. M. Adejolu, L. Huo, E. Rohren, et al., False-positive lesions mimicking breast cancer on FDG PET and PET/CT. AJR Am J Roentgenol. 198,W304-314 (2012).
13. M. Scheffler, C. Kobe, T. Zander, et al., Monitoring reversible and irreversible EGFR inhibition with erlotinib and afatinib in a patient with EGFR-mutated non-small cell lung cancer (NSCLC) using sequential [18F]fluorothymidine (FLT-)PET. Lung Cancer. 77, 617-620 (2012).
14. A.J. de Langen, M. Lubberink, R. Boellaard, et al., Reproducibility of tumor perfusion measurements using 15O-labeled water and PET. J Nucl Med. 49, 1763-1768 (2008).
15. F.G. Blankenberg. Imaging the molecular signatures of apoptosis and injury with radiolabeled annexin V. Proc Am Thorac Soc. 6, 469-476 (2009).
16. L.S. Mortensen, J. Johansen, J. Kallehauge, et al., FAZA PET/CT hypoxia imaging in patients with squamous cell carcinoma of the head and neck treated with radiotherapy: results from the DAHANCA 24 trial. Radiother Oncol. 105, 14-20 (2012).
17. L.M. Peterson, B.F. Kurland, E.K. Schubert, et al. A phase 2 study of 16α-[^{18}F]-fluoro-17β-estradiol positron emission tomography (FES-PET) as a marker of hormone sensitivity in metastatic breast cancer (MBC). Mol Imaging Biol. Epub ahead of print (2013).
18. A. Verhagen, M. Studeny, G. Luurtsema, et al. Metabolism of a [^{18}F]fluorine labeled progestin (21-[^{18}F]fluoro-16 alpha-ethyl-19-norprogesterone) in humans: a clue for future investigations. Nucl Med. Biol. 21, 941-952 (1994).

19. F. Dehdashti, J. Picus, J.M. Michalski, et al. Positron tomographic assessment of androgen receptors in prostatic carcinoma. Eur J Nucl Med Mol Imaging. 32, 344-350 (2005).
20. D.A. Mankoff, J.M. Link, H.M. Linden, et al., Tumor receptor imaging. J Nucl Med. 49 suppl, 149S-163S (2008).
21. M. van Kruchten, E.G. de Vries, E.F. de Vries, et al., PET imaging of oestrogen receptors in patients with breast cancer. Lancet Oncol. 14, e465-e475 (2013).
22. F. Dehdashti, A.H. McGuire, H.F. van Brocklin, et al., Assessment of 21-[18F]fluoro-16 alpha-ethyl-19-norprogesterone as a positron-emitting radiopharmaceutical for the detection of progestin receptors in human breast carcinomas. J Nucl Med. 32, 1532-1537 (1991).
23. H.B. Zhou, J.H. Lee, C.G. Mayne, et al., Imaging progesterone receptor in breast tumors: synthesis and receptor binding affinity of fluoroalkyl-substituted analogues of tanaproget. J Med Chem. 53:3349-3360 (2010).
24. S.M. Larson, M. Morris, I. Gunther, et al., Tumor localization of 16beta-18F-fluoro-5alpha-dihydrotestosterone versus 18F-FDG in patients with progressive, metastatic prostate cancer. J Nucl Med. 45, 366-373 (2004).
25. J.A. Ruizeveld de Winter, P.J. Janssen, H.M. Sleddens. Androgen receptor status in localized and locally progressive hormone refractory human prostate cancer. Am J Pathol. 144,735-746 (1994).
26. I. Velikyan, A.L. Sundberg, O. Lindhe, et al., Preparation and evaluation of 68Ga-DOTA-hEGF for visualization of EGFR expression in malignant tumors. J Nucl Med. 46, 1881–1888 (2005).
27. W. Li, G. Niu, L. Lang, et al., PET imaging of EGF receptors using [18F]FBEM-EGF in a head and neck squamous cell carcinoma model. Eur J Nucl Med Mol Imaging. 39, 300–308 (2012).
28. P.M. Smith-Jones, D.B. Solit, T. Akhurst, et al., Imaging the pharmacodynamics of HER2 degradation in response to Hsp90 inhibitors. Nat Biotechnol. 22, 701-706 (2004).
29. Z. Miao, G. Ren, H. Liu, et al., Small-animal PET imaging of human epidermal growth factor receptor positive tumor with a 64Cu labeled affibody protein. Bioconjugate Chem. 21, 947–954 (2010).
30. Z. Miao, G. Ren, H. Liu, et al., PET of EGFR expression with an 18F-labeled affibody molecule. J Nucl Med. 53, 1110-1118 (2012).
31. C. Xavier, I. Vaneycken, M. D'huyvetter, et al., Synthesis, preclinical validation, dosimetry, and toxicity of 68Ga-NOTA-anti-HER2 Nanobodies for iPET imaging of HER2 receptor expression in cancer. J Nucl Med. 54, 776-784 (2013).
32. H. Gong, L. Sampath, J. L. Kovar, et al. (2012). Targeting EGFR and HER2 for Molecular Imaging of Cancer, Molecular Imaging, Prof. Bernhard Schaller (Ed.), ISBN: 978-953-51-0359-2]. InTech, Available from: http://www.intechopen.com/books/molecular-imaging/targeting-egfr-and-her2-for-molecular-imaging-of-cancer.
33. F. Teng, X. Meng, X. Sun, et al., New strategy for monitoring targeted therapy: molecular imaging. Int J Nanomedicine. 8, 3703-3713 (2013).
34. W. Cai, K. Chen, L. He, et al., Quantitative PET of EGFR expression in xenograft-bearing mice using 64Cu-labeled cetuximab, a chimeric anti-EGFR monoclonal antibody. Eur J Nucl Med Mol Imaging. 34, 850-858 (2007).

35. H.J. Aerts, L. Dubois, L. Perk, et al., Disparity between in vivo EGFR expression and 89Zr-labeled cetuximab uptake assessed with PET. J Nucl Med. 50, 123-131 (2009).
36. E.B. Corcoran, R.N. Hanson. Imaging EGFR and HER2 by PET and SPECT: a review. Med Res Rev. 34, 596-643 (2014).
37. C.C. Wagner, O. Langer, Approaches using molecular imaging technology – use of PET in clinical microdose studies. Adv Drug Deliv Rev. 63, 539-546 (2011).
38. Office of new drugs in the Center for Drug Administration and Research (CDER). Guidance for industry, investigators and reviewers. (Food and Drug Administration 2006), http://www.fda.gov/downloads/Drugs/GuidanceComplianceRegulatoryInformation/Guidances/ucm078933.pdf. Accessed 3 January 2014.
39. B. van den Bossche, C. van de Wiele, Receptor imaging in oncology by means of nuclear medicine: current status. J Clin Oncol. 22, 3593-3607 (2004).
40. P. Slobbe, A.J. Poot, A.D. Windhorst, et al., PET imaging with small-molecule tyrosine kinase inhibitors: TKI-PET. Drug Discov Today. 17, 1175-1187 (2012).
41. M.W. Brechbiel, Bifunctional chelates for metal nuclides. Q J Nucl Mol Imaging. 52, 166-173 (2008).
42. A.B. Riemer, M. Klinger, S. Wagner, Generation of Peptide mimics of the epitope recognized by trastuzumab on the oncogenic protein Her-2/neu. J Immunol. 173, 394-401 (2004).
43. G.A. van Dongen, G.W. Visser, M.N. Lub-de Hooge, et al., Immuno-PET: a navigator in monoclonal antibody development and applications. The oncologist. 12, 1379-1389 (2007).
44. A.A. Memon, S. Jakobsen, F. Dagnaes-Hansen, et al., Positron emission tomography (PET) imaging with [11C]-labeled erlotinib: a micro-PET study on mice with lung tumor xenografts. Cancer Res. 69, 873-878 (2009).
45. A.J. Poot, B. van der Wildt, M. Stigter-van Walsum, et al., [^{11}C]Sorafenib: radiosynthesis and preclinical evaluation in tumor-bearing mice of a new TKI-PET tracer. Nucl Med Biol. 40, 488-97 (2013).
46. H. Su, Y. Seimbille, G.Z. Ferl, et al., Evaluation of [18F]gefitinib as a molecular imaging probe for the assessment of the epidermal growth factor receptor status in malignant tumors. Eur J Nucl Med Mol Imaging. 35, 1089-1099 (2008).
47. Y. Seimbille, F. Bénard, J. Rousseau, et al., Impact on estrogen receptor binding and target tissue uptake of [18F]fluorine substitution at the 16alpha-position of fulvestrant (faslodex; ICI 182,780). Nucl Med Biol. 31, 691-698 (2004).
48. D. Yang, L.R. Kuang, A. Cherif, et al. Synthesis of [18F]fluoroalanine and [18F] fluorotamoxifen for imaging breast tumors. J Drug Target. 1, 259-267 (1993).
49. A.A. van der Veldt, E.F. Smit, A.A. Lammertsma, Positron emission tomography as a method for measuring drug delivery to tumors in vivo: the example of [^{11}C] docetaxel. Front Oncol 13:103389 (2013).
50. A.A. Lammertsma, C.J. Bench, S.P. Hume, et al. Comparison of methods for analysis of clinical [^{11}C]raclopride studies. J Cereb Blood Flow Metab. 16, 42-52 (1996).
51. R.N. Gunn, S.R. Gunn, V.J. Cunningham, Positron emission tomography compartmental models. J Cereb Blood Flow Metab. 21, 635-652 (2001).
52. A.A. Lammertsma, in In Vivo Imaging of Cancer Therapy, ed. By A.F. Shields, P. Price (Humana Press, New Jersey, 2007), p. 155-167.

53. M. Yaqub, R. Boellaard, M.A. Kropholler, et al., Optimization algorithms and weighting factors for analysis of dynamic PET studies. Phys Med Biol. 51, 4217-4232 (2006).
54. K.S. Gleisner, M. Nickel, O. Lindén, et al., Parametric images of antibody pharmacokinetics based on serial quantitative whole-body imaging and blood sampling. J Nucl Med. 48, 1369-1378 (2007).
55. M.C. Adams, T.G. Turkington, J.M. Wilson, et al., A systematic review of the factors affecting accuracy of SUV measurements. AJR Am J Roentgenol. 195, 310-320 (2010).
56. I. Bahce, E.F. Smit, M. Lubberink, et al., Development of [^{11}C]erlotinib positron emission tomography for in vivo evaluation of EGF receptor mutational status. Clin Cancer Res. 19, 183-193 (2013).
57. M. Bergström, A. Grahnén, B. Langström. Positron emission tomography microdosing: a new concept with application in tracer and early clinical drug development. Eur J Clin Pharmacol. 59, 357-366 (2003).
58. A. Saleem, G. Searle, L.M. Kenny, et al., Brain and tumor penetration of carbon-11-labeled lapatinib in patients with HER2-overexpressing metastatic breast cancer. J Clin Oncol. 31, suppl 15:635 (2013).
59. A.J. Fischman, A.A. Bonab, R.H. Rubin, Regional pharmacokinetics of orally administered PET tracers. Curr Pharm Des. 6,1625-1629 (2000).
60. J.E. Mortimer, F. Dehdashti, B.A. Siegel, et al., Metabolic flare: indicator of hormone responsiveness in advanced breast cancer. J Clin Oncol. 19, 2797-2803 (2001).
61. F. Dehdashti, J.E. Mortimer, K. Trinkaus, et al., PET-based estradiol challenge as a predictive biomarker of response to endocrine therapy in women with estrogen-receptor-positive breast cancer. Breast Cancer Res Treat. 113, 509-517 (2009).
62. C. Liedtke, K. Broglio, S. Moulder, et al., Prognostic impact of discordance between triple-receptor measurements in primary and recurrent breast cancer. Ann Oncol. 20, 1953-1958 (2009).
63. E. Amir, M. Clemons, C.A. Purdie, Tissue confirmation of disease recurrence in breast cancer patients: pooled analysis of multi-centre, multi-disciplinary prospective studies. Cancer Treat Rev. 38, 708-714 (2012).
64. T. Foukakis, G. Astrom, L. Lindstrom, et al., When to order a biopsy to characterise a metastatic relapse in breast cancer. Ann Oncol. 23 (suppl 10) x349–353 (2012).
65. K. Tamura, H. Kurihara, K. Yonemori, et al., 64Cu-DOTA-trastuzumab PET imaging in patients with HER2-positive breast cancer. J Nucl Med. 51, 1869-1875 (2013).
66. J.E. Mortimer, J.R. Bading, D.M. Colcher, et al., Functional imaging of human epidermal growth factor receptor 2-positive metastatic breast cancer using 64Cu-DOTA-trastuzumab PET. J Nucl Med. 55, 23-29 (2014).
67. E.C. Dijkers, T.H. Oude Munnink, J.G. Kosterink, et al., Biodistribution of 89Zr-trastuzumab and PET imaging of HER2-positive lesions in patients with metastatic breast cancer. Clin Pharmacol Ther. 87, 586-592 (2010).
68. E.C. Gootjes, M.C. Huisman, D. Vughts, et al., [^{89}Zr] labeled cetuximab PET imaging in advanced colorectal cancer patients: a feasibility study. Abstract O3.6 of the 12th international congress on targeted anticancer therapies 2014. http://www.tatcongress.org/download-abstracts.html. Accessed 18 April 2014.
69. S.B. Gaykema, A.H. Brouwers, M.N. Lub-de Hooge, et al., 89Zr-bevacizumab PET imaging in primary breast cancer. J Nucl Med. 54, 1014-1018 (2013).

70. A.A. van der Veldt, G. Luurtsema, M. Lubberink, et al., Individualized treatment planning in oncology: role of PET and radiolabelled anticancer drugs in predicting tumour resistance. Curr Pharm Des. 14, 2914-2931 (2008).
71. R. Sharma R, E. Aboagye. Development of radiotracers for oncology--the interface with pharmacology. Br J Pharmacol. 163, 1565-1585 (2011).
72. A.A. van der Veldt, M. Lubberink, R.H. Mathijssen, et al., Toward prediction of efficacy of chemotherapy: a proof of concept study in lung cancer patients using [^{11}C]docetaxel and positron emission tomography. Clin Cancer Res. 19, 4163-4173 (2013).
73. M. Moehler, A. Dimitrakopoulou-Strauss, F. Gutzler, et al., 18F-labeled fluorouracil positron emission tomography and the prognoses of colorectal carcinoma patients with metastases to the liver treated with 5-fluorouracil. Cancer. 83, 245-253 (1998).
74. T. Inoue, E.E. Kim, S. Wallace, et al., Positron emission tomography using [18F] fluorotamoxifen to evaluate therapeutic responses in patients with breast cancer: preliminary study. Cancer Biother Radiopharm. 11, 235-245 (1996).
75. N. Godin-Heymann, L. Ulkus, B.W. Brannigan, et al., The T790M “gatekeeper” mutation in EGFR mediates resistance to low concentrations of an irreversible EGFR inhibitor. Mol Cancer Ther. 7, 874-879 (2008).
76. A.A. Memon, B. Weber, M. Winterdahl, et al., PET imaging of patients with non-small cell lung cancer employing an EGF receptor targeting drug as tracer. Br J Cancer. 105, 1850-1855 (2011).
77. Y.Y. Janjigian, N. Viola-Villegas, J.P. Holland, et al., Monitoring afatinib treatment in HER2-positive gastric cancer with 18F-FDG and 89Zr-trastuzumab PET. J Nucl Med 54, 936-943 (2013).
78. Y. Miyata, H. Nakamoto, L. Neckers. The therapeutic target Hsp90 and cancer hallmarks. Curr Pharm Des. 19, 347-365 (2013).
79. G. Niu, W. Cai, K. Chen, et al., Non-invasive PET imaging of EGFR degradation induced by a heat shock protein 90 inhibitor. Mol Imaging Biol. 10, 99-106 (2008).
80. G. Niu, Z. Li, Q. Cao, et al., Monitoring therapeutic response of human ovarian cancer to 17-DMAG by noninvasive PET imaging with (64)Cu-DOTA-trastuzumab. Eur J Nucl Med Mol Imaging. 36, 1510-1519 (2009).
81. T.H. Oude Munnink, M.A. Korte, W.B. Nagengast, et al., (89)Zr-trastuzumab PET visualises HER2 downregulation by the HSP90 inhibitor NVP-AUY922 in a human tumour xenograft. Eur J Cancer. 46, 678-684 (2010).
82. W.B. Nagengast, M.A. de Korte, T.H. Oude Munnink, et al., 89Zr-bevacizumab PET of early antiangiogenic tumor response to treatment with HSP90 inhibitor NVP-AUY922. J Nucl Med. 51, 761-767 (2010).
83. A.J. Chang, R. Sohn. Z. Hong Lu, et al., Detection of rapalog-mediated therapeutic response in renal cancer xenogrefts using ^{64}Cu-bevacizumab immunoPET. PLoS One. 8:101371 (2013).
84. A.R. van der Bilt, A.G. Terwisscha van Scheltinga, H. Timmer-Bosscha, et al., Measurement of tumor VEGF-A levels with 89Zr-bevacizumab PET as an early biomarker for the antiangiogenic effect of everolimus treatment in an ovarian cancer xenograft model. Clin Cancer Res. 18, 6306-6314 (2012).
85. S. Oosting, A.H. Brouwers, S.C. van Es, et al., ^{89}Zr-bevacizumab PET imaging in metastatic renal cell carcinoma patients before and during antiangiogenic treatment. J Clin Oncol. 30, suppl 15:10581 (2012).

86. J. Tol, M. Koopman, A. Cats, et al. Chemotherapy, bevacizumab, and cetuximab in metastatic colorectal cancer. N Engl J Med. 360:563-572 (2009)
87. J.R. Hecht, E. Mitchell, T. Chidiac, et al., A randomized phase IIIB trial of chemotherapy, bevacizumab and panitumumab compared with chemotherapy and bevacizumab alone for metastatic colorectal cancer. J Clin Oncol. 27, 672-680 (2009).
88. M. Arjaans, T.H. Oude Munnink, S.F. Oosting, et al., Bevacizumab-induced normalization of blood vessels in tumors hampers antibody uptake. Cancer Res. 73, 3347-3355 (2013).
89. M.H. Zissen, P. Kunz, M. Subbarayan, et al., 18F-5-fluorouracil dynamic positron emission tomography/computed tomography shows decreased tracer activity after bevacizumab in colorectal metastases. Nucl Med Commun. 32, 343-347 (2011).
90. A.A.M. van der Veldt, M. Lubberink, I. Bahce, et al., Rapid decrease in delivery of chemotherapy to tumors after anti-VEGF therapy: implications for scheduling of anti-angiogenic drugs. Cancer Cell. 21, 82-91 (2012).
91. R.J.A. Harte, J.C. Matthews, S.M. O'Reilly, et al., Tumor, normal tissue, and plasma pharmacokinetic studies of fluorouracil biomodulation with n-phosphonacetyl-l-aspartate, folinic Acid, and interferon alfa. J Clin Oncol. 17, 1580-1588 (1999).
92. W. Löscher, H. Potschka. Drug resistance in brain diseases and the role of drug efflux transporters. Net Rev Neurosci. 6, 591-602 (2005).
93. V.S. Narang, C. Fraga, N. Kumar, et al., Dexamethasone increases expression and activity of multidrug resistance transporters at the rat blood-brain barrier. Am J Physiol Cell Physiol. 295, C440-450 (2008).
94. M.S. Gordon, K. Margolin, M. Talpaz, et al., Phase I safety and pharmacokinetic study of recombinant human anti-vascular endothelial growth factor in patients with advanced cancer. J Clin Oncol 19,843-818 (2001).
95. B. Leyland-Jones, Dose scheduling: Herceptin. Oncology 61, suppl 2,31-36 (2001).
96. J. Baselga, D. Pfister, M.R. Cooper, et al., Phase I studies of anti-epidermal growth factor receptor chimeric antibody C225 alone and in combination with cisplatin. J Clin Oncol. 18, 904-914 (2000).
97. L.R. Perk, O.J. Visser, M. Stigter-van Walsum, et al., Preparation and evaluation of (89)Zr-Zevalin for monitoring of (90)Y-Zevalin biodistribution with positron emission tomography. Eur J Nucl Med Mol Imaging. 33, 1337-1345 (2006).
98. S.N. Rizvi, O.J. Visser, M.J. Vosjan, et al., Biodistribution, radiation dosimetry and scouting of ^{90}Y-ibritumomab tiuxetan therapy in patients with relapsed B-cell non-Hodgkin's lymphoma using ^{89}Zr-ibritumomab tiuxetan and PET. Eur J Nucl Med Mol Imaging. 39, 512-520 (2012).
99. K. Taniguchi, J. Okami, K. Kodama, et al., Intratumor heterogeneity of epidermal growth factor receptor mutations in lung cancer and its correlation to the response to gefitinib. Cancer Sci. 99, 929-935 (2008).
100. S. Artale, A. Sartore-Bianchi, S.M. Veronese, et al., Mutations of KRAS and BRAF in primary and matched metastatic sites of colorectal cancer. J Clin Oncol. 26, 4217-4219 (2008).
101. G. Curigliano, V. Bagnardi, G. Viale, et al., Should liver metastases of breast cancer be biopsied to improve treatment choice? Ann Oncol. 22, 2227-2233 (2011).
102. R. Boellaard, M.J. O'Doherty, W.A.Weber, et al., FDG PET and PET/CT: EANM procedure guidelines for tumour PET imaging: version 1.0. Eur J Nucl Med Mol Imaging. 37, 181-200 (2010)

103. R.L. Wahl, H. Jacene, Y. Kasamon,et al., From RECIST to PERCIST: Evolving Considerations for PET response criteria in solid tumors. J Nucl Med. 50 Suppl 1, 122S-50S (2009).
104. S.J O'Day, O. Hamid, W.J. Urba. Targeting cytotoxic T-lymphocyte antigen-4 (CTLA-4): a novel strategy for the treatment of melanoma and other malignancies. Cancer. 110, 2614-2627 (2007).
105. D.J. Yang, C. Li, L.R. Kuang, et al. Imaging, biodistribution and therapy potential of halogenated tamoxifen analogues. Life Sci. 55, 53-67 (1994).
106. J.R. Petrulli, J.M. Sullivan, M.Q. Zheng, et al., quantitative Analysis of [(11)C]-erlotinib PET demonstrates specific binding for activating mutations of the EGFR kinase domain. Neoplasia. 15, 1347-1353 (2013)
107. M.R. Zhang, K. Kumata, A. Hatori, et al., [11C]Gefitinib ([11c]Iressa): radiosynthesis, in vitro uptake, and in vivo imaging of intact murine fibrosarcoma. Mol Imaging Biol. 12, 181-191 (2010).
108. K. Kawamura, T. Yamasaki, J Yui, et al., In vivo evaluation of P-glycoprotein and breast cancer resistance protein modulation in the brain using [(11)C]gefitinib. Nucl Med Biol. 36, 239-246 (2009).
109. K.E. Kil, Y.S. Ding, K.S. Lin, et al., Synthesis and positron emission tomography studies of carbon-11-labeled imatinib (Gleevec). Nucl Med Biol. 34, 153-163 (2007).
110. F. Basuli, H. Wu, C. Li, et al., A first synthesis of 18F-radiolabeled lapatinib: a potential tracer for positron emission tomographic imaging of ErbB1/ErbB2 tyrosine kinase activity. J Label Compd Radiopharm. 54, 633-636 (2011).
111. C. Asakawa, M. Ogawa, K. Kumata, et al., [11C]sorafenib: radiosynthesis and preliminary PET study of brain uptake in P-gp/Bcrp knockout mice. Bioorg Med CHem Lett. 21, 2220-2223 (2011).
112. J.Q Wang, K.D. Miller, G.W. Sledge, et al., Synthesis of [18F]SU11248, a new potential PET tracer for imaging cancer tyrosine kinase. Bioorg Med Chem Lett. 15, 4380-4384 (2005).
113. M. Gao, C.M. Lola, M. Wang, et al. Radiosynthesis of [11C]Vandetanib and [11C] chloro-Vandetanib as new potential PET agents for imaging of VEGFR in cancer. Bioorg Med Chem Lett. 21, 3222-3226 (2011).
114. B. Paudyal, P. Paudyal, N. Oriuchi, et al., Positron emission tomography imaging and biodistribution of vascular endothelial growth factor with 64Cu-labeled bevacizumab in colorectal cancer xenografts. Cancer Sci. 102, 117-121 (2011).
115. T.K. Nayak, K. Garmestani, K.E. Baidoo, et al., PET imaging of tumor angiogenesis in mice with VEGF-A-targeted (86)Y-CHX-A"-DTPA-bevacizumab. Int J Cancer. 128, 920-926 (2011).
116. W.B. Nagengast, E.G. de Vries, G.A. Hospers, et al., In vivo VEGF imaging with radiolabeled bevacizumab in a human ovarian tumor xenograft. J Nucl med. 48, 1313-1319 (2007).
117. W. Ping Li, L.A. Meyer, D.A. Capretto, et al., Receptor-binding, biodistribution, and metabolism studies of 64Cu-DOTA-cetuximab, a PET-imaging agent for epidermal growth-factor receptor-positive tumors. Cancer Biother Radiopharm. 23, 158-171 (2008).
118. M. Eiblmaier, L.A. Meyer, M.A. Watson, et al., Correlating EGFR expression with receptor-binding properties and internalization of 64Cu-DOTA-cetuximab in 5 cervical cancer cell lines. J Nucl Med. 49, 1472-1479 (2008).

119. G. Niu, X. Sun, Q. Cao, et al., Cetuximab-based immunotherapy and radioimmunotherapy of head and neck squamous cell carcinoma. Clin Cancer Res. 16, 2095-2105 (2010).
120. A. Achmad, H. Hanaoka, H. Yoshioka, et al., Predicting cetuximab accumulation in KRAS wild-type and KRAS mutant colorectal cancer using 64Cu-labeled cetuximab positron emission tomography. Cancer Sci. 103, 600-605 (2012).
121. T.K. Nayak, C.A. Regino, K.J. Wong, et al., PET imaging of HER1-expressing xenografts in mice with 86Y-CHX-A''-DTPA-cetuximab. Eur J Nucl Med Mol Imaging. 37, 1368-1376 (2010).
122. T.K. Nayak, K. Garmestani, D.E. Milenic, et al., HER1-targeted 86Y-panitumumab possesses superior targeting characteristics than 86Y-cetuximab for PET imaging of human malignant mesothelioma tumors xenografts. PLoS One. 25:101371 (2011).
123. L.R. Perk, G.W. Visser, M.J. Vosjan, et al., (89)Zr as a PET surrogate radioisotope for scouting biodistribution of the therapeutic radiometals (90)Y and (177)Lu in tumor-bearing nude mice after coupling to the internalizing antibody cetuximab. J Nucl Med. 46, 1898-1906 (2005).
124. G. Niu, Z. Li, J. Xie, et al., PET of EGFR antibody distribution in head and neck squamous cell carcinoma models. J Nucl Med. 50, 1116-1123 (2009).
125. T.K. Nayak, K. Garmestani, K.E. Baidoo, et al., Preparation, biological evaluation, and pharmacokinetics of the human anti-HER1 monoclonal antibody panitumumab labeled with 86Y for quantitative PET of carcinoma. J Nucl Med. 51, 942-950 (2010).
126. T.K. Nayak, K. Garmestani, D.E. Milenic, et al., PET and MRI of metastatic peritoneal and pulmonary colorectal cancer in mice with human epidermal growth factor receptor 1-targeted 89Zr-labeled panitumumab. J Nucl Med. 53, 113-120 (2012).
127. A.J. Chang, R.A. De Silva, S.E. Lapi, PET and MRI of metastatic peritoneal and pulmonary colorectal cancer in mice with human epidermal growth factor receptor 1-targeted 89Zr-labeled panitumumab. Mol Imaging. 12, 17-27 (2013).
128. S. Bhattacharyya, K. Kurdziel, L. Wei, et al., Zirconium-89 labeled panitumumab: a potential immuno-PET probe for HER1-expressing carcinomas. Nucl Med Biol. 40, 451-457 (2013).
129. A. Natarajan, G. Gowrishankar, C.H. Nielsen, et al., Positron emission tomography of 64Cu-DOTA-Rituximab in a transgenic mouse model expressing human CD20 for clinical translation to image NHL. Mol Imaging Biol. 14, 608-616 (2012).
130. A. Natarajan, F. Habte, H. Liu, et al., Evaluation of 89Zr-rituximab tracer by Cerenkov luminescence imaging and correlation with PET in a humanized transgenic mouse model to image NHL. Mol Imaging Biol. 15, 468-475 (2013).
131. E. Mume, A. Orlova, P.U. Malmström, et al., Radiobromination of humanized anti-HER2 monoclonal antibody trastuzumab using N-succinimidyl 5-bromo-3-pyridinecarboxylate, a potential label for immunoPET. Nucl Med Biol. 32, 613-622 (2005).
132. E.C. Dijkers, J.G. Kosterink, A.P. Rademaker, et al., Development and characterization of clinical-grade 89Zr-trastuzumab for HER2/neu immunoPET imaging. J Nucl med. 50, 974-981 (2009).
133. A.J. Chang, R. Desilva, S. Jain, et al., 89Zr-radiolabeled trastuzumab imaging in orthotopic and metastatic breast tumors. Pharmaceuticals (Basel). 5, 79-93 (2012).

PART I

Visualizing targets: *hormone receptor imaging*

CHAPTER 2

Androgen and estrogen receptor imaging in metastatic breast cancer patients as a surrogate for tissue biopsies

Clasina M. Venema*, Lemonitsa H. Mammatas*, Carolina P. Schröder, Michel van Kruchten, Giulia Apollonio, Andor W.J.M. Glaudemans, Alfons H.H. Bongaerts, Otto S. Hoekstra, Henk M.W. Verheul, Epie Boven, Bert van der Vegt, Erik F.J. de Vries, Elisabeth G.E. de Vries, Ronald Boellaard, C. Willemien Menke-van der Houven van Oordt and Geke A.P. Hospers

*Co-leading authors

Published in: J Nucl Med. 2017;58:1906-12

ABSTRACT

In addition to the well-known estrogen receptor (ER) and human epidermal growth factor receptor 2, the androgen receptor (AR) is also a potential drug target in breast cancer treatment. Whole-body imaging can provide information across lesions within a patient. ER expression in tumor lesions can be visualized by ^{18}F-fluoroestradiol (^{18}F-FES) PET, and AR expression has been visualized in prostate cancer patients with ^{18}F-fluorodihydrotestosterone (^{18}F-FDHT) PET. Our aim was to assess the concordance between ^{18}F-FDHT and ^{18}F-FES PET and tumor AR and ER expression measured immunohistochemically in patients with metastatic breast cancer. **Methods:** Patients with ER-positive metastatic breast cancer were eligible for the study, irrespective of tumor AR status. The concordance of ^{18}F-FDHT and ^{18}F-FES uptake on PET with immunohistochemical expression of AR and ER in biopsies of corresponding metastases was analyzed. Patients underwent ^{18}F-FDHT PET and ^{18}F-FES PET. A metastasis was biopsied within 8 wk of the PET procedures. Tumor samples with more than 10% and 1% nuclear tumor cell staining were considered, respectively, AR- and ER-positive. Correlations between PET uptake and semiquantitative immunohistochemical scoring (percentage positive cells × intensity) were calculated. The optimum threshold of SUV to discriminate positive and negative lesions for both AR and ER was determined by receiver-operating-characteristic analysis. **Results:** In the 13 evaluable patients, correlation (R^2) between semiquantitative AR expression and ^{18}F-FDHT uptake was 0.47 (P = 0.01) and between semiquantitative ER expression and ^{18}F-FES uptake 0.78 (P = 0.01). The optimal cutoff for AR-positive lesions was an SUV_{max} of 1.94 for ^{18}F-FDHT PET, yielding a sensitivity of 91% and a specificity of 100%; the optimal cutoff was an SUV_{max} of 1.54 for ^{18}F-FES PET, resulting in a sensitivity and specificity of 100% for ER. **Conclusion:** ^{18}F-FDHT and ^{18}F-FES uptake correlate well with AR and ER expression levels in representative biopsies. These results show the potential use of whole-body imaging for receptor status assessment, particularly in view of biopsy-associated sampling errors and heterogeneous receptor expression in breast cancer metastases.

INTRODUCTION

The estrogen receptor (ER) is expressed in 75% of the breast carcinomas, which makes patients with such tumors eligible for ER-targeted therapy (1). Although the ER, human epidermal growth factor receptor 2, and progesterone receptor are routinely determined in breast cancer for prognosis and treatment decision making, this is not the case for the androgen receptor (AR). Nevertheless, several studies have shown that the AR is also present in 70%–80% of the breast carcinomas, which offers a potential new treatment strategy with AR-affecting drugs (2).

Patients with metastatic breast cancer received androgens in the first half of the 20th century, with response rates of 19%–36% (3,4). However, side effects of androgens, including hirsutism and lowering of voice, combined with awareness of the conversion of androgens into estrogens resulted in the discontinuation of androgen therapy in breast cancer patients. With several emerging, less toxic AR-targeted therapies for patients with prostate cancer, and the development of resistance to current breast cancer treatment options, AR-targeted therapies in breast cancer have reentered clinical trials.

A challenge in this era of rapidly emerging drug targets and treatment options is to administer the right drug to the right patient. It is well recognized that only those patients with ER-expressing tumors can benefit from endocrine therapies (1). Because the ER is functionally and structurally highly comparable to the AR, response to AR-targeting drugs may also rely on AR expression in the tumor.

Standard immunohistochemical staining of the primary tumor is inexpensive, easy to apply, and well established in decision making for adjuvant therapies. However, discordant ER expression between the primary breast tumor and metastases has been observed in 18%–40% of the patients (5–8). Molecular imaging offers the possibility to noninvasively determine the presence of relevant drug targets in all metastases within an individual patient. Tumor ER expression can be visualized by ^{18}F-fluoroestradiol (^{18}F-FES) PET in breast cancer patients (9). AR expression in prostate cancer patients has been evaluated using ^{18}F-fluorodihydrotestosterone (^{18}F-FDHT) PET (10,11). If ^{18}F-FDHT PET is also able to determine the AR status in metastatic breast cancer patients, this technique has the potential to select patients eligible for AR-targeted therapies. The aim of the present study was to assess whether uptake on ^{18}F-FES and ^{18}F-FDHT PET correlates with levels of both ER and AR expression on a simultaneous biopsied metastasis.

MATERIALS AND METHODS

Patients

Postmenopausal patients with metastatic breast cancer with previous ER-positive primary tumor were eligible if they had a metastasis outside the liver that was safe to biopsy. Patients were staged with full-body bone scintigraphy (bone scan) and a contrast-enhanced CT scan (chest/abdomen) within 6 wk before the PET examinations. A tumor biopsy was performed within 8 wk of the PET examinations. Exclusion criteria for the study were the use of ER ligands less than 6 wk before entering the study, and a life expectancy of less than 3 mo. Aromatase inhibitors and chemotherapy were allowed. All patients gave written informed consent before study participation, according to the Declaration of Helsinki, and the protocol was approved by the local Ethical Committee (EudraCT no., 2012-003981-42)

Study Design

We performed a prospective, 2-center feasibility trial (NCT01988324). The primary endpoint was the concordance of ^{18}F-FDHT and ^{18}F-FES uptake with, respectively, AR and ER expression in a newly obtained biopsy of a metastasis measured by immunohistochemistry. Secondary endpoints were the optimum threshold to discriminate positive and negative lesions for both AR and ER on PET, inter- and intrapatient ^{18}F-FDHT and ^{18}F-FES heterogeneity, and correlation between tracer uptake and serum hormone levels at the time of scanning. Venous blood was collected before ^{18}F-FES tracer injection to evaluate serum estradiol (luminescence immune assay), luteinizing hormone, follicle-stimulating hormone (both fluorescence immune assay), and sex hormone–binding globulin (chemiluminescence microparticle immune assay). These have been reported to affect tumor ^{18}F-FES uptake in breast cancer studies (12). Before ^{18}F-FDHT injection, blood was collected for serum testosterone and dihydrotestosterone levels (both liquid chromatography-mass spectrometry assay).

Tumor histology

All patients underwent a biopsy of a metastasis, detectable by conventional imaging, within 8 wk of the PET procedures. Biopsies were formalin-fixed and paraffin-embedded. Biopsies were centrally revised by a dedicated breast pathologist. ER (CONFIRM anti-Estrogen Receptor [SP1] Rabbit Monoclonal Primary Antibody; Ventana) and AR (anti-Androgen Receptor [SP107] Rabbit Monoclonal Primary Antibody; Ventana) were stained with a Benchmark automated stainer (Ventana) at the Department of Pathology of the University Medical Center Groningen. Antibodies were prediluted by the supplier. ER was scored according to the guideline of the American Society of Clinical Oncologypathologists (13) and semiquantitatively: the percentage of positive

tumor nuclei was multiplied by the intensity of staining (0, negative; 1, weak; 2, moderate; and 3, strong). This led to a score of 0–300 (14). Because AR is not a routine staining in breast cancer, a threshold of more than 10% positive nuclear staining was used as a discriminator for AR positivity, based on current use in literature (2).

Imaging

CT scans were evaluated by a radiologist. Bone scans were evaluated by 2 nuclear physicians. All tumor lesions visible on CT (>1 cm) and bone scans were documented. Patients underwent ^{18}F-FDHT PET and ^{18}F-FES PET on separate days within 14 d. ^{18}F-FES and ^{18}F-FDHT were produced as described previously (15,16). Patients received approximately 200 MBq of ^{18}F-FDHT and ^{18}F-FES. Whole-body PET/CT was performed 60 min after tracer injection with a Siemens 64-slice mCT (PET/CT) (University Medical Center Groningen) or a Philips Gemini 64 TF PET/CT camera (VU University Medical Center) using the European Association of Nuclear Medicine Research Limited (EARL)–approved protocols (17). Low-dose CT (for attenuation and scatter correction) and PET imaging were performed within 1 procedure. All images were reconstructed according to the specifications of the EARL accreditation program (17).

Tumor ^{18}F-FES uptake was quantified for all lesions seen on CT and bone scans, as well as for nonphysiologic uptake visible above background with an SUV_{max} of greater than 1.5 based on previous studies (18,19). All lesions detected on bone, CT, and ^{18}F-FES PET scans were also quantified on the ^{18}F-FDHT PET scan. In line with previous studies, we used the SUV_{max} to calculate tumor ^{18}F-FDHT and ^{18}F-FES uptake (18,19). We also measured the SUV_{mean} using a 50% isocontour of the hottest pixel to assess the average SUV computed in the volume of interest. The SUV_{peak} was used to calculate uptake in a 1-cm^3 spheric volume of interest surrounding the voxel with the highest activity. Background correction was applied using a volume of interest at the unaffected contralateral site whenever available, or at the surrounding tissue of the same origin and deducted from the SUV of the tumor (i.e., lesion $SUV_{max/mean/peak}$ minus background $SUV_{max/mean/peak}$, resulting in background corrected $SUV_{max/mean/peak}$.

Statistical analysis

^{18}F-FDHT PET/CT and ^{18}F-FES PET/CT findings were compared with immunohistochemical findings for AR and ER expression, respectively. The optimum threshold of SUV to discriminate positive and negative lesions for both AR and ER was determined by receiver-operating-characteristic analysis. Correlations between semiquantitative receptor analysis and SUV were calculated using the Pearson correlation coefficient. A *P* value of 0.05 or less was considered significant.

RESULTS

Patient characteristics

Twenty-one patients were included between September 2014 and August 2015 (Table 1), and 13 were evaluable for the primary study endpoint. Nonevaluable were 5 patients with a nonvital tumor biopsy (24%), and 3 patients (14%) with biopsied lesions not visible on conventional imaging or PET (*n* = 2 skin lesions, *n* = 1 intestinal lesion). All evaluable patients had an ER-positive and AR-positive primary breast cancer based on immunohistochemistry. Three patients (23%) showed conversion between the primary tumor and the metastasis of either ER (8%), AR (8%), or both (8%) measured with immunohistochemistry.

Concordance between SUV and immunohistochemistry of same tumor lesion

Figure 1 shows 2 representative examples of AR immunohistochemical staining results and corresponding ^{18}F-FDHT PET scans. Mean ^{18}F-FDHT SUV_{max} of the biopsies in AR-positive lesions was 3.1 (SD, 0.90) versus a mean ^{18}F-FDHT SUV_{max} in AR-negative lesions of 1.9 (SD, 0.01). Mean ^{18}F-FES SUV_{max} of the biopsied ER-positive lesions was 4.3 (SD, 2.4) versus a mean ^{18}F-FES SUV_{max} in biopsied ER-negative lesions of 1.1 (SD, 0.4). The correlation between semiquantitative AR expression and ^{18}F-FDHT uptake was R^2 = 0.47 (P = 0.01), and between semiquantitative ER expression and ^{18}F-FES uptake it was R^2 = 0.78 (P = 0.01) (Fig. 2). The correction for background uptake did not improve the correlation between semiquantitative AR and ER expression and ^{18}F-FDHT and ^{18}F-FES uptake, because background correction resulted in a correlation of R^2 = 0.39 and 0.78, respectively. The correlations between immunohistochemistry and SUV_{peak}, SUV_{mean}, and background-corrected SUV_{peak} and SUV_{mean} did not differ from the correlations observed between immunohistochemistry and SUV_{max} (Supplemental Table 1; supplemental materials are available at http://jnm.snmjournals.org).

The optimal SUV_{max} cutoff for ^{18}F-FDHT PET was 1.9, leading to a sensitivity of 91% and a specificity of 100% (area under the curve, 0.91; 95% confidence interval, 0.74–1.0). Receiver-operating-characteristic analysis showed an optimal cutoff value for ^{18}F-FES PET to be SUV_{max} 1.5, resulting in a sensitivity and specificity of 100%. The correction of tracer uptake for background or using SUV_{mean} or SUV_{peak} instead of SUV_{max} did not improve the results (Supplemental Table 2).

Table 1. Patient characteristics

Characteristic	*n*	%
Mean age (y)	64	
Sex		
Female	11	85
Male	2	15
Primary tumor characteristics IHC		
ER+/AR+	13	100
ER+/AR−	0	
ER−/AR+	0	
ER−/AR−	0	
Primary tumor stage		
T1N0M0	4	31
T1N1M0	1	8
T2N0M0	4	31
T2N1M0	1	8
T3N2M0	3	23
Metastatic tumor characteristics IHC		
ER+/AR+	10	77
ER+/AR−	1	8
ER−/AR+	1	8
ER−/AR−	1	8
Treatment at time of ^{18}F-FES and ^{18}F-FDHT PET scans		
Aromatase inhibitor	5	38
Chemotherapy	4	31
None	4	31

ER+ = ER-positive; AR+ = AR-positive; ER− = ER-negative; AR− = AR-negative; IHC = immunohistochemistry.

Heterogeneity in uptake

Heterogeneity in lesion uptake was seen between patients and across lesions within individual patients for both ^{18}F-FES and ^{18}F-FDHT uptake. An example of a typical ^{18}F-FDHT and ^{18}F-FES PET is shown in Figure 3. With the cutoff at 1.9 for ^{18}F-FDHT PET, all patients had both ^{18}F-FDHT–positive and ^{18}F-FDHT–negative lesions. SUV_{max} on ^{18}F-FDHT for tumor lesions varied within patients (median, 2.8; range, 0.8–6.5) and between patients (median, 2.7; range, 1.7–3.7). Eleven of 13 patients had visually both ^{18}F-FES–positive and ^{18}F-FES–negative lesions. SUV_{max}

on ^{18}F-FES PET varied widely between lesions (median, 3.2; range, 0.6–12.2) and patients (median, 2.4; range, 1.3–6.0).

Figure 1. Comparison of immunohistochemistry staining of AR between an AR-negative (0% AR staining) lesion (A, top) and AR-positive (100% staining) lesion (B, top). (Bottom) Horizontal ^{18}F-FDHT PET/CT fusion images. (A, bottom) Physiologic uptake in small intestines and kidneys. Arrow indicates biopsied lesion (rib) with no visual enhanced uptake. (B, bottom) Physiologic uptake in small intestines and high uptake throughout pelvic bones. Arrow indicates biopsied lesion in iliac bone with visually enhanced uptake.

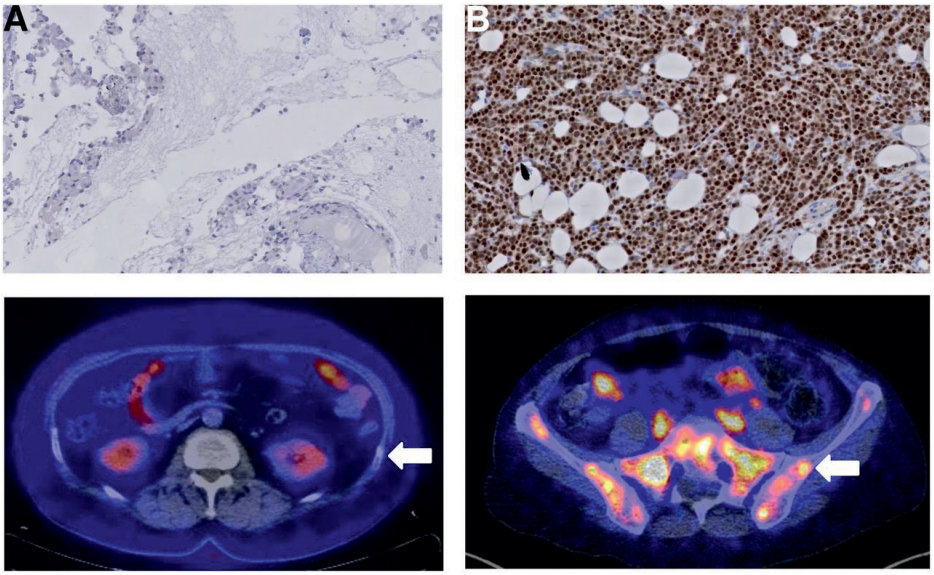

Figure 2. Correlation plot of semiquantitative analysis of receptor status and SUV_{max} as measured by PET scan for AR (left) and ER (right).

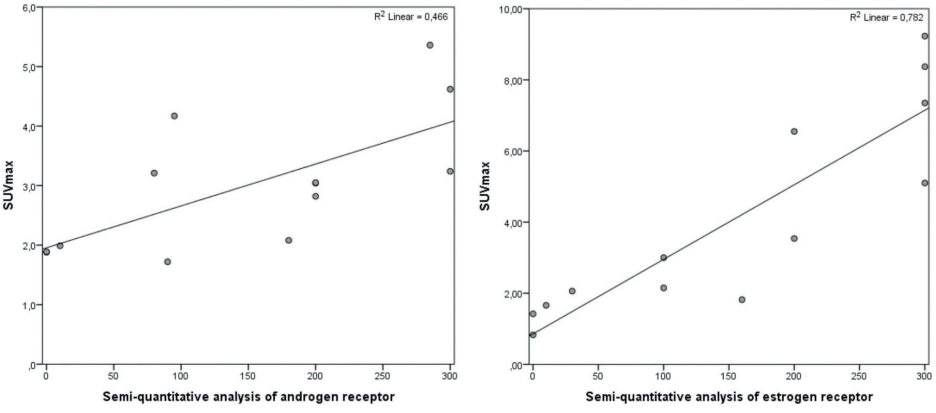

Figure 3. Example of typical ^{18}F-FES (A–C) and ^{18}F-FDHT (D–F) distribution in same patient with multiple bone metastases. (A) Sagittal ^{18}F-FES PET/CT fusion image with physiologic uptake in liver, small intestine, and urinary tract and pathologic uptake in multiple vertebrae. (B) ^{18}F-FES PET maximum-intensity-pixel format to allow visualization of biodistribution of ^{18}F-FES tracer. (C) Horizontal ^{18}F-FES PET/CT fusion image with physiologic uptake in small intestine and pathologic uptake throughout pelvic bones. (D) Maximum-intensity-pixel format of ^{18}F-FDHT PET scan, with physiologic uptake in blood pool of heart and liver and excretion via bile to small intestine, and urinary tract. (E) Sagittal ^{18}F-FDHT PET/CT fusion image with physiologic uptake and pathologic uptake in multiple vertebrae. (F) Horizontal ^{18}F-FES PET/CT fusion image with physiologic uptake in large vessels and small intestines and pathologic uptake throughout pelvic bones.

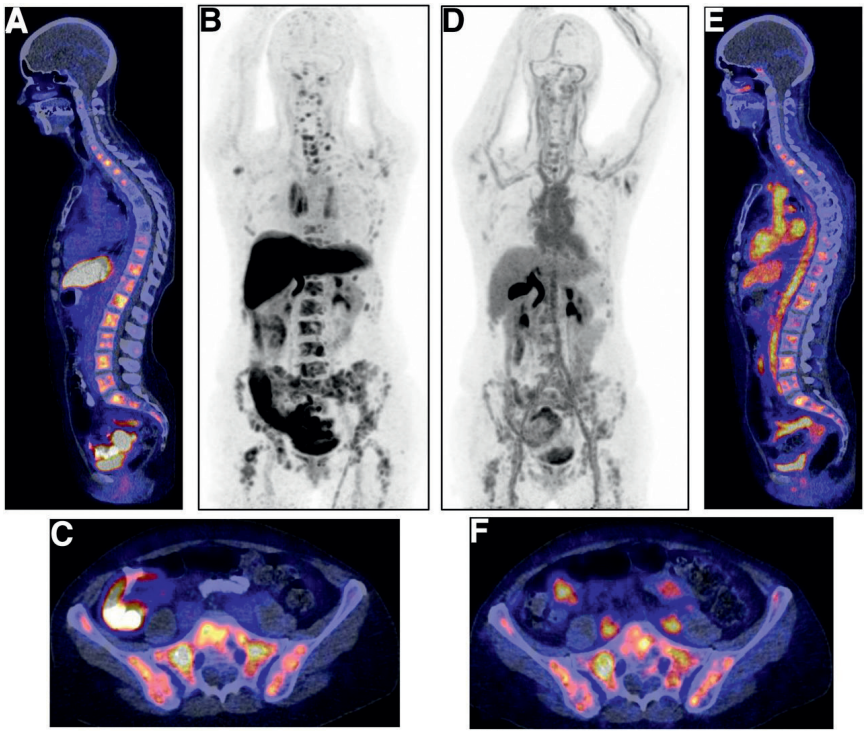

A total of 298 lesions were detected with CT scans (*n* = 95), bone scans (*n* = 126), or ^{18}F-FES PET scans (*n* = 239). Most lesions (81%) showed uptake above background on ^{18}F-FES PET. CT or bone scan identified 59 lesions that showed no ^{18}F-FES uptake above background. ^{18}F-FES PET identified 48 lesions not visible on conventional imaging. In total, 278 lesions could be used for ^{18}F-FES PET analysis. Because of the high physiologic background uptake near the lesion such as in the liver and intestines, 20 lesions could not be reliably quantified. Most of the lesions were in the bone (*n* = 219); 34 lesions were in the lymph nodes, and 25 were visceral lesions (Fig. 4).

Figure 4. Distribution of SUV_{max} per lesion per patient measured by ^{18}F-FES PET. Lesions are divided into bone (blue), lymph nodes (red), lung (green), and others (purple). Orange circles are biopsied lesions. Blue boxes indicate ER-positive biopsies (>1% staining); numbers indicate score of biopsy (i.e., intensity times percentage positive cells). Dashed line indicates threshold set based on receiver-operating-characteristic analysis. White boxes indicate negative biopsies (<1% staining).

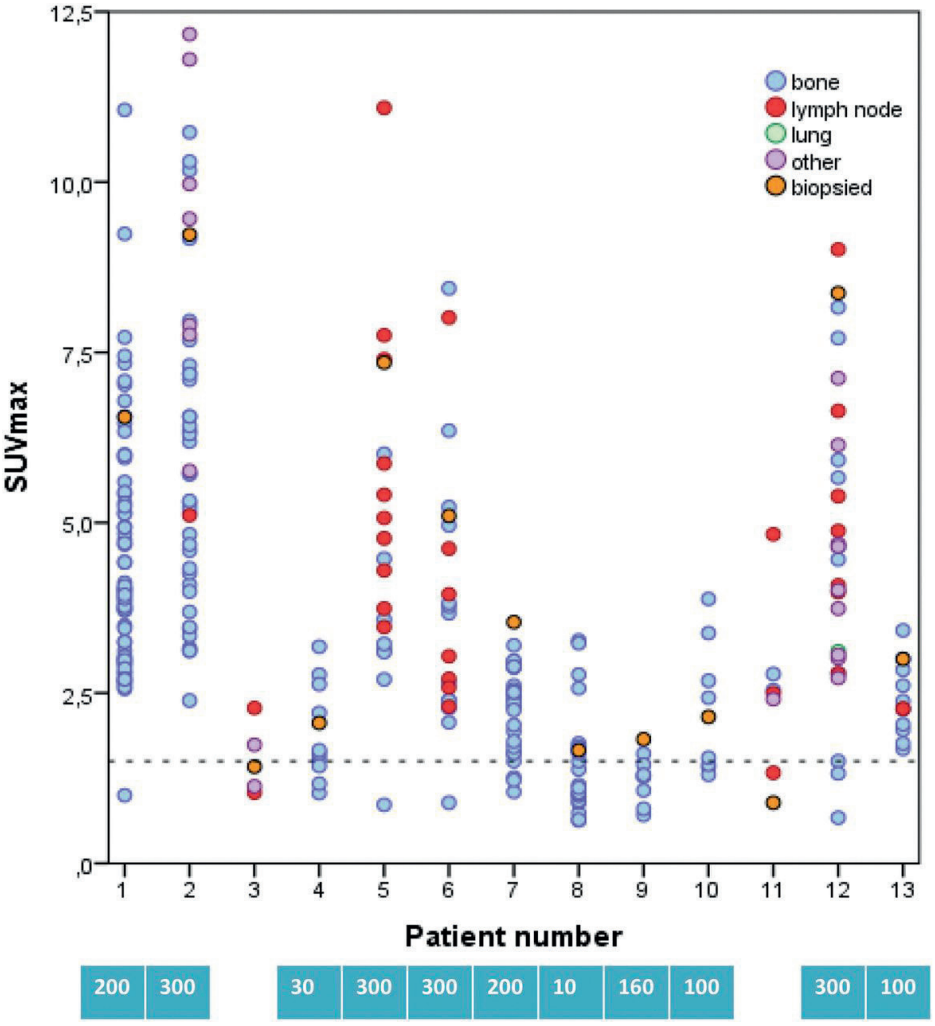

On ^{18}F-FDHT PET scans, 196 lesions (66%) were visible above background, of which 42 lesions could not be reliably quantified because of high physiologic background uptake near the lesion (e.g., the liver, blood vessels, and intestines). One hundred two lesions were not visible above background but were visible on either CT scan, bone scan, or ^{18}F-FES PET scan. In total, 256 lesions were

included for ^{18}F-FDHT PET analysis. Most of the lesions were bone lesions (n = 222), 14 lesions were lymph nodes, and the remaining 20 lesions were visceral lesions (Fig. 5).

Figure 5. Distribution of SUV_{max} per lesion per patient measured by ^{18}F-FDHT PET. Lesions are divided into bone (blue), lymph nodes (red), lung (green), and others (purple). Orange circles are biopsied lesions. Orange boxes indicate AR-positive biopsies (i.e., >10% staining); white boxes indicate negative biopsies. Numbers in boxes indicate score of biopsy (i.e., intensity times percentage positive cells). Dashed line indicates threshold set based on receiver-operating-characteristic analysis.

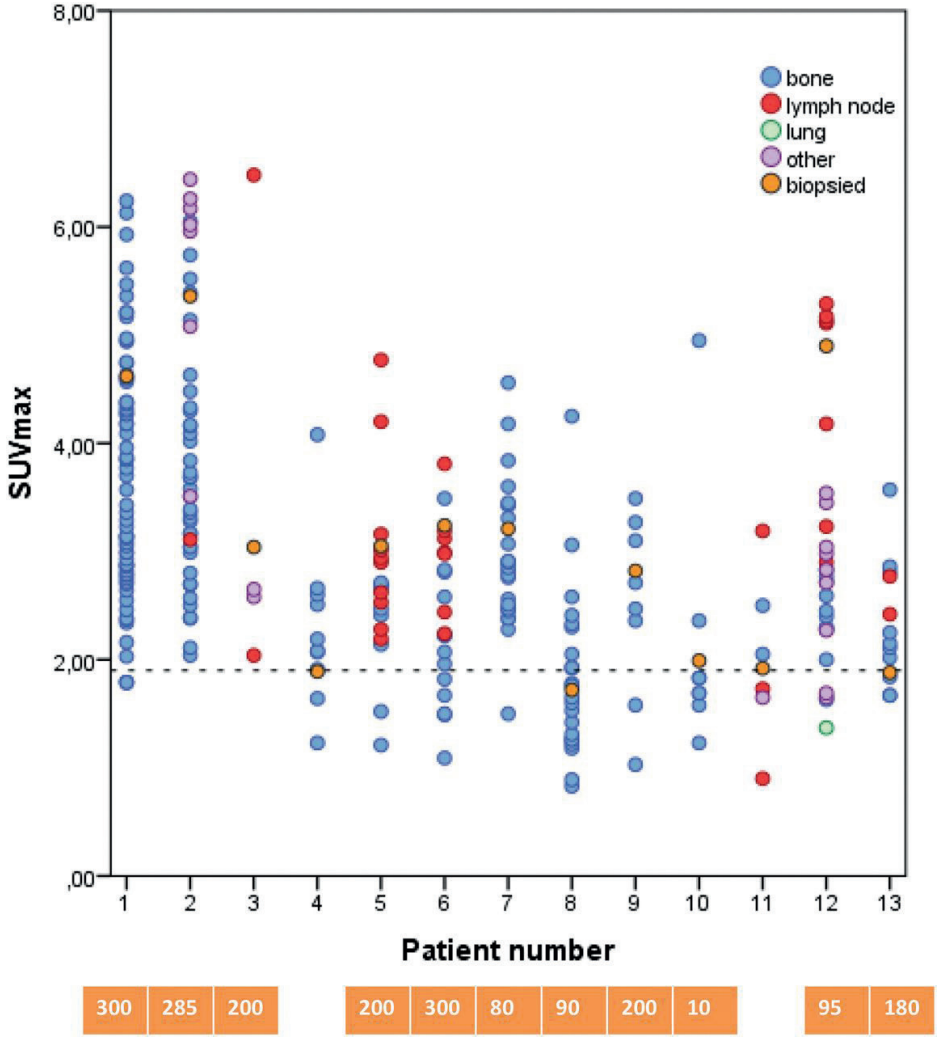

Uptake in healthy liver tissue was high on both ^{18}F-FDHT PET and ^{18}F-FES PET scans, rendering analysis of liver metastases impossible. The mean liver uptake on ^{18}F-FDHT SUV_{mean} was 4.4 (range, 3.6–5.8) versus the mean liver uptake on ^{18}F-FES SUV_{mean} of 12.8 (range, 8.2–19.6). Several lesions were nonquantifiable due to high blood-pool accumulation on the ^{18}F-FDHT PET. The blood-pool accumulation measured in the descending thoracic artery was higher on ^{18}F-FDHT PET than ^{18}F-FES PET: SUV_{mean} of 4.6 (range, 3.8–6.2) versus SUV_{mean} of 1.3 (range, 0.9–2.1), respectively.

Correlation between PET uptake and serum hormone levels and sex hormone–binding globulin

^{18}F-FDHT tumor uptake did not correlate with serum sex hormone–binding globulin, DHT, or testosterone levels (Supplemental Tables 3–5). Serum estradiol levels correlated positively with^{18}F-FES tumor uptake (R^2 = 0.52; P = 0.01). ^{18}F-FES tumor uptake did not correlate with sex hormone–binding globulin, luteinizing hormone, or follicle-stimulating hormone serum levels.

DISCUSSION

This is the first study in which the ^{18}F-FDHT uptake is evaluated in breast cancer patents and in which ^{18}F-FDHT tracer uptake was correlated with semiquantitative AR analysis in a biopsy of the corresponding metastasis. ^{18}F-FDHT uptake shows a moderate correlation with AR expression, and ^{18}F-FES uptake shows a strong correlation with ER expression.

In this study, we showed that ^{18}F-FDHT can identify AR-positive metastases in breast cancer patients. ^{18}F-FDHT PET may therefore be an interesting tool to select patients eligible for clinical trials with AR antagonists and to analyze the receptor occupancy of these drugs. AR-targeted therapy is not yet standard in breast cancer patients, but preliminary results of phase II trials are promising, with stable disease in 35% of metastatic breast cancer patients (20,21). More clinical studies exploring the efficacy of AR-targeted therapy in AR-positive metastatic breast cancer are currently ongoing (e.g., NCT00468715, NCT00755885). Even combined AR- and ER-targeted therapies are currently under way (NCT02910050, NCT02953860).

To date ^{18}F-FDHT PET has been used only in trials with metastatic prostate cancer patients. A comparison of 59 metastatic prostate cancer lesions visible on conventional imaging showed that 97% were also visible on the ^{18}F-FDHT PET (10). Here, conventional imaging also included ^{18}F-FDG PET. In our study, we found that 66% of the lesions visible on conventional imaging were visible on ^{18}F-FDHT PET.

With serial ^{18}F-FES PET scans in patients treated with ER modulators such as fulvestrant, we were able to visualize residual ER availability during therapy, which was associated with early progression (22). For other ER modulators such as GDC0810 and Z-endoxifen, ^{18}F-FES PET provided information about ER occupancy and guided dose selection for phase II trials (23,24). ^{18}F-FDHT uptake in tumor lesions of patients with prostate cancer diminished in 3 patients after treatment with a high dose of testosterone. Treatment with the AR blocker enzalutamide also resulted in a reduced uptake on ^{18}F-FDHT PET in prostate cancer patients (10). We are currently investigating the effect of the AR blocker bicalutamide on residual AR availability assessed by ^{18}F-FDHT PET in patients with metastatic breast cancer. Secondary endpoints are the relation between percentage decreased uptake on ^{18}F-FDHT PET and response to treatment measured by RECIST in the case of measurable disease (NCT02697032).

This study enforces the earlier observed correlation between ^{18}F-FES uptake and ER expression. Correlations between the ^{18}F-FES PET uptake parameters and immunohistochemistry on the metastatic biopsy using an SUV_{max} of greater than 1.5 showed a 100% sensitivity and specificity similar to previously published results (9,18,19). The parameters SUV_{max}, SUV_{mean}, and SUV_{peak} did not differ, and correction for background did not influence the correlation. Therefore, for ^{18}F-FES PET analysis in the diagnostic setting SUV_{max} can be used, and correction for background is not required. The correlation between uptake on ^{18}F-FDHT PET scans and immunohistochemical staining was lower than on ^{18}F-FES PET and immunohistochemical staining. The kinetic properties and metabolism of ^{18}F-FES and ^{18}F-FDHT are similar (25,26). But ^{18}F-FDHT has a lower relative binding affinity of 0.43 for AR than FES, which has a binding affinity of 0.83 for ER (21). Furthermore, SUV might not be the best quantification method for ^{18}F-FDHT uptake. In a small study with 4 metastatic prostate cancer patients, SUV corrected for plasma ^{18}F-FDHT concentration showed a better correlation (27).

We analyzed factors that potentially could influence tracer uptake such as circulating hormone levels. We found only estradiol levels to be correlated with higher uptake on ^{18}F-FES PET scans, which might be related to higher ER expressions in tumor lesions in postmenopausal patients with higher residual estradiol levels. In fact, we found a correlation of R^2 of 0.42 (P = 0.02) between serum estradiol levels and ER expression determined by immunohistochemical staining on a metastasis biopsy. There was no correlation between other serum hormone levels and ^{18}F-FES or ^{18}F-FDHT tumor uptake. These data indicate that physiologic circulating hormone levels are too low to directly affect tracer uptake in the tumor. Tracer uptake can be influenced by volume, that is, partial-volume effect, where smaller tumor sizes result in an underestimation of uptake

(28). However, in our study there was no correlation found between the volumes of interest of the lesions and ^{18}F-FES or ^{18}F-FDHT uptake.

Because of the feasibility setting of this study, only a limited number of patients were evaluable for primary endpoint. Therefore, larger studies should confirm the optimal cutoff value for ^{18}F-FDHT PET. In our study, 5 of the 21 entered patients did not have vital tumor tissue in their metastatic biopsies. CT may have also shown bone lesions that were no longer active, as patients were heavily pretreated. This might have resulted in an overestimation of ^{18}F-FES– and ^{18}F-FDHT–negative sites. Others have used ^{18}F-FDG PET to visualize hormone receptor–negative lesions. We refrained from doing so, because ^{18}F-FDG PET can also be negative in hormone receptor–positive breast cancer lesions (29). PET imaging of hormone receptors also has some restrictions. Liver lesions are nonevaluable by ^{18}F-FES and ^{18}F-FDHT PET because of high uptake of both tracers in the liver. In addition, ^{18}F-FDHT PET has the disadvantage of high accumulation in the blood pool, rendering it difficult to analyze lesions near large veins. This has also been described in a ^{18}F-FDHT PET study in prostate cancer patients (9). If the ^{18}F-FDHT PET would be used as a diagnostic tool, this would be complementary to the current conventional imaging.

CONCLUSION

In our heavily pretreated patient population, hormone receptor conversion in the metastasis, when compared with the primary tumor, occurred in 23% of the patients. This is similar to previously reported conversion rates (7,8). Heterogeneous uptake in tumor lesions on both ^{18}F-FES and ^{18}F-FDHT PET was seen in most patients, suggesting that both receptor-positive and -negative lesions are present in 1 patient. Current guidelines advise on a biopsy being performed when metastatic disease presents. This may not always be feasible. However, when omitted, changes in receptor status over time might lead to suboptimal therapy choices. ^{18}F-FDHT and ^{18}F-FES PET have the potential to serve as a surrogate for metastasis biopsy, especially when lesions are difficult to access or sampling errors are prone to occur.

DISCLOSURE

This work was supported by CTMM-MAMMOTH WP5, the Alpe d'HuZes/Dutch Cancer Society (RUG 2013-5960), the Ubbo Emmius Fund grant (510215), the van der Meer-Boerema Foundation, and the Anna Dorothea Hingst Foundation. No other potential conflict of interest relevant to this article was reported.

REFERENCES

1. Blamey RW, Hornmark-Stenstam B, Ball G, et al. ONCOPOOL: a European database for 16,944 cases of breast cancer. Eur J Cancer. 2010;46:56-71.
2. Collins LC, Cole KS, Marotti JD, Hu R, Schnitt SJ, Tamimi RM. Androgen receptor expression in breast cancer in relation to molecular phenotype: results from the Nurses' Health Study. Mod Pathol. 2011;24:924-931.
3. Adair FE, Herrmann JB. The use of testosterone propionate in the treatment of advanced carcinoma of the breast. Ann Surg. 1946;123:1023-1035.
4. Olson KB. Fluoxymesterone (halotestin) in the treatment of advanced breast cancer. N Y State J Med. 1959;59:248-252.
5. Layfield LJ, Saria E, Mooney EE, Liu K, Dodge RR. Tissue heterogeneity of immunohistochemically detected estrogen receptor: implications for image analysis quantification. Am J Clin Pathol. 1998;110:758-764.
6. Chung GG, Zerkowski MP, Ghosh S, Camp RL, Rimm DL. Quantitative analysis of estrogen receptor heterogeneity in breast cancer. Lab Invest. 2007;87:662-669.
7. Simmons C, Miller N, Geddie W, et al. Does confirmatory tumor biopsy alter the management of breast cancer patients with distant metastases. Ann Oncol. 2009;20:1499-1504.
8. Amir E, Miller N, Geddie W, et al. Prospective study evaluating the impact of tissue confirmation of metastatic disease in patients with breast cancer. J Clin Oncol. 2012;30:587-592.
9. Linden HM, Stekhova SA, Link JM, et al. Quantitative fluoroestradiol positron emission tomography imaging predicts response to endocrine treatment in breast cancer. J Clin Oncol. 2006;24:2793-2799.
10. Larson SM, Morris M, Gunther I, et al. Tumor localization of 16b-18F-fluoro-5adihydrotestosterone versus 18F-FDG in patients with progressive, metastatic prostate cancer. J Nucl Med. 2004;45:366-373.
11. Scher HI, Beer TM, Higano CS, et al. Antitumour activity of MDV3100 in castration-resistant prostate cancer: a phase 1-2 study. Lancet. 2010;375:1437-1446.
12. Peterson LM, Kurland BF, Link JM, et al. Factors influencing the uptake of 18F-fluoroestradiol in patients with estrogen receptor positive breast cancer. Nucl Med Biol. 2011;38:969-978.
13. Hammond MEH, Hayes DF, Dowsett M, et al. American Society of Clinical Oncology/College of American Pathologists guideline recommendations for immunohistochemical testing of estrogen and progesterone receptor in breast cancer. J Clin Oncol. 2010;28:2784-2795.
14. McCarty KS Jr, Miller LS, Cox EB, Konrath J, McCarty KS Sr. Estrogen receptor analyses. Correlation of biochemical and immunohistochemical methods using monoclonal antireceptor antibodies. Arch Pathol Lab Med. 1985;109:716-721.
15. Liu A, Dence CS, Welch MJ, Katzenellenbogen JA. Fluorine-18-labeled androgens: radiochemical synthesis and tissue distribution studies on six fluorinesubstituted androgens, potential imaging agent for prostatic cancer. J Nucl Med. 1992;33:724-734.
16. Römer J, Steinbach J, Kasch H. Studies on the synthesis of 16a [18 F] fluoroestradiol. Appl Radiat Isot. 1996;47:395-399.

17. Boellaard R, Delgado-Bolton R, Oyen WJ, et al. FDG PET/CT: EANM procedure guidelines for tumour imaging: version 2.0. Eur J Nucl Med Mol Imaging. 2015;42:328–354.
18. Venema CM, Apollonio G, Hospers GA, et al. Recommendations and technical aspects of 16a-[18F] fluoro-17b estradiol PET to image the estrogen receptor in vivo: the Groningen experience. Clin Nucl Med. 2016;41:844–851.
19. van Kruchten M, de Vries EG, Brown M, et al. PET imaging of oestrogen receptors in patients with breast cancer. Lancet Oncol. 2013;14:e465–e475.
20. Overmoyer B, Sanz-Altamira P, Taylor RP, et al. Enobosarm: a targeted therapy for metastatic, androgen receptor positive, breast cancer [abstract]. J Clin Oncol. 2014;32:5S.
21. Traina TA, O'Shaughnessy J, Kelly CM, et al. A phase 2 single-arm study of the clinical activity and safety of enzalutamide in patinets with advanced androgen-receptor-positive triple-negative breast cancer [abstract]. J Clin Oncol. 2014;32:5S.
22. van Kruchten M, de Vries EG, Glaudemans AW, et al. Measuring residual estrogen receptor availability during fulvestrant therapy in patients with metastatic breast cancer. Cancer Discov. 2015;5:72–81.
23. Lin FI, Gonzales EM, Kummar S, et al. Utility of 18F-fluoroestradiol (18F-FES) PET/CT imaging as a pharmacodynamic marker in patients with refractory estrogen receptor-positive solid tumors receiving Z-endoxifen therapy. Eur J Nucl Med Mol Imaging. 2017;44:500–508.
24. Wang Y, Ayres K, Goldman DA, et al. 18F-fluoroestradiol PET/CT measurement of estrogen receptor suppression during a phase I trial of the novel estrogen receptor targeted therapeutic GDC-0810. Clin Cancer Res. 2017;23:3053–3060.
25. Beattie BJ, Smith-Jones PM, Jhanwar YS, et al. Pharmacokinetic assessment of the uptake of 16a-18F-fluoro-5a-dihidrotestosterone in prostate tumors as measured by PET. J Nucl Med. 2010;51:183–192.
26. Kumar P, Mercer J, Doerkson C, Tonkin K, McEwan AJ. clinical production, stability studies and PET imaging with 16a-[18F]fluoroestradiol ([18F]FES) in ER positive breast cancer patients. J Pharm Pharm Sci. 2007;10:256s.
27. Kramer G, Yaqub M, Schuit R, et al. Assessment of simplified methods for quantification of 18F-FDHT uptake in patients with metastasized castrate resistant prostate cancer [abstract]. J Nucl Med. 2016;57(suppl 2):464.
28. Soret M, Bacharach SL, Buvat I. Partial volume effect in PET tumor imaging. J Nucl Med. 2007;48:932–945.
29. Groheux D, Majdoub M, Tixier F, et al. Do clinical, histological or immunohistochemical primary tumour characteristics translate into different 18F-FDG PET/CT volumetric and heterogeneity features in stage II/III breast cancer? Eur J Nucl Med Mol Imaging. 2015;42:1682–1691.

CHAPTER 3

Visual and quantitative evaluation of [^{18}F]FES and [^{18}F]FDHT PET in patients with metastatic breast cancer: *an interobserver variability study*

Lemonitsa H. Mammatas*, Clasina M. Venema*, Carolina P. Schröder, Henrica C.W. de Vet, Michel van Kruchten, Andor W.J.M. Glaudemans, Maqsood M. Yaqub, Henk M.W. Verheul, Epie Boven, Bert van der Vegt, Erik F.J. de Vries, Elisabeth G.E. de Vries, Otto S. Hoekstra, Geke A.P. Hospers, C. Willemien Menke-van der Houven van Oordt

*Co-leading authors

Published in: EJNMMI Res. 2020;19:40

ABSTRACT

Purpose: Correct identification of tumour receptor status is important for treatment decisions in breast cancer. [^{18}F]FES PET and [^{18}F]FDHT PET allow non-invasive assessment of the oestrogen (ER) and androgen receptor (AR) status of individual lesions within a patient. Despite standardized analysis techniques interobserver variability can significantly affect the interpretation of PET results and thus clinical applicability. The purpose of this study was to determine visual and quantitative interobserver variability of [^{18}F]FES PET and [^{18}F]FDHT PET interpretation in patients with metastatic breast cancer.

Methods: In this prospective, two-centre study, patients with ER-positive metastatic breast cancer underwent both [^{18}F]FES and [^{18}F]FDHT PET/CT. In total, 120 lesions were identified in 10 patients with either conventional imaging (bone scan or lesions > 1 cm on high-resolution CT, n = 69) or only with [^{18}F]FES and [^{18}F]FDHT PET (n = 51). All lesions were scored visually and quantitatively by two independent observers. Visually PET-positive lesions were defined as uptake above background. For quantification, we used standardised uptake values (SUV): SUV_{max}, SUV_{peak} and SUV_{mean}.

Results: Visual analysis showed an absolute positive and negative interobserver agreement for [^{18}F]FES PET of 84% and 83%, respectively (kappa = 0.67, 95% CI 0.48-0.87), and 49% and 74% for [^{18}F]FDHT PET, respectively (kappa = 0.23, 95% CI -0.04-0.49). Intraclass correlation coefficients (ICC) for quantification of SUV_{max}, SUV_{peak} and SUV_{mean} were 0.98 (95% CI 0.96-0.98), 0.97 (95% CI 0.96-0.98) and 0.89 (95% CI 0.83-0.92) for [^{18}F]FES, and 0.78 (95% CI 0.66-0.85), 0.76 (95% CI 0.63-0.84) and 0.75 (95% CI 0.62-0.84) for [^{18}F]FDHT, respectively.

Conclusion: Visual and quantitative evaluation of [^{18}F]FES PET showed high interobserver agreement. These results support the use of [^{18}F]FES PET in clinical practice. In contrast, visual agreement for [^{18}F]FDHT PET was relatively low due to low tumour to background ratios, but quantitative agreement was good. This underscores the relevance of quantitative analysis of [^{18}F]FDHT PET in breast cancer.

INTRODUCTION

Breast cancer is the most common malignancy in women in the Western World. The majority of breast tumours express the oestrogen receptor (ER), which is the main indicator of potential response to anti-oestrogen therapies [1, 2]. Therefore, it is mandatory to determine ER expression in breast cancer. Recently, the androgen receptor (AR) emerged as a possible target for breast cancer therapy. The AR is present in 70-80% of patients with breast cancer and AR antagonists are under investigation in clinical trials [3-6].

A tumour biopsy is the gold standard to determine receptor expression. However, this is an invasive procedure, is not always feasible in case of inaccessible tumour sites, and is subject to sampling errors [7]. The 16α-[18F]fluoro-17β-oestradiol ([18F]FES) and 16β-[18F]fluoro-5α-dihydrotestosterone ([18F]FDHT) PET/CT have been developed to non-invasively visualise, respectively, the ER and AR status in the tumour lesions within a patient. Previously, it has been shown that [18F]FES and [18F]FDHT uptake correlate well with ER and AR expression levels in representative breast cancer biopsies [8-10]. As a diagnostic tool, [18F]FES PET leads to better diagnostic understanding in 88% and to a change of therapy in 48% of the patients presenting with a clinical dilemma [11]. To predict treatment effects, [18F]FES PET can be used to assess residual ER availability during treatment with e.g. fulvestrant, a selective ER down regulator. Inadequate reduction of the [18F]FES PET signal (< 75%) by fulvestrant treatment was associated with early progression [12]. Similarly, in patients with prostate cancer, [18F]FDHT PET was used to determine the optimal dose of the AR blocker enzalutamide in a phase 1 trial [13]. Lastly, patients with ER-positive breast cancer and high [18F]FDG uptake showed a worse progression free survival if [18F]FES uptake was low in comparison to high [18F]FES uptake (3 versus 8 months, respectively) [14].

For all these potential applications, reliable, observer-independent identification and quantification of [18F]FES and [18F]FDHT uptake in tumour lesions is essential for translation to daily clinical practice. Up till now, there are no data on the interobserver variability of [18F]FES and [18F]FDHT PET in breast cancer. Therefore, the primary objective of this study was to examine interobserver variability in visual and quantitative assessment of [18F]FES and [18F]FDHT PET. Secondary objectives included the effect of tumour to background ratio (TBR), tracer accumulation, tumour size and the use of different SUV parameters ($SUV_{max,}$ SUV_{peak} or SUV_{mean}) on interobserver agreement. Also, the added value of quantitative assessment in comparison to visual assessment was examined and the number of lesions detected on [18F]FES and [18F]FDHT were compared

with those detected on conventional imaging methods (contrast enhanced CT scan and bone scan).

MATERIALS AND METHODS

Patient population

This prospective two-centre interobserver variability study was part of a study investigating the correlation between [^{18}F]FES and [^{18}F]FDHT uptake and ER- and AR-expression in simultaneously biopsied metastases, of which the results have been published elsewhere [8]. Patients were recruited from September 2014 to August 2015 at the CCA-VUmc University Medical Center Amsterdam and the University Medical Center Groningen in the Netherlands.

Eligibility criteria included metastatic breast cancer and an ER-positive primary tumour, ≥ 1 extrahepatic tumour lesion, ECOG performance status of ≤ 2 and a postmenopausal status or use of LHRH-agonists. Patients were excluded if they had used ER- or AR-binding drugs during the 6 weeks before study entry, because these ligands compete with tracer binding.

All patients had to give written informed consent before study participation. The study was conducted in compliance with the ethical principles originating in or derived from the Declaration of Helsinki and in compliance with all International Conference on Harmonization Good Clinical Practice guidelines. The local medical ethics committee approved the study (NCT01988324).

Imaging protocols

[^{18}F]FES and [^{18}F]FDHT were produced as described previously [15, 16]. On separate days ≤ 14 days apart, 200 MBq (± 10%) of each tracer was injected. After 60 minutes (± 5 minutes) a low-dose CT was performed during tidal breathing for attenuation correction, followed by a whole-body PET scan (skull vertex to mid-thigh, 2 minutes per bed position). PET/CT scans were made using a Philips Gemini TF-64 PET/CT (Amsterdam) or Siemens 64 slice mCT PET/CT (Groningen). Acquisition and reconstruction protocols used on both scanners were according to the recommendations of the European Association of Nuclear Medicine (EARL) [17].

In addition, a high-resolution, contrast-enhanced CT chest-abdomen and bone scan were performed within 6 weeks of the PET scans for comparison.

Image analyses

Contrast enhanced CT scans were examined by experienced radiologists and bone scans by experienced nuclear medicine physicians, respectively, masked

for the [18F]FES and [18F]FDHT PET results. Two independent observers from each centre (LM and CV) trained and supervised by two experienced nuclear medicine physicians, performed visual and quantitative analyses. The observers had knowledge of conventional imaging results (contrast enhanced CT and bone scans).

A visually PET-positive lesion was defined as focal uptake above local background incompatible with physiological uptake. Liver metastases were excluded from all analyses in this study because of high physiological [18F]FES and [18F]FDHT uptake in healthy liver tissue, making reliable identification of metastases difficult. In addition, if visual interpretation of uptake in a (potential) lesion was impossible, e.g. due to overlap with adjacent organs with high physiological tracer, the readers independently reported it as 'not evaluable' in the visual ratings and these were excluded from further analyses. For each patient the observers made a list that consisted of all lesions already detected on conventional imaging, followed by additional lesions discovered on [18F]FES or [18F]FDHT PET. An anatomical description of all the lesions was reported in order to match the results. In case a lesions was not reported by one of the two observers it was scored as not visible for that observer. All visually PET-positive lesions were quantified, as well as PET-negative lesions that were identified on conventional imaging (i.e. lesions on bone scintigraphy and/or high resolution CT > 1 cm).

Each observer manually drew volumes of interest (VOI) on the tumour contours, using PET images for PET-positive lesions and low dose CT images for PET-negative lesions (lesions only seen on bone scan or high resolution CT were visually matched on the low dose CT). Lesions were separately analysed based on visibility on either PET or conventional imaging alone to investigate the influence of visibility on imaging techniques on interobserver agreement.

For every VOI the standardised uptake values (SUV), i.e. the tracer uptake within a VOI normalised to the injected dose and body weight, were calculated using the software programs accurate (in-house build using IDL, observer 1) and syngo.via version VB10B, Siemens (observer 2). Both programs yielded identical results on test images. Three types of SUV were compared in this study: SUV_{max} (voxel with highest SUV within the VOI), SUV_{peak} (average SUV of a 1 cm^3 sphere containing the hottest voxels of the VOI) and SUV_{mean} with isocontour 50% of SUV_{max} (average SUV of all voxels with uptake ≥ 50% of SUV_{max}).

Based on previous studies an SUV_{max} [18F]FES cut-off ≥ 1.5 was used to define ER-positivity (corresponding with a IHC cut-off of ≥ 1%) and an SUV_{max} [18F]FDHT cut-off ≥ 1.9 for AR-positivity (corresponding with a IHC cut-off of ≥ 10%) [8, 9].

For [^{18}F]FES and [^{18}F]FDHT, the SUV_{max} tumour-background ratio (TBR) was defined as the ratio of the SUV_{max} of a tumour lesion and the SUV_{mean} of healthy background tissue. To determine the SUV_{mean} of healthy background tissue a VOI was drawn on reference tissue in the unaffected contralateral site whenever available or in the unaffected surrounding tissue of the same origin [18].

Statistical analyses

For visual assessments, agreement was calculated with absolute and relative measures of interobserver agreement. Absolute agreement is the probability that if one observer would score a lesion as visible (positive agreement) or not visible (negative agreement) on the PET scan, the other observer would do the same. It is calculated by the following formulas: positive agreement = 2 x lesions visible to both observers/(2 x lesions visible to both observers + lesions only visible to observer 1 + lesions only visible to observer 2) and negative agreement = 2 x lesions not visible to both observers/ (2x lesions not visible to both observers + lesions only not visible to observer 1 + lesions only not visible to observer 2) [19]. In order to compare results with previous studies, also reliability (relative agreement) was calculated according to Cohen's kappa and results were interpreted as follows: kappa 0.01-0.20 as slight, 0.21-0.40 as fair, 0.41-0.60 as moderate, 0.61-0.80 as substantial and 0.81-1.00 as almost perfect interobserver agreement [20]. To account for potential within-person correlation in visual assessments, a Chi square test was performed to examine whether the percentage visual agreement differed per patient.

For quantitative assessments, parameters are presented as mean ± SD, and reliability was calculated with intraclass correlation coefficients (ICC) using a two-way random effect model with absolute agreement. For the interpretation of the ICCs, the following guideline was used: ≥ 0.90 as excellent, ≥ 0.75 as good, ≥ 0.50 as moderate and < 0.50 as poor [21].

Absolute agreement on quantitative assessments were analysed with Bland-Altman plots (differences between observers showed a normal distribution). For each lesion it graphically shows the average SUV of observers 1 and 2 on the x-axes and on the y-axes the difference between observers for each lesion, expressed as percentage of the average SUV value. Percentage differences were used instead of absolute differences to achieve independence of magnitude of differences from magnitude of SUV values and it facilitates comparisons between the SUV parameters SUV_{max}, SUV_{mean} and SUV_{peak}, which may show large differences in absolute values.

To investigate the effect of TBRs on interobserver variability, differences between TBRs of [^{18}F]FES and [^{18}F]FDHT PETs were tested with Wilcoxon

matched pairs signed rank tests. In addition, correlations between tracer uptake or tumour size and percentage interobserver differences were determined using the Spearman correlation coefficient (r). Finally, linear regression was performed to find the linear function between SUV_{max}, SUV_{peak} and SUV_{mean} for [18F]FES and [18F]FDHT PET and Cochran's Q and McNemar tests were used to analyse differences between visibility and quantitative uptake above or below cut-off for SUV_{max}, SUV_{peak} and SUV_{mean}. P value < 0.05 was considered significant. Statistical analyses were generated using SPSS software (version 22; IBM, SPSS statistics).

RESULTS

Patient Characteristics

A total of 120 lesions were identified in 10 patients using the different imaging modalities (Table 1). Most lesions were skeletal (66%), followed by lymph node (25%) and visceral metastases (9%). The median number of lesions per patient was 9 (range 2-32).

Comparison of lesion detection on different imaging modalities

Of the 120 lesions in total (Table 1), most were identified on [18F]FES PET (n = 64 [53%] and n = 69 [58%] by observer 1 and 2, respectively), followed by high resolution CT (n = 54 [45%]), bone scintigraphy (n = 40 [33%]) and [18F]FDHT PET (n = 36 [30%] and n = 37 [31%]). Fifty and 42% of the lesions identified on [18F]FES PET by observer 1 and 2, respectively, were also detected on high resolution CT or bone scintigraphy (Figure 1). For [18F]FDHT PET, 55% and 49% of the identified lesions were seen with conventional imaging. Conversely, 46 and 42% of the lesions identified on conventional imaging were visible on [18F]FES PET by, respectively, observer 1 and 2, and 29% and 26% were seen on [18F]FDHT PET. In particular, more lymph node lesions were detected on [18F]FES PET and [18F]FDHT PET compared to conventional imaging: 97% and 53% versus 27% of all detected lymph node lesions, respectively.

Visual analysis of [18F]FES and [18F]FDHT PET images

Out of 120 lesions, a total of 87 and 74 on [18F]FES and [18F]FDHT PET, respectively, were analysed for visual interobserver agreement. The other lesions were excluded because one or both observers reported these as 'not evaluable' due to overlap with adjacent organs with high physiological tracer uptake.

Table 1. Patient characteristics.

Characteristic	**Number (n = 10)**	**%**
Age in years, mean (range)	67 (48-79)	
Biopsy of primary tumour:		
ER+/AR+	10	100%
Biopsy of metastases:		
ER+/AR+	8	80%
ER+/AR-	1	10%
ER-/AR-	1	10%
Previous treatment lines:		
0-1	3	30%
2-4	7	70%
Visible lesions: total; median per patient (range)	120; 9 (2-32)	
Conventional imaging (CT; bone scan)	69 (54; 40)	58% (45%; 33%)
Visible on PET alone ([^{18}F]FES or [^{18}F]FDHT PET)	51 (33; 20)	42% (28%; 16%)
Total visible on [^{18}F]FES PET (observer 1; 2)	64; 69	53; 58%
Total visible on [^{18}F]FDHT PET (observer 1; 2)	36; 37	30; 31%
Location:		
Bone (conventional imaging; [^{18}F]FES; [^{18}F]FDHT PET)	79 (55; 45; 37)	66% (80%; 54%; 64%)
Lymph node (conventional imaging; [^{18}F]FES; [^{18}F]FDHT PET)	30 (8; 29; 16)	25% (12%; 35%; 28%)
Visceral* (conventional imaging; [^{18}F]FES; [^{18}F]FDHT PET)	11 (6; 9; 5)	9% (9%; 11%; 9%)

*Excluding liver

For lesions *visible on conventional imaging*, [^{18}F]FES PET readings (Table 2) had substantial positive and negative agreement of 84% (95% CI 72-92%) and 83% (95% CI 70-91%), respectively (kappa = 0.67, 95% CI 0.48-0.87). By including lesions that were only visible on [^{18}F]FES PET, the positive agreement improved to 88% (95% CI 80-93%) for *all* lesions scored on [^{18}F]FES PET (negative agreement remained the same). [^{18}F]FDHT PET showed lower positive agreement of 49% (95% CI 32-65%) for lesions *visible on conventional imaging*, while negative agreement was 74% (95% CI 62-83%) (kappa = 0.23, 95% CI -0.04-0.49). Positive agreement for *all* lesions scored on [^{18}F]FDHT PET was 58% (95% CI 43-71%). By looking at lesions *only visible on PET* and not on conventional imaging, the positive agreement rate was the highest: 91% (95% CI 81-96%) for [^{18}F]FES PET and 80% (95% CI 55-93%) for [^{18}F]FDHT PET. Visual interobserver agreement was not significantly different between the 10 different patients in this study: P = 0.159 for [^{18}F]FES PET and P = 0.387 for [^{18}F]FDHT PET.

An important aspect in the identification of tumour lesions is how well tracer uptake can be distinguished from background uptake in normal reference tissue. The TBR of [18F]FDHT was significantly lower than that of [18F]FES (Figure 2). In bone lesions, the mean TBR of [18F]FDHT was 2.0 (± SD 0.6) versus 3.3 (± SD 2.2) for [18F]FES (P = 0.003). In addition, in lymph node lesions, the mean [18F]FDHT TBR was 4.6 (± SD 1.9) compared to 10.7 (± SD 8.4) for [18F]FES (P < 0.0001).

Figure 1. Tumour lesions detected with conventional imaging, [18F]FES and [18F]FDHT PET.

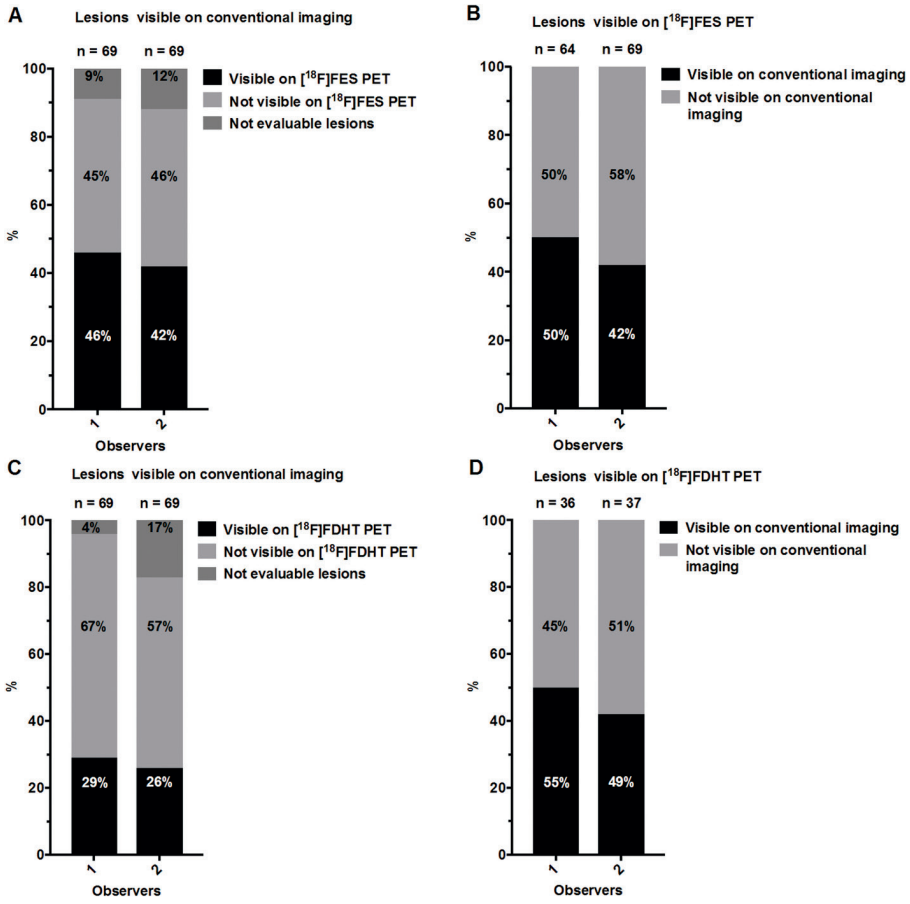

Quantitative analyses of [18]FES and [18F]FDHT PET images

Out of 120 lesions, a total of 94 and 95 were quantified by both observers on [18F]FES and [18F]FDHT PET, respectively. The other lesions were not quantified by one or both of the observers as a result of overlap with adjacent organs with high physiological tracer uptake, unless there was a clear anatomical substrate on other imaging modalities allowing for reliable VOI definition.

Table 2. Visual interobserver agreement for lesions visible (A, C) and not visible on conventional imaging (B, D) on [^{18}F]FES and [^{18}F]FDHT PET, respectively.

A Visual interobserver agreement on [^{18}F]FES PET for lesions visible on conventional imaging

	OBSERVER 1			
OBSERVER 2	**VISIBLE**	**NOT VISIBLE**	**NOT EVALUABLE§**	**TOTAL**
VISIBLE	24	3	2	29
NOT VISIBLE	6	22	4	32
NOT EVALUABLE§	2	6	0	8
TOTAL	32	31	6	69

B Visual interobserver agreement on [^{18}F]FES PET for lesions not visible on conventional imaging

	OBSERVER 1			
OBSERVER 2	**VISIBLE**	**NOT VISIBLE**	**NOT EVALUABLE§**	**TOTAL**
VISIBLE	26	3	11	40
NOT VISIBLE	2	1*	3	6
NOT EVALUABLE§	4	1	0	5
TOTAL	32	5	14	51

C Visual interobserver agreement on [^{18}F]FDHT PET for lesions visible on conventional imaging

	OBSERVER 1			
OBSERVER 2	**VISIBLE**	**NOT VISIBLE**	**NOT EVALUABLE§**	**TOTAL**
VISIBLE	9	8	1	18
NOT VISIBLE	11	27	1	39
NOT EVALUABLE§	0	11	1	12
TOTAL	20	46	3	69

D Visual interobserver agreement on [^{18}F]FDHT PET for lesions not visible on conventional imaging

	OBSERVER 1			
OBSERVER 2	**VISIBLE**	**NOT VISIBLE**	**NOT EVALUABLE§**	**TOTAL**
VISIBLE	6	2	11	19
NOT VISIBLE	1	10#	6	17
NOT EVALUABLE§	9	4	2	15
TOTAL	16	16	19	51

§Not evaluable lesions due to overlap with adjacent organs with high physiological tracer uptake. *Lesions identified on [^{18}F]FDHT PET, #Lesions identified on [^{18}F]FES PET.

In general, interobserver agreement was excellent for PET quantification (Figure 3) of *all* lesions combined (i.e. visible on PET or seen on conventional imaging). The ICCs for quantification of SUV_{max}, SUV_{peak} and SUV_{mean} on [18F]FES PET were 0.98 (95% CI 0.96-0.98), 0.97 (95% CI 0.96-0.98) and 0.89 (95% CI 0.83-0.92). For [18F]FDHT PET the ICCs were lower with 0.78 (95% CI 0.66-0.85), 0.76 (95% CI 0.63-0.84) and 0.75 (95% CI 0.62-0.84), respectively.

In addition, [18F]FES (Figure 4) and [18F]FDHT PET (Figure 5) quantification was analysed separately with Bland Altman plots for all lesions *visible on PET* or lesions *only visible on conventional imaging* (hence, PET-negative lesions). For [18F]FES PET, PET-positive lesions showed excellent quantitative interobserver agreement with mean differences < 2% and 95% limits of agreement ($LOA_{95\%}$) being narrower for SUV_{max} ($LOA_{95\%}$ -31.3% to 34.3%) and SUV_{peak} ($LOA_{95\%}$ -31.1% to 28.4%), compared to SUV_{mean} ($LOA_{95\%}$ -46.5% to 44.3%). More differences were shown for PET-negative lesions with mean interobserver differences < 14% and larger $LOA_{95\%}$ (within ± 75%), but note that absolute differences between observers were generally low due to a low SUV. Similarly, for [18F]FDHT PET interobserver agreement was better for PET-positive (mean interobserver differences < 7%, $LOA_{95\%}$ within ± 45 %) compared to PET-negative lesions (mean interobserver differences < 12%, $LOA_{95\%}$ within ± 76%). SUV_{max} and SUV_{peak} showed a better interobserver agreement in comparison to SUV_{mean} for the quantification of lesions visible on [18F]FES PET, while on [18F]FDHT PET the different SUV parameters were comparable.

Higher levels of tracer accumulation in PET positive lesions were not associated with improved interobserver agreement (for [18F]FES PET: Spearman r = 0.04, 0.26 and 0.14 for $SUV_{max,}$ SUV_{peak} and SUV_{mean}, respectively and for [18F]FDHT PET: Spearman r = 0.00, r = 0.03 and r = -0.17, respectively). In addition, there was no correlation between tumour size and interobserver agreement (for [18F]FES PET: Spearman r = 0.10, r = 0.08 and r = 0.06, for $SUV_{max,}$ SUV_{peak} and SUV_{mean}, respectively and for [18F]FDHT PET: Spearman r = -0.07, r = -0.16 and r = -0.42, respectively).

The added value of quantitative assessment in comparison to visual assessment

Based on previous studies, [18F]FES and [18F]FDHT SUV_{max} cut-off levels of 1.5 and 1.9, respectively, have been identified. There are however limited data on quantitative thresholds and corresponding cut-off values for SUV_{peak} and SUV_{mean}. Based on linear regression of all lesions quantified in this study, an SUV_{max} cut-off of 1.5 on [18F]FES PET corresponded with an SUV_{peak} of 1.2 and an SUV_{mean} of 1.1 (Supplementary figure S1), and for [18F]FDHT PET, an SUV_{max} cut-off of 1.9 corresponded with an SUV_{peak} of 1.6 and an SUV_{mean} of 1.3.

Figure 2. The difference in tumour to background ratio between [^{18}F]FES and [^{18}F]FDHT PET shown visually (A) and quantitatively (mean ± SD) for bone and lymph node lesions (B).

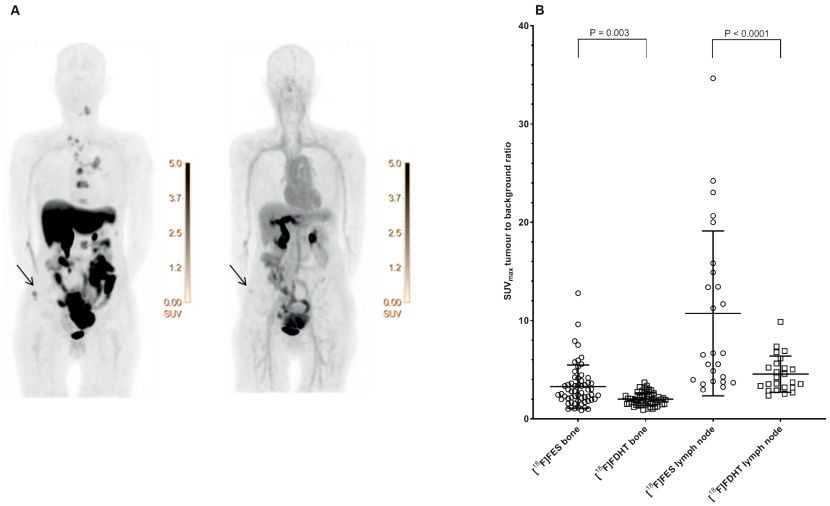

The arrows in Fig 2A show a bone lesion in the right os ilium visible on [^{18}F]FES PET which is only subtly visible on [^{18}F]FDHT PET. Note there is physiological tracer uptake of [^{18}F]FES in liver, gallbladder, intestine, bladder and for [^{18}F]FDHT also in the blood pool.

Figure 3. Intraclass correlation coefficients for all quantified tumour lesions on [^{18}F]FES (n = 94) using SUV_{max}, SUV_{peak} and SUV_{mean} (A, B and C) and [^{18}F]FDHT PET (n = 95) (D, E and F). Note: not quantifiable lesions by one or both of the observers were excluded as a result of overlap with adjacent organs with high physiological tracer uptake.

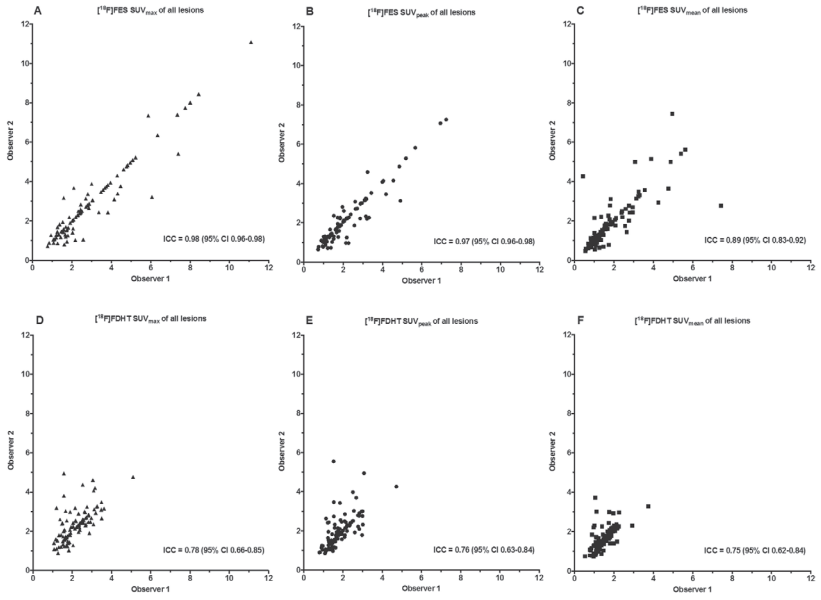

Figure 4. Bland Altman plots showing the % differences in $SUV_{max,}$ SUV_{peak} and SUV_{mean} between observers for lesions visible on [18F]FES PET (A, B, C) or only visible on conventional imaging (D, E, F). The dashed lines represent the mean difference between observers ± 95% limits of agreement ($LOA_{95\%}$).

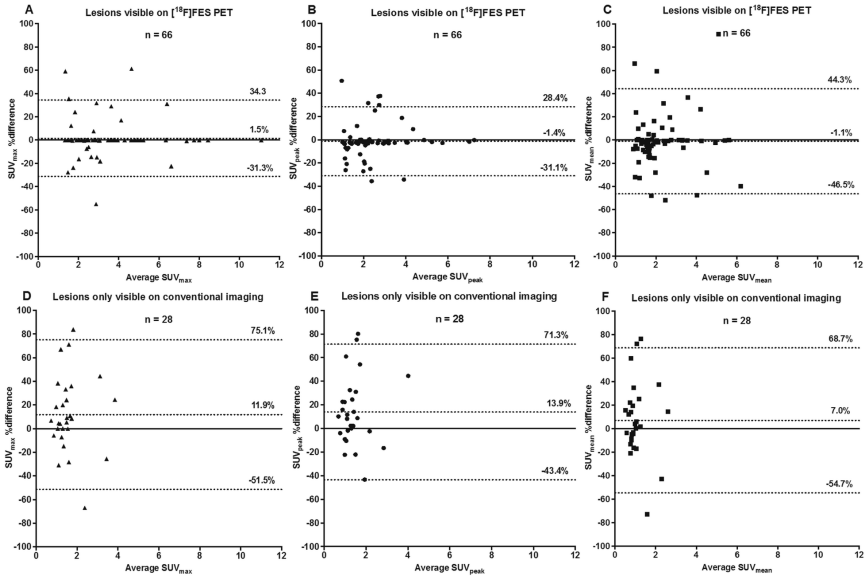

Figure 5. Bland Altman plots showing the % differences in $SUV_{max,}$ SUV_{peak} and SUV_{mean} between observers for lesions visible on [18F]FDHT PET (A, B, C) or only visible on conventional imaging (D, E, F).

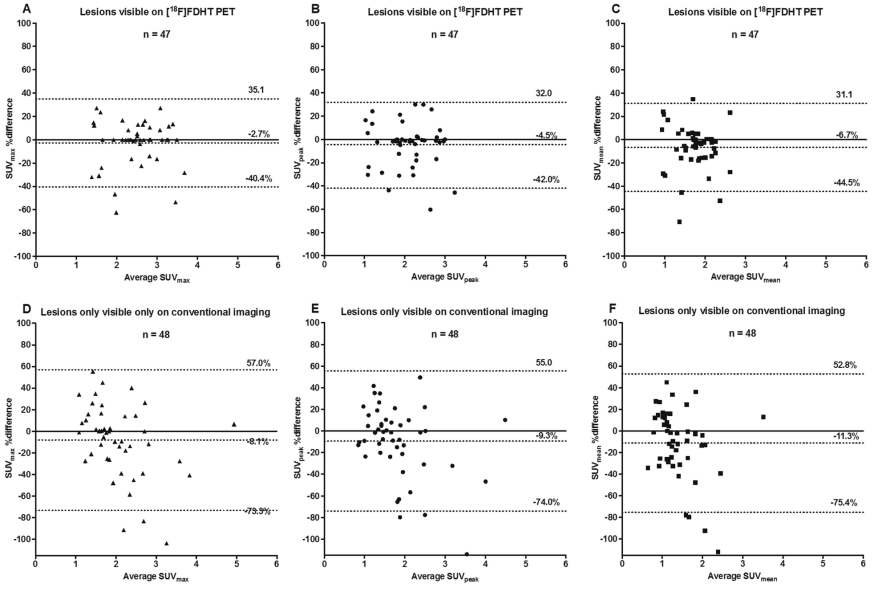

For diagnostic purposes it is important to identify all receptor positive tumour lesions. Therefore, we compared visual and quantitative tracer uptake above/below cut-off levels (Table 3). In 3% and 1% of the lesions scored visually positive on [^{18}F]FES PET by observer 1 and 2 respectively, SUV_{max} was below the threshold of 1.5. For [^{18}F]FDHT PET, 14% of the visually positive lesions scored by observer 1 as well as observer 2 had an SUV_{max} below the threshold of 1.9. There were no structural differences between observer 1 and 2. The discrepancies were mostly seen in lesions located in tissue with low background uptake such as skin and lung metastases (Supplementary table S1). Conversely, in 44% and 39% of the lesions scored visually negative on [^{18}F]FES PET by observer 1 and 2, respectively, SUV_{max} was ≥ 1.5. Similarly, respectively 31% and 52% of the visually negative lesions had an SUV_{max} ≥ 1.9 on [^{18}F]FDHT PET, respectively. However, in most cases (60%) we observed overlap with organs having high physiological tracer accumulation such as liver and bowel, followed by lesions that were determined to be visually positive at second glance (32%). After correction for these effects, ≤ 4% of the visually negative lesions had an SUV_{max} above cut-off for both tracers.

Table 3. Discrepancies between visual and quantitative assessments (above/below cut-off values for receptor positivity) for [^{18}F]FES (A) and [^{18}F]FDHT PET (B). Note: not evaluable lesions were excluded

A [^{18}F]FES	**OBSERVER 1**		**OBSERVER 2**	
	VISIBLE (n = 64)	**NOT VISIBLE (n = 36)**	**VISIBLE (n = 69)**	**NOT VISIBLE (n = 38)**
SUV_{MAX} ≥ 1.5	62 (97%)	16 (44%)	68 (99%)	15 (39%)
SUV_{MAX} < 1.5	2 (3%)	20 (56%)	1 (1%)	23 (61%)
SUV_{PEAK} ≥ 1.2	54 (84%)	19 (53%)	67 (97%)	16 (42%)
SUV_{PEAK} < 1.2	10 (16%)	17 (47%)	2 (3%)	22 (58%)
SUV_{MEAN} ≥ 1.1	57 (89%)	8 (22%)	67 (97%)	11 (29%)
SUV_{MEAN} < 1.1	7 (11%)	28 (78%)	2 (3%)	27 (71%)
B [^{18}F]FDHT	**OBSERVER 1**		**OBSERVER 2**	
	VISIBLE (n = 36)	**NOT VISIBLE (n = 62)**	**VISIBLE (n = 37)**	**NOT VISIBLE (n = 56)**
SUV_{MAX} ≥ 1.9	31 (86%)	19 (31%)	32 (86%)	29 (52%)
SUV_{MAX} < 1.9	5 (14%)	43 (69%)	5 (14%)	27 (48%)
SUV_{PEAK} ≥ 1.6	30 (83%)	25 (40%	33 (89%)	30 (54%)
SUV_{PEAK} < 1.6	6 (17%)	37 (60%)	4 (11%)	26 (46%)
SUV_{MEAN} ≥ 1.3	31 (86%)	20 (32%)	33 (89%)	30 (54%)
SUV_{MEAN} < 1.3	5 (14%)	42 (68%)	4 (11%)	26 (46%)

Comparing the impact of the different SUV parameters on discrepancies between visual and quantitative assessments, showed no significant differences with the only exception that SUV_{mean} showed less visually negative lesions above cut-off on [18FES]PET than SUV_{max} or SUV_{peak} for observer 1 (P = 0.008 and P = 0.001, respectively), but not for observer 2 (P = 0.125 and P = 0.063, respectively).

DISCUSSION

Interobserver variability is an important step in the clinical application of diagnostic tools. Here, we showed that both visual and quantitative evaluation were highly reproducible between independent observers evaluating [18F]FES PET at separate centres using different scanners and software. Visual positive and negative absolute agreement was > 80%, with a kappa of 0.67. Also, the interobserver reliability of quantitative metrics was excellent for SUV_{max} and SUV_{peak} (ICC of 0.98 and 0.97, respectively) and good for SUV_{mean} (ICC of 0.89). In comparison, staging patients with breast cancer showed similar results for bone scintigraphy (kappa 0.62-0.78) and [18F]FDG PET (kappa 0.65 and an ICC of 0.93 for the quantification of [18F]FDG uptake) [22-26].

[18F]FDHT PET also showed good interobserver reliability for quantitative assessments with ICCs ≥ 0.75. These values are slightly lower than those of [18F]FES PET, and this was probably due to the lower lesional [18F]FDHT uptake, because quantitative agreement according to Bland Altman analyses were comparable for both tracers. The TBR of [18F]FDHT was considerably lower compared to [18F]FES. This probably explains the higher variability in visual interpretation (kappa = 0.23), mainly caused by a low visual positive agreement (49%) in lesions already identified by conventional imaging modalities, while positive agreement in lesions not identified by conventional imaging was much higher (80%), as well as negative visual agreement between observers (74%). An important impeding factor was the significantly lower TBR of [18F]FDHT in bone and lymph node lesions compared to [18F]FES PET. The TBR of [18F]FDHT in the current study (2.0 for bone and 4.6 for lymph nodes) was also lower than in prostate cancer metastases (3.3 for bone and 5.7 for soft tissue metastases) with an SUV_{max} three times higher in prostate cancer (7.1-9.1 versus 2.0 in the present breast cancer study) [27, 28]. This suggests that higher AR expression likely results in better interobserver reliability.

Our study had some limitations. There were only a limited number of patients included in this study. However, receptor expression between lesions within a single patient can be heterogeneous [29], which was confirmed in the present study resulting in the coverage of a large range of data in 120 lesions

[8]. In addition, we showed there was no within-patient correlation in visual assessments. A second limitation is a substantial number of 'not evaluable' lesions, due to overlap with adjacent organs with high physiological background. The decision for evaluability was left to each observer individually, which may have contributed to the low agreement (≤ 6%) on these 'not evaluable lesions'. For future studies we recommend that all lesions with physiological background overlap from liver, gallbladder, intestine, bladder and for [^{18}F]FDHT also from bloodpool are regarded as not evaluable. A third limitation is the lack of robust [^{18}F]FES and [^{18}F]FDHT thresholds for test positivity. We used an SUV_{max} cut-off of 1.5 for [^{18}F]FES and 1.9 for [^{18}F]FDHT PET based on previous data corresponding with ER and AR positivity in biopsies and so far showing the best predictive value for response to endocrine therapy [8, 9, 30, 31]. Some studies suggested an SUV_{max} cut-off of 2.0 for [^{18}F]FES PET, taking into account the background [^{18}F]FES uptake in normal tissues which can exceed the cut-off of 1.5 [29-31]. Tissue specific cut-off values may indeed be more appropriate as there are responders to endocrine therapy with a tumour SUV_{max} < 2.0. In the current study, up to 20% of the visually positive lesions had an SUV_{max} < 2.0, while < 3% had an SUV_{max} < 1.5 (Supplementary table S2).

For diagnostic purposes simple visual assessment of [^{18}F]FES uptake may suffice to determine the receptor status of a tumour lesion (agreement was high between visual assessment and the applied SUV_{max} cut-off value of 1.5 for ER-positivity). True discrepancies between visibility and corresponding uptake above or below cut-off were low (< 4%), making quantification of visually negative lesions not only cumbersome, but also unnecessary. Also, quantification of lesions without visual [^{18}F]FES uptake leads to higher interobserver variability due to differences in VOI definition. However, quantification remains a helpful tool for nuclear medicine physicians in 'equivocal [^{18}F]FES lesions'. In addition, quantification is useful to measure receptor availability over time for the evaluation of treatment effects. In contrast, quantification of [^{18}F]FDHT uptake is still required in future breast cancer studies, as we have shown relatively low visual agreement.

The role of [^{18}F]FES and [^{18}F]FDHT PET in addition to conventional imaging modalities needs to be defined further. It has to be taken into account that besides partial volume effects and constraints due to background tracer uptake limiting their detection, receptor expression can be heterogeneous and variable during the course of the disease [11, 32]. In addition, treatment may induce changes in receptor expression, but also eradicated tumour cells can leave a visible lesion on conventional imaging (e.g. sclerotic bone lesions), in absence of viable tumour cells. In the current study with heavily pretreated patients, 42-46% and 26-29% of the lesions identified by conventional imaging

were detected on [18F]FES and [18F]FDHT PET, respectively. Vice versa, only approximately 50% of the lesions observed on [18F]FES PET and [18F]FDHT PET, were identified by conventional imaging.

Therefore, a potential role for [18F]FES PET may be in staging of early ER-positive breast cancer as an addition to existing imaging techniques. Standard staging with [18F]FDG PET can miss low-intermediate grade ER-positive lesions due to their low metabolic activity [33]. We are currently investigating [18F]FES PET in staging patients with low grade, ER-positive locally advanced or recurrent breast cancer versus [18F]FDG PET (NCT03726931), and in metastatic breast cancer versus addition to conventional diagnostics (NCT01957332). The *non-invasive* visualisation of receptor status in metastatic lesions with PET offers a number potential clinical advantages. For example, in case conventional diagnostics cannot establish a final diagnosis of suspected metastatic breast cancer lesions (e.g. as a result of inaccessible biopsy sites or repeated biopsy sampling errors). Also, PET imaging may help to determine the hormone receptor status of *different tumour sites within a patient* and guide treatment decisions. For instance, to decide on the origin of a metastatic lesion in case of multiple primary tumours or to determine whether receptor conversion occurred in metastases from a single primary tumour [11]. If validated, this may help with multimodality treatment strategies for heterogeneous tumour sites of breast cancer, such as endocrine therapy for [18F]FES positive lesions combined with a local modality such as radiotherapy for concurrent [18F]FES negative lesions [34].

CONCLUSION

In conclusion, our findings demonstrate that visual and quantitative evaluation of [18F]FES PET has a high interobserver concordance and support the use in clinical practice. Although [18F]FDHT PET showed relatively low visual agreement, presumably a result of the low AR expression and consequently low TBR in patients with breast cancer, there was good quantitative agreement between observers, acceptable for further [18F]FDHT PET imaging studies in breast cancer.

Abbreviations

ER: oestrogen receptor, AR: androgen receptor, [18F]FES: 16α-[18F]fluoro-17β-oestradiol, [18F]FDHT: 16β-[18F]fluoro-5α-dihydrotestosterone, VOI: volume of interest, SUV: standardised uptake value, TBR: tumour-background ratio, ICC: intraclass correlation coefficient, $LOA_{95\%}$: 95% limits of agreement.

Acknowledgements
We thank the patients who participated in this study and their families. In addition, we acknowledge the efforts of the clinical and imaging teams at the university medical centres participating in this study.

Authors' contributions
CS, MvK, AG, HV, EB, ErdV, EldV, OH, GH, WM were responsible for the study concept and design. LM, CV, OH and AG carried out the data acquisition. MY, OH and AG performed the quality control of the data. HdV supervised the statistical analyses. BvdV performed the pathological analyses. LM and CV prepared the manuscript. CS, MvK, AG, HV, EB, ErdV, EldV, OH, GH, WM, MY, HdV and BvdV edited and revised the manuscript. All authors read and approved of the final manuscript.

Funding
This study was financially supported by the Centre for Translational Molecular Medicine (CTMM) project as part of the Mammary Carcinoma Molecular Imaging for Diagnosis and Therapeutics (MAMMOTH) project.

Availability of data and materials
The datasets used and/or analysed during the current study are available from the corresponding author on reasonable request.

Ethics approval and consent to participate
All procedures performed in studies involving human participants were in accordance with the ethical standards of the Institutional Review Board of University Medical Center, Groningen, and also approved by the Institutional Review Board of the Amsterdam UMC, location VUmc University Medical Center, Amsterdam, the Netherlands (File no. 2014.501-NL41954.042.13) and with the 1964 Helsinki Declaration and its later amendments or comparable ethical standards. Informed consent was obtained from all individual participants included in the study.

Consent for publication
Not applicable.

Competing interests
The authors declare that they have no competing interests.

SUPPLEMENTAY MATERIAL

Supplementary table S1. Biodistribution of [18F]FES and [18F]FDHT in various organs (n = 10)

ORGAN	[18F]FES SUV_{MEAN}	[18F]FDHT SUV_{MEAN}
	Mean (± SD)	Mean (± SD)
Galbladder	49.7 (± 28.3)	30.4 (± 26.6)
Bladder	14.5 (± 7.3)	14.1 (± 6.7)
Liver	12.0 (± 4.0)	3.9 (± 0.4)
Intestine	4.1 (± 1.9)	2.9 (± 1.0)
Kideney	2.3 (± 0.5)	3.2 (± 0.4)
Uterus	1.7 (± 0.6)	2.0 (± 0.3)
Pancreas	1.4 (± 0.3)	1.6 (± 0.5)
Bloodpool	1.3 (± 0.6)	3.9 (± 0.7)
Adrenal Gland	1.2 (± 0.1)	1.9 (± 0.4)
Spleen	1.0 (± 0.3)	2.1 (± 0.3)
Lung	0.9 (± 0.3)	1.0 (± 0.1)
Bone	0.9 (± 0.3)	1.1 (± 0.1)
Ovary	0.8 (± 0.2)	1.3 (± 0.3)
Stomach	0.6 (± 0.4)	0.9 (± 0.6)
Breast	0.6 (± 0.3)	0.8 (± 0.2)
Muscle	0.6 (± 0.1)	0.8 (± 0.1)
Brain	0.5 (± 0.1)	0.4 (± 0.1)
Fat	0.5 (± 0.2)	0.6 (± 0.1)

Supplementary table S2. Discrepancies between visual and quantitative assessments (above/below cut-off values for receptor positivity) for [18F]FES using higher cut-off values

[18F]FES	OBSERVER 1		OBSERVER 2	
	VISIBLE (n = 64)	NOT VISIBLE (n = 36)	VISIBLE (n = 69)	NOT VISIBLE (n = 38)
$SUV_{max} \geq 2.0$	51 (80%)	7 (19%)	64 (93%)	6 (16%)
$SUV_{max} < 2.0$	13 (20%)	29 (80%)	5 (7%)	32 (84%)
$SUV_{peak} \geq 1.6$	45 (70%)	9 (25%)	57 (83%)	7 (18%)
$SUV_{peak} < 1.6$	19 (30%)	27 (75%)	12 (17%)	31 (82%)
$SUV_{mean} \geq 1.5$	45 (70%)	6 (17%)	57 (83%)	6 (16%)
$SUV_{mean} < 1.5$	19 (30%)	30 (83%)	12 (17%)	32 (84%)

Supplementary figure S1. Linear regression showing the relationship between SUV_{max}, SUV_{peak} and SUV_{mean} for [^{18}F]FES and [^{18}F]FDHT PET (n = 95)

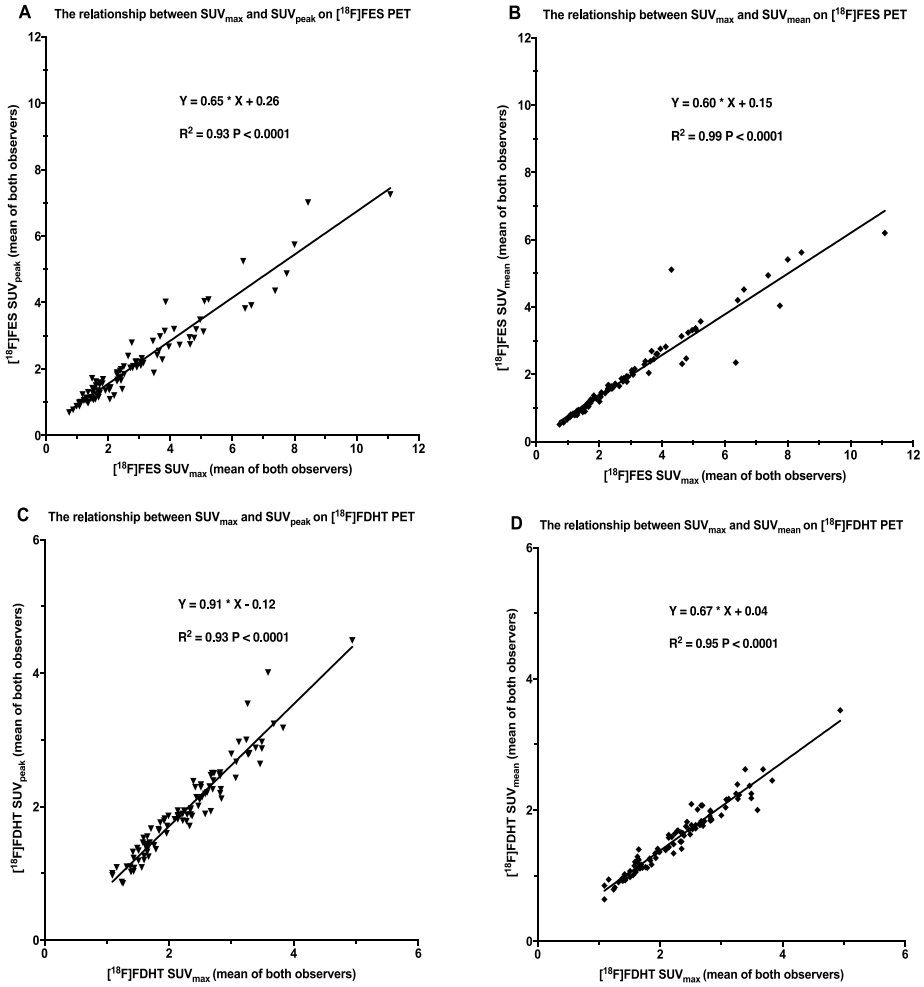

REFERENCES

1. Blamey RW, Hornmark-Stenstam B, Ball G, Blichert-Toft M, Cataliotti L, Fourquet A, et al. ONCOPOOL - a European database for 16,944 cases of breast cancer. Eur J Cancer. 2010;46:56-71. doi:10.1016/j.ejca.2009.09.009.
2. Yamashita H, Yando Y, Nishio M, Zhang Z, Hamaguchi M, Mita K, et al. Immunohistochemical evaluation of hormone receptor status for predicting response to endocrine therapy in metastatic breast cancer. Breast Cancer. 2006;13:74-83.
3. Collins LC, Cole KS, Marotti JD, Hu R, Schnitt SJ, Tamimi RM. Androgen receptor expression in breast cancer in relation to molecular phenotype: results from the Nurses' Health Study. Mod Pathol. 2011;24:924-31. doi:10.1038/modpathol.2011.54.
4. Krop I, Colleoni M, Traina T, Holmes F, Estevez L, et al. Results from a randomized placebo-controlled phase 2 trial evaluating exemestane ± enzalutamide in patients with hormone receptor-positive breast cancer. Abstract GS4-07. San Antonio Breast Cancer Symposium. San Antonio, Texas; 2017.
5. Gucalp A, Tolaney S, Isakoff SJ, Ingle JN, Liu MC, Carey LA, et al. Phase II trial of bicalutamide in patients with androgen receptor-positive, estrogen receptor-negative metastatic Breast Cancer. Clin Cancer Res. 2013;19:5505-12. doi:10.1158/1078-0432.CCR-12-3327.
6. Traina TA, Yardley DA, Schwartzberg LS, O'Shaughnessy J, Cortes J, Awada A, et al. Overall survival (OS) in patients (Pts) with diagnostic positive (Dx+) breast cancer: Subgroup analysis from a phase 2 study of enzalutamide (ENZA), an androgen receptor (AR) inhibitor, in AR+ triple-negative breast cancer (TNBC) treated with 0-1 prior lines of therapy. Journal of Clinical Oncology. 2017;35:1089-. doi:10.1200/JCO.2017.35.15_suppl.1089.
7. Youk JH, Kim EK, Kim MJ, Lee JY, Oh KK. Missed breast cancers at US-guided core needle biopsy: how to reduce them. Radiographics. 2007;27:79-94. doi:10.1148/rg.271065029.
8. Venema CM, Mammatas LH, Schroder CP, van Kruchten M, Apollonio G, Glaudemans A, et al. Androgen and Estrogen Receptor Imaging in Metastatic Breast Cancer Patients as a Surrogate for Tissue Biopsies. J Nucl Med. 2017;58:1906-12. doi:10.2967/jnumed.117.193649.
9. van Kruchten M, de Vries EG, Brown M, de Vries EF, Glaudemans AW, Dierckx RA, et al. PET imaging of oestrogen receptors in patients with breast cancer. Lancet Oncol. 2013;14:e465-75. doi:10.1016/S1470-2045(13)70292-4.
10. Chae SY, Ahn SH, Kim SB, Han S, Lee SH, Oh SJ, et al. Diagnostic accuracy and safety of 16alpha-[(18)F]fluoro-17beta-oestradiol PET-CT for the assessment of oestrogen receptor status in recurrent or metastatic lesions in patients with breast cancer: a prospective cohort study. Lancet Oncol. 2019;20:546-55. doi:10.1016/S1470-2045(18)30936-7.
11. van Kruchten M, Glaudemans AW, de Vries EF, Beets-Tan RG, Schroder CP, Dierckx RA, et al. PET imaging of estrogen receptors as a diagnostic tool for breast cancer patients presenting with a clinical dilemma. J Nucl Med. 2012;53:182-90. doi:10.2967/jnumed.111.092734.

12. van Kruchten M, de Vries EG, Glaudemans AW, van Lanschot MC, van Faassen M, Kema IP, et al. Measuring residual estrogen receptor availability during fulvestrant therapy in patients with metastatic breast cancer. Cancer Discov. 2015;5:72-81. doi:10.1158/2159-8290.CD-14-0697.
13. Scher HI, Beer TM, Higano CS, Anand A, Taplin ME, Efstathiou E, et al. Antitumour activity of MDV3100 in castration-resistant prostate cancer: a phase 1-2 study. Lancet. 2010;375:1437-46. doi:10.1016/S0140-6736(10)60172-9.
14. Kurland BF, Peterson LM, Lee JH, Schubert EK, Currin ER, Link JM, et al. Estrogen Receptor Binding (18F-FES PET) and Glycolytic Activity (18F-FDG PET) Predict Progression-Free Survival on Endocrine Therapy in Patients with ER+ Breast Cancer. Clin Cancer Res. 2017;23:407-15. doi:10.1158/1078-0432.CCR-16-0362.
15. Liu A, Dence CS, Welch MJ, Katzenellenbogen JA. Fluorine-18-labeled androgens: radiochemical synthesis and tissue distribution studies on six fluorine-substituted androgens, potential imaging agents for prostatic cancer. J Nucl Med. 1992;33:724-34.
16. Römer J, Steinbach J, Kasch H. Studies on the synthesis of 16α-[18F] fluoroestradiol. Applied radiation and isotopes. 1996;47:395-9.
17. Boellaard R, Delgado-Bolton R, Oyen WJ, Giammarile F, Tatsch K, Eschner W, et al. FDG PET/CT: EANM procedure guidelines for tumour imaging: version 2.0. Eur J Nucl Med Mol Imaging. 2015;42:328-54. doi:10.1007/s00259-014-2961-x.
18. Jansen BHE, Kramer GM, Cysouw MCF, Yaqub MM, de Keizer B, Lavalaye J, et al. Healthy Tissue Uptake of (68)Ga-Prostate Specific Membrane Antigen (PSMA), (18) F-DCFPyL, (18)F-Fluoromethylcholine (FCH) and (18)F-Dihydrotestosterone (FDHT). J Nucl Med. 2019. doi:10.2967/jnumed.118.222505.
19. de Vet HC, Mokkink LB, Terwee CB, Hoekstra OS, Knol DL. Clinicians are right not to like Cohen's kappa. BMJ. 2013;346:f2125. doi:10.1136/bmj.f2125.
20. Landis JR, Koch GG. An application of hierarchical kappa-type statistics in the assessment of majority agreement among multiple observers. Biometrics. 1977:363-74.
21. Portney LG, Watkins MP. Foundations of clinical research: applications to practice: Pearson/Prentice Hall Upper Saddle River, NJ; 2009.
22. Sawicki LM, Grueneisen J, Schaarschmidt BM, Buchbender C, Nagarajah J, Umutlu L, et al. Evaluation of 18 F-FDG PET/MRI, 18 F-FDG PET/CT, MRI, and CT in whole-body staging of recurrent breast cancer. European journal of radiology. 2016;85:459-65.
23. van der Hoeven JJ, Hoekstra OS, Comans EF, Pijpers R, Boom RP, van Geldere D, et al. Determinants of diagnostic performance of [F-18] fluorodeoxyglucose positron emission tomography for axillary staging in breast cancer. Annals of surgery. 2002;236:619.
24. Shackleton M, Yuen K, Little AF, Schlicht S, McLachlan SA. Reliability of X-rays and bone scans for the assessment of changes in skeletal metastases from breast cancer. Intern Med J. 2004;34:615-20. doi:10.1111/j.1445-5994.2004.00637.x.
25. Gutzeit A, Doert A, Froehlich JM, Eckhardt BP, Meili A, Scherr P, et al. Comparison of diffusion-weighted whole body MRI and skeletal scintigraphy for the detection of bone metastases in patients with prostate or breast carcinoma. Skeletal Radiol. 2010;39:333-43. doi:10.1007/s00256-009-0789-4.

26. Jacene HA, Leboulleux S, Baba S, Chatzifotiadis D, Goudarzi B, Teytelbaum O, et al. Assessment of interobserver reproducibility in quantitative 18F-FDG PET and CT measurements of tumor response to therapy. J Nucl Med. 2009;50:1760-9. doi:10.2967/jnumed.109.063321.
27. Fox JJ, Autran-Blanc E, Morris MJ, Gavane S, Nehmeh S, Van Nuffel A, et al. Practical approach for comparative analysis of multilesion molecular imaging using a semiautomated program for PET/CT. J Nucl Med. 2011;52:1727-32. doi:10.2967/jnumed.111.089326.
28. Vargas HA, Wassberg C, Fox JJ, Wibmer A, Goldman DA, Kuk D, et al. Bone metastases in castration-resistant prostate cancer: associations between morphologic CT patterns, glycolytic activity, and androgen receptor expression on PET and overall survival. Radiology. 2014;271:220-9. doi:10.1148/radiol.13130625.
29. Nienhuis HH, van Kruchten M, Elias SG, Glaudemans A, de Vries EFJ, Bongaerts AHH, et al. (18)F-Fluoroestradiol Tumor Uptake Is Heterogeneous and Influenced by Site of Metastasis in Breast Cancer Patients. J Nucl Med. 2018;59:1212-8. doi:10.2967/jnumed.117.198846.
30. Dehdashti F, Mortimer JE, Trinkaus K, Naughton MJ, Ellis M, Katzenellenbogen JA, et al. PET-based estradiol challenge as a predictive biomarker of response to endocrine therapy in women with estrogen-receptor-positive breast cancer. Breast Cancer Res Treat. 2009;113:509-17. doi:10.1007/s10549-008-9953-0.
31. Mortimer JE, Dehdashti F, Siegel BA, Trinkaus K, Katzenellenbogen JA, Welch MJ. Metabolic flare: indicator of hormone responsiveness in advanced breast cancer. J Clin Oncol. 2001;19:2797-803. doi:10.1200/JCO.2001.19.11.2797.
32. Amir E, Miller N, Geddie W, Freedman O, Kassam F, Simmons C, et al. Prospective study evaluating the impact of tissue confirmation of metastatic disease in patients with breast cancer. J Clin Oncol. 2012;30:587-92. doi:10.1200/JCO.2010.33.5232.
33. Groheux D, Giacchetti S, Moretti JL, Porcher R, Espie M, Lehmann-Che J, et al. Correlation of high 18F-FDG uptake to clinical, pathological and biological prognostic factors in breast cancer. Eur J Nucl Med Mol Imaging. 2011;38:426-35. doi:10.1007/s00259-010-1640-9.
34. Mammatas LH, Verheul HM, Hendrikse NH, Yaqub M, Lammertsma AA, Menke-van der Houven van Oordt CW. Molecular imaging of targeted therapies with positron emission tomography: the visualization of personalized cancer care. Cell Oncol (Dordr). 2015;38:49-64. doi: 10.1007/s13402-014-0194-4.

PART II

Visualizing targeted anticancer therapies and effects: *sorafenib imaging*

CHAPTER 4

^{11}C-sorafenib and ^{15}O-H_2O PET for early evaluation of sorafenib therapy

Lemonitsa H. Mammatas, Maqsood Yaqub, N. Harry Hendrikse, Otto S. Hoekstra, Richard J. Honeywell, Robert C. Schuit, Martijn Meijerink, Lothar A. Schwarte, Godefridus J. Peters, Henk M.W. Verheul, Adriaan A. Lammertsma, C. Willemien Menke-van der Houven van Oordt

Published in: J Nucl Med. 2020; online ahead of print

ABSTRACT

Purpose: Sorafenib leads to clinical benefit in a subgroup of patients, while all are exposed to potential toxicity. Currently, no predictive biomarkers are available. The purpose of this study was to evaluate whether ^{11}C-sorafenib and ^{15}O-H_2O PET have potential to predict treatment efficacy.

Methods: In this prospective exploratory study, 8 patients with advanced solid malignancies and an indication for sorafenib treatment were included. Microdose ^{11}C-sorafenib and perfusion ^{15}O-H_2O dynamic PET scans were performed before and after two weeks of sorafenib therapy. The main objective was to assess whether tumor ^{11}C-sorafenib uptake predicts sorafenib concentrations during therapy in corresponding tumor biopsies measured with liquid chromatography tandem mass spectrometry (LC-MS/MS). Secondary objectives included the association of ^{11}C-sorafenib PET, perfusion ^{15}O-H_2O PET and sorafenib concentrations after therapeutic dosing with response.

Results: ^{11}C-sorafenib PET did not predict sorafenib concentrations in tumor biopsies during therapy. In addition, sorafenib plasma and tumor concentrations, were not associated with clinical outcome in this exploratory study. Higher ^{11}C-sorafenib accumulation in tumors at baseline and day 14 of treatment showed association with poorer prognosis and was correlated with tumor perfusion (r_s = 0.671, P = 0.020). Interestingly, a decrease in tumor perfusion measured with ^{15}O-H_2O PET after only 14 days of therapy showed an association with response, with a decrease in tumor perfusion of 56% ± 23% (mean ± SD) versus 18% ± 32% in patients with stable and progressive disease, respectively.

Conclusion: Microdose ^{11}C-sorafenib PET did not predict intratumoral sorafenib concentrations after therapeutic dosing, but the association between a decrease in tumor perfusion and clinical benefit warrants further investigation.

INTRODUCTION

Since the discovery of Rapidly Accelerated Fibrosarcoma (RAF) kinases in 1983 as oncoproteins involved in cancer proliferation, migration and survival, protein kinase inhibitors have been developed in an attempt to inhibit these RAF kinases (*1*). Sorafenib was the first clinically successful RAF inhibitor (*2*). The molecular properties of sorafenib (~ 637 Daltons) enable diffusion and transporter mediated uptake into the cell. Sorafenib competes with adenosine triphosphate in order to occupy the hydrophobic pocket directly adjacent to its binding site, thereby trapping protein kinases in an inactive state (*3*). Apart from RAF kinases, sorafenib has shown affinity for multiple other protein kinases, thereby suppressing angiogenesis and inducing apoptosis (*4*). Sorafenib has been approved for treatment of locally advanced and metastatic hepatocellular carcinoma, renal cell carcinoma and iodine-refractory differentiated thyroid carcinoma (*5-7*). However, response to sorafenib is variable, resulting in clinical benefit for only a subgroup of patients, while all are exposed to potential toxicity (*5-7*). Most common side effects include gastrointestinal symptoms, fatigue, and (hand-foot) skin reactions (*5-7*). Currently, no biomarkers are available to identify which patients are likely to benefit from sorafenib.

The response to sorafenib is thought to be directly related to drug concentrations in tumor tissue (*8*). Non-invasive quantification of drug uptake in tumors and normal tissues at different time points using positron emission tomography (PET) imaging may provide insight in tissue pharmacokinetics in relation to therapeutic effects. For some protein kinase inhibitors, such as [^{11}C]erlotinib PET, this approach already has shown clinical relevance (*9*). PET is a highly sensitive method to detect tracer concentrations in the body at the lower picomolar range (10^{-12} mol/L) (*10*). This enables the use of a microdose drug tracer, i.e. a drug dose < 1% of the expected pharmacologically active concentration, avoiding toxicity of the studied drug (*11*). The tracer ^{11}C-sorafenib has been developed without changing the molecular structure of the drug itself (*12*). In mice, ^{11}C-sorafenib PET showed tumor uptake in the RAF-expressing human renal cell carcinoma xenograft RXF393 (*12*).

The purpose of the present study was to explore whether ^{11}C-sorafenib uptake in tumors can be used as a potential biomarker for treatment efficacy. The primary objective was to assess whether microdose ^{11}C-sorafenib PET at baseline or a change in uptake after 14 days of treatment (steady state), could predict sorafenib concentrations after therapeutic dosing as measured in corresponding tumor biopsies. Secondary objectives were to investigate the effect of tumor perfusion on ^{11}C-sorafenib delivery and to assess the anti-angiogenic effects of sorafenib on tumor perfusion. Finally, ^{11}C-sorafenib

uptake and sorafenib concentrations in tumors, together with tumor perfusion (changes), were related to patient outcome.

MATERIALS AND METHODS

Study Design

This prospective exploratory study, with a planned sample size of n = 8, was conducted at the Amsterdam UMC, location VUmc, The Netherlands. Patients underwent dynamic microdose ^{11}C-sorafenib PET scans before ('baseline') and after two weeks of treatment with sorafenib 400 mg twice daily ('on treatment') when steady state levels of sorafenib were reached (*13*). Within 2 hours of the on treatment ^{11}C-sorafenib PET scan, a tumor biopsy and a venous blood sample were taken to measure (unlabeled) steady state sorafenib concentrations during therapy. Prior to each ^{11}C-sorafenib PET scan, a dynamic ^{15}O-H_2O PET scan was performed to measure tumor perfusion (Figure 1). For all patients, sorafenib treatment was continued until progressive disease, severe toxicity, or refusal by the patient.

Figure 1. Study design.

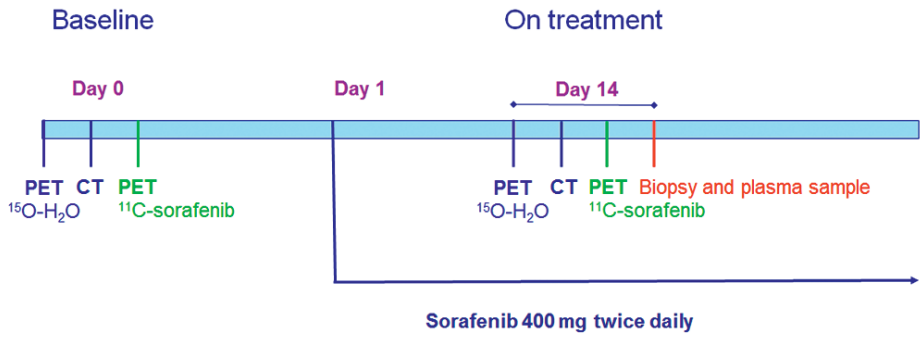

Patient Population

Adult patients with a histologically confirmed, metastatic solid malignancy accessible for tumor biopsy, who were eligible for standard palliative treatment with sorafenib, were included i.e. hepatocellular carcinoma, renal cell carcinoma and iodine-refractory differentiated thyroid carcinoma (other in- and exclusion criteria are shown in Supplement Table 1).

The study was approved by the Medical Ethics Review Committee of Amsterdam UMC, location VUmc (NCT02111889) and all subjects signed a written informed consent.

Tracer Synthesis

^{11}C-sorafenib and ^{15}O-H_2O were produced according to good manufacturing practice guidelines, as described previously (*12,14*). Carbon-11 was incorporated in the molecular structure of sorafenib at the terminal methylamide position.

PET Scanning

Scans were performed using a Gemini TF-64 PET-CT scanner (Philips Medical Systems, Best, The Netherlands) with an 18.4 cm axial field of view, divided into 45 contiguous planes. Patients received two venous catheters (for tracer injection and manual venous sampling, respectively) and an indwelling catheter in the radial artery for continuous arterial blood sampling during PET/CT. Patients were positioned supine on the scanner bed. Elastic body-restraining bandages were used to minimize movement during PET-CT scanning. A CT based topogram was performed to determine that both tumor and left ventricle were within the field of view of the scanner. Next, a 10 minutes dynamic scan was performed, starting at the time of an intravenous injection of ~370 MBq ^{15}O-H_2O (5 mL at a rate of 0.8 mL·sec^{-1}, followed by a 35 mL saline flush at a rate of 2.0 mL·sec^{-1}). Finally, a 60 minutes dynamic scan was acquired, starting at the time of an intravenous injection of ~370 MBq ^{11}C-sorafenib (5 mL at a rate of 0.8 mL·sec^{-1}, followed by a 35 mL saline flush at a rate of 2.0 mL·sec^{-1}). A 30 mAs low-dose CT scan was performed between ^{11}C-sorafenib and ^{15}O-H_2O dynamic PET scans for attenuation correction and segmentation purposes.

Using the three-dimensional row action maximum likelihood reconstruction algorithm (3D RAMLA), ^{15}O-H_2O scans were reconstructed into 26 frames with increasing duration (1 x 10, 8 x 5, 4 x 10, 2 x 15, 3 x 20, 2 x 30 and 6 x 60 s). ^{11}C-sorafenib scans were reconstructed into 36 frames (1 x 10, 8 x 5, 4 x 10, 3 x 20, 5 x 30, 5 x 60, 4 x 150, 4 x 300 and 2 x 600 sec). All data were normalized and corrected for dead time, decay, randoms, scatter and attenuation. Resulting PET images consisted of 128 x 128 x 90 isotropic voxels, with 4 x 4 x 4 mm^3 voxel size, and a final resolution of 5 mm FWHM.

Blood Sampling

During ^{15}O-H_2O and ^{11}C-sorafenib scans, arterial blood was withdrawn continuously at a rate of 300 mL·h^{-1} for the first five minutes and 150 mL·h^{-1} thereafter until the end of the scan, using an online detection system (Comecer, Joure, The Netherlands) (*15*). In addition, 7 mL arterial and venous samples were collected manually in lithium heparine containing tubes at 5, 7 and 9 minutes after injection of ^{15}O-H_2O and at 5, 10, 20, 30, 40 and 60 minutes after injection of ^{11}C-sorafenib. After each sample the line was flushed with 2 mL saline. These venous samples were used for measuring plasma-to-whole blood ratios, and for measuring plasma fractions of parent ^{11}C-sorafenib and

radiolabeled metabolites. The arterial samples were used for calibration of the continuous arterial input curve. Because of the invasive character of an arterial catheter, a non-invasive image derived input function (IDIF) was also investigated (Supplement Figure S1).

Blood Radioactivity Concentrations of Tracer and Metabolites
Whole blood and plasma radioactivity concentrations of the parent drug and its radiolabeled metabolites were determined in the blood samples using a well-counter, cross-calibrated against the PET scanner (Supplement Table S2).

Volume of Interest Definition
Volume of interests (VOIs) of tumor lesions were defined manually on low dose CT scans, avoiding large blood vessels and normal liver tissue. In addition to the complete tumor volume, a separate VOI was defined for the rim of each tumor lesion using 2 voxels from the outer border of the tumor contour for comparison with tracer uptake in the whole tumor VOI, as central tumor necrosis may affect tracer uptake. Next, low-dose CT VOIs were projected onto corresponding dynamic PET images to generate time-activity curves (TAC) for ^{11}C-sorafenib and ^{15}O-H_2O. In addition, VOIs were defined on normal organs for ^{11}C-sorafenib biodistribution (*16*).

Analysis of Tumor Perfusion
Tumor perfusion (F in mL/cm^3/min) was obtained by fitting each ^{15}O-H_2O TAC to the single-tissue compartment model in combination with the arterial input function, as described previously (*17*). This model was implemented in Matlab R2017B software (MathWorks, Natick, USA).

Biodistribution of ^{11}C-sorafenib in Healthy Tissues
The biodistribution of ^{11}C-sorafenib in healthy tissues was measured during the 40-60 minutes interval of the dynamic PET scan and expressed as the mean standardized uptake value (SUV_{mean}), which is routinely used for evaluating the biodistribution in normal tissues (*18*).

^{11}C-sorafenib Pharmacokinetics in Tumors
Tumor TACs derived from ^{11}C-sorafenib scans at baseline and after 14 days therapy were fitted to three different compartment models (i.e. 1-tissue, irreversible 2-tissue and reversible 2-tissue models) using the arterial plasma input function, corrected for radiolabeled metabolites. All models included a blood volume parameter to account for intravascular activity. The optimal model for describing the TAC data was selected based on Akaike Information and Schwartz Criteria (*19,20*).

Sorafenib Concentrations in Tumor and Plasma during Therapy

Using 14-16 Gauge biopsy needles, experienced intervention radiologists obtained tumor biopsies. In case of central necrosis, as seen on CT, samples were taken from the rim of the tumor. Samples were snap frozen within 1 minute of the biopsy, followed by storage under -80 °C conditions. Both plasma and tumor tissue samples were obtained within 2 hours of the on treatment ^{11}C-sorafenib PET scan. Liquid chromatography tandem mass spectrometry (LC-MS/MS) was used as a reference method to measure sorafenib concentrations, as described previously (*21*).

Safety and Response Evaluation

Safety evaluations were performed in all patients with grading of adverse events according to the National Cancer Institute Common Terminology Criteria for Adverse Events, version 4.0. Tumor response evaluation was performed every 2 months during sorafenib therapy according to Response Evaluation Criteria in Solid Tumors (RECIST) version 1.1 (*22*).

Statistical Analysis

Statistical analyses were performed using SPSS software for Windows version 22.0 (SPSS Inc. Chicago, USA). Tumor uptake of ^{11}C-sorafenib (both at baseline and on treatment PET scan) was compared with corresponding tumor and plasma sorafenib concentrations and with the calculated tumor-to-plasma concentration ratio of sorafenib after therapeutic dosing. PET measures are presented as mean ± SD. Correlations were explored using Spearman's correlation coefficient (r_s). The Wilcoxon signed rank test was used to compare PET measures before and after 14 days of sorafenib treatment, and to compare whole tumor and tumor rim values. A 2-tailed probability value of < 0.05 was considered significant.

RESULTS

Patient Characteristics

Eight patients were included (Table 1) between September 2013 and November 2015. There were no side effects during tracer injection or imaging procedures. Patients received 100% of the therapeutic dose during sorafenib treatment, except for patient 4. This patient had to end study participation within 2 weeks of treatment as a result of unexpected rapid clinical progression. In the other patients at least one contrast-enhanced CT scan was obtained for response evaluation. Five patients had progressive disease at first evaluation and two patients had stable disease for 20 and 44 weeks, respectively.

Table 1. Tumor and plasma sorafenib concentrations measured with LC-MS/MS and ^{11}C-sorafenib tumor V_T on day 0 and 14. DTC = differentiated thyroid carcinoma, RCC = renal cell carcinoma, HCC = hepatocellular carcinoma, PD = progressive disease, SD = stable disease.

Patient	Age (years)	Sex	Tumor	Biopsy site	Tumor (µg/L)	Plasma (µg/L)	Tumor-to-plasma ratio	V_T day 0	V_T day 14	Response
1	52	F	DTC	Skin	3390	6100	0.56	0.72	0.27	PD
2	55	M	RCC	Spleen	3480	4860	0.72	0.40	0.23	PD
3	59	M	RCC	Adrenal gland	5700	6880	0.83	0.33	0.11	SD
4	69	M	HCC	-	-	6180	-	1.52	-	PD
5	66	M	RCC	Lung	11750	9610	1.22	0.34	0.10	SD
6	60	F	RCC	Adrenal gland	3000	6490	0.46	2.11	0.71	PD
7	66	M	HCC	Liver	13400	6860	1.95	1.26	0.28	PD
8	59	M	RCC	Lung	13200	7550	1.75	0.14	0.26	PD

Figure 2. Biodistribution of ^{11}C-sorafenib in different healthy tissues and tumor tissue. PRE = baseline, POST = after 14 days of sorafenib therapy.

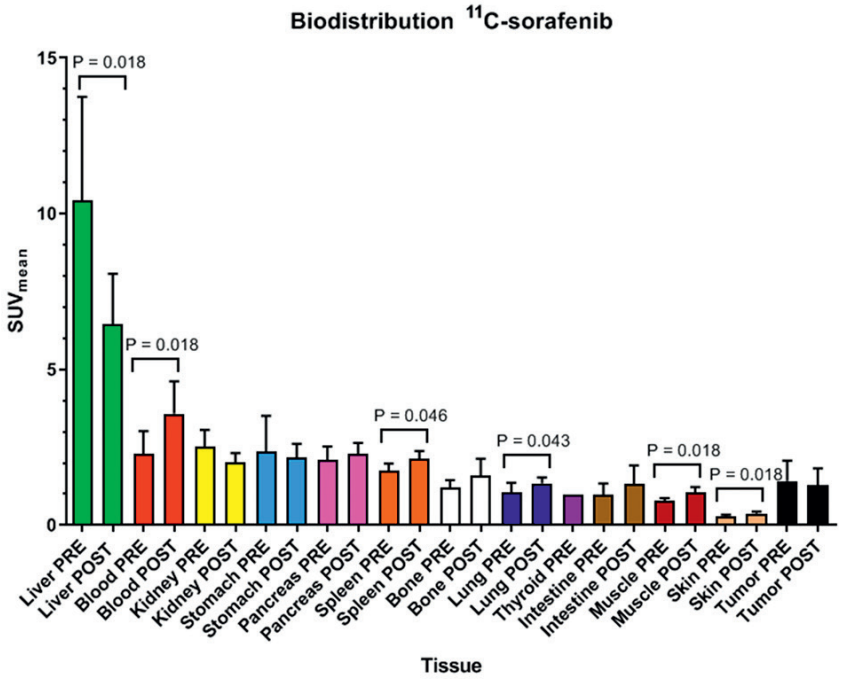

Biodistribution of ^{11}C-sorafenib

The highest ^{11}C-sorafenib accumulation was in the liver (SUV_{mean} 10.4 ± 3.3 at baseline and 6.4 ± 1.6 on treatment), whereas concentrations in skin were lowest (SUV_{mean} 0.3 ± 0.1 at baseline and 0.01 ± 0.01 on treatment) (Figure 2).

Comparison of ^{11}C-sorafenib uptake at baseline with that on treatment showed the largest differences in the liver with an SUV_{mean} decrease from 10.4 to 6.4 (P = 0.018) and in blood with an SUV_{mean} increase from 2.3 to 3.6 (P = 0.018).

No association was seen between the biodistribution of ^{11}C-sorafenib and treatment related toxicities.

Quantitative Analysis of ^{11}C-sorafenib Uptake in Tumors

A total of 15 lesions could be evaluated. Tumor volumes were highly variable, with a median size of 10 cm^3 and range of 4-2527 cm^3. Patient 4 only had a baseline ^{11}C-sorafenib scan due to early clinical deterioration.

A PET tracer dose of 347 ± 66 MBq (mean ± SD) ^{11}C-sorafenib was given with a specific activity of 35350 ± 9929 MBq/μmol sorafenib. As the molecular weight of sorafenib is 464.8 μg/μmol this corresponded with 4.9 ± 1.6 μg of unlabeled sorafenib. After injection, ^{11}C-sorafenib was quite stable, with only < 5% labeled metabolites formed during the 60 minutes scan. The reversible 2-tissue compartment model with four rate constants and additional blood volume parameter best described ^{11}C-sorafenib tumor kinetics (Supplement Figure S2). Therefore, the total volume of distribution (V_T) = $K_1/k_2*(1+k_3/k_4)$ was used as outcome parameter, which represents the tumor-to-plasma ratio of ^{11}C-sorafenib at equilibrium.

At baseline, 3/8 patients had a tumor V_T > 1, i.e. ^{11}C-sorafenib accumulation in the tumor was higher than in plasma (Figure 3). After 14 days of treatment, no patients were left with a tumor V_T > 1. Overall, tumor V_T values of ^{11}C-sorafenib were higher at baseline than at day 14 of treatment (0.68 ± 0.55 versus 0.29 ± 0.20, P = 0.007).

Figure 3. Fusion ^{11}C-sorafenib PET/CT (sum 40-60 min), low-dose CT and PET images from three patients showing ^{11}C-sorafenib uptake in tumor lesions (red arrows)). Patient A with hepatocellular carcinoma has a metastasis in the left costa 4, patient B with renal cell carcinoma has a metastasis in the left adrenal gland, and patient C with hepatocellular carcinoma has a large intra-abdominal metastasis. Physiologic uptake can be seen in the liver (white *) and kidneys (yellow Δ).

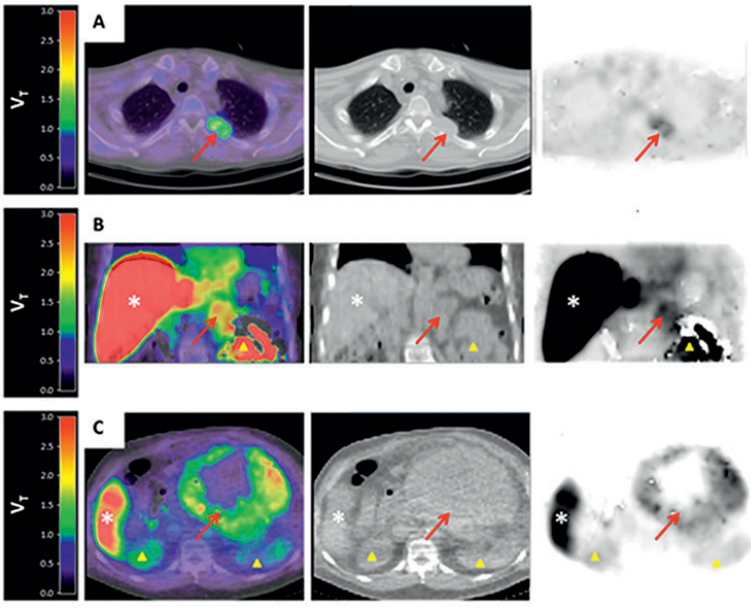

Figure 4. Tumor ^{11}C-sorafenib V_T on days 0 (A) and 14 (B) in lesions of patients with progressive (PD) and stable (SD) disease.

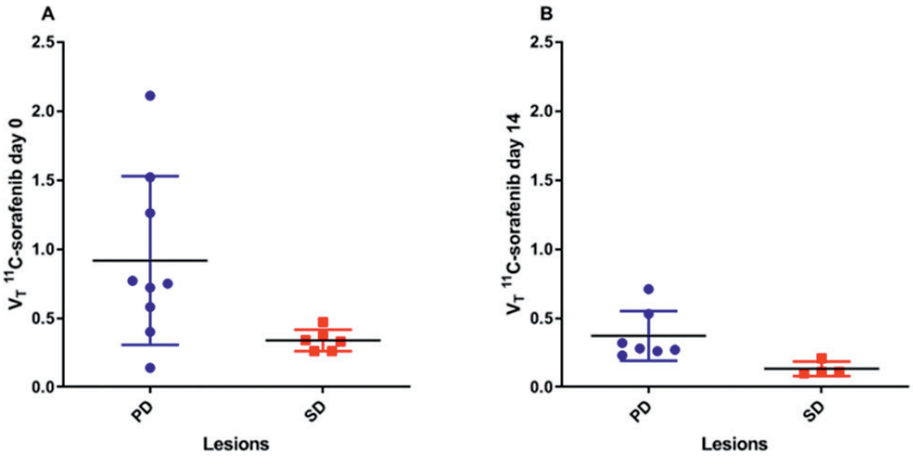

No significant differences in ^{11}C-sorafenib V_T were established between whole tumor and outer tumor rim (P = 0.944 at baseline and P = 0.138 at day 14). In addition, total tumor volume was not correlated with the amount of tracer uptake (r_s = 0.196, P = 0.483 at baseline and r_s = -0.134, P = 0.713 at day 14). Surprisingly, patients with clinical benefit had a lower tumor ^{11}C-sorafenib V_T in comparison to patients with progressive disease at baseline (0.34 ± 0.08 versus 0.92 ± 0.61) as well as after 14 days of treatment (0.13 ± 0.05 versus 0.37 ± 0.18) (Figure 4 A and 4B). In contrast, the percentage decrease in ^{11}C-sorafenib V_T between baseline and on treatment scans was not associated with clinical outcome (stable disease -58% ± 26% versus progressive disease -34% ± 55%).

Comparison of LC-MS/MS and ^{11}C-sorafenib PET Results

Sorafenib concentrations in tumor biopsies and plasma after two weeks of treatment as measured using LC-MS/MS are presented in Table 1. In plasma, the median sorafenib concentration was 6680 μg·L^{-1} (range: 4860-9610 μg·L^{-1}). The median sorafenib concentration in tumor biopsies was 5700 μg·L^{-1} (range: 3000-13400 μg·L^{-1}), which was lower than in plasma in 4 out of 8 patients. There was no correlation between plasma and tumor sorafenib concentrations (r_s = 0.607, P = 0.148). PET derived tumor ^{11}C-sorafenib V_T both at baseline and during therapy were not correlated with corresponding LC-MS/MS measured sorafenib concentrations in tumor biopsies (r_s = -0.429, P = 0.337 at baseline and r_s = -0.250, P = 0.589 at day 14) (Figure 5A). In addition, the calculated tumor-to-plasma concentration ratio of sorafenib after therapeutic dosing was not related to ^{11}C-sorafenib V_T (baseline as well as day 14 r_s = -0.357, P = 0.432) (Figure 5B). Also, the percentage difference of V_T between baseline

and on treatment PET were not correlated with sorafenib concentrations in tumor biopsies (r_s = -0.500, P = 0.267), nor with the calculated tumor-to-plasma concentration ratio of sorafenib after therapeutic dosing (r_s = -0.321, P = 0.498). Moreover, plasma and tumor concentrations of sorafenib measured with LC-MS/MS during treatment were not associated with treatment outcome (plasma concentrations: 8245 µg/L ± 1930 µg/L versus 6807 µg/L ± 1483 µg/L and tumor concentrations: 8725 µg/L ± 4278 µg/L versus 7294 µg/L ± 5486 µg/L for stable versus progressive disease, respectively).

Tumor Perfusion Effects Measured using ^{15}O-H_2O PET

Tumor perfusion, measured using ^{15}O-H_2O PET, at baseline could be compared with that after 14 days of treatment in five out of eight patients. In the other patients only one ^{15}O-H_2O PET scan was performed as a result of technical problems (n = 2) or early study dropout (n = 1). Higher perfusion of the tumor rim at baseline and after 14 days of treatment was associated with higher ^{11}C-sorafenib V_T in the tumor (baseline r_s = 0.671, P = 0.020 and day 14 r_s = 0.641, P = 0.025), (Figure 6A). However, no significant correlation between ^{11}C-sorafenib uptake and total tumor perfusion at baseline and after 14 days of treatment was observed (baseline r_s = 0.574, P = 0.056 and day 14 r_s = 0.485, P = 0.058).

Analysis of tumor perfusion and clinical response revealed that patients with stable disease had larger decrease in total tumor perfusion (56% ± 23%) after 14 days of sorafenib treatment than patients with progressive disease (18% ± 32%) (Figure 6B).

Figure 5. Correlation between tumor ^{11}C-sorafenib V_T values and the tumor sorafenib concentrations (A) and sorafenib tumor-to-plasma ratio (B) measured with LC-MS/MS.

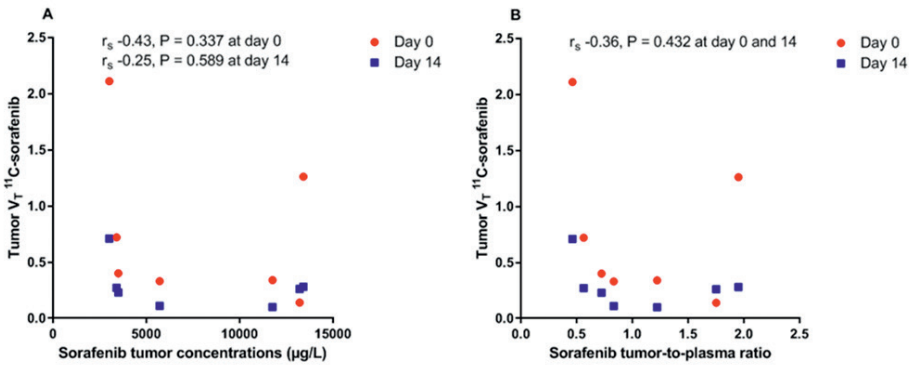

Figure 6. Correlation between tumor V_T values of ^{11}C-sorafenib and perfusion of the tumor rim (A). Tumor perfusion difference after 14 days of sorafenib treatment in patients with PD and SD (B).

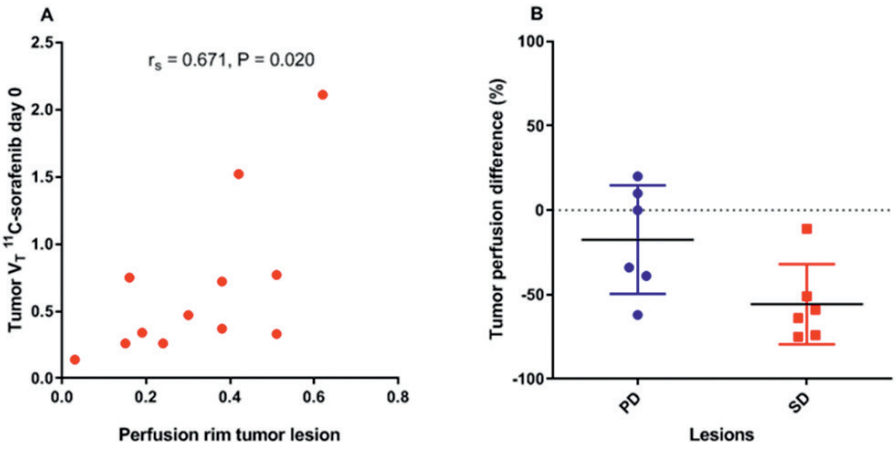

DISCUSSION

To the best of our knowledge, this is the first clinical study directly comparing tracer uptake with drug concentrations after therapeutic dosing measured with LC-MS/MS in corresponding tumor biopsies. In contrast to expectations, this study showed that sorafenib concentrations in tumors during treatment could not be predicted by microdose ^{11}C-sorafenib PET. Both LC-MS/MS and PET are very accurate for the quantification of drug concentrations, with low test-retest variability in the range of 5-10% (*10,21,23,24*). However, there are biopsy and tracer dependent factors that may explain the observed discrepancies between LC-MS/MS and PET.

Biopsies only provide one sample of the tumor lesion. In case of intratumor heterogeneity this may lead to an under- or overestimation of sorafenib concentrations in the whole tumor. Overall, no significant intralesional heterogeneity of ^{11}C-sorafenib uptake between the whole tumor and its outer rim was established in this study. However, in larger tumors, regional differences in ^{11}C-sorafenib uptake were seen (Figure 3), supporting sample effects as a potential contributing factor to the discrepancies observed between LC-MS/MS and PET.

Another reason for discrepancies between LS/MS-MS and PET may be tracer dependent. Linearity in tumor pharmacokinetics, in other words dose proportionality, between microdose ^{11}C-sorafenib and standard dose sorafenib

therapy was not observed in this study (Table 1). Non-linearity has been reported in 27% of the ascending drug dose studies by comparison of plasma drug concentrations, which can be due to the levels of drug transporters, metabolic enzymes and drug-target occupation (*25,26*).

First, drug transporting systems may become (partially) saturated after (prolonged) exposure to therapy in comparison to the tracer dose. Sorafenib is a substrate for organic anion and cation transporters, but uptake mostly depends on passive diffusion into cells (*27,28*). In addition, sorafenib is a substrate for efflux transporters, in particular breast cancer resistance protein (BCRP/ABCG2) and P-glycoprotein (P-gp/ABCB1). Sorafenib has demonstrated capacity to inhibit BCRP and P-gp in a dose-dependent manner (*29,30*). This could potentially result in less tumor efflux of higher concentrations sorafenib. However, the affinity of sorafenib for these efflux transporters has shown to be weak and therefore tumor accumulation is not likely influenced by transporter-mediated alterations (*27*). The ^{11}C-sorafenib V_T in this study, which did not increase after 14 days of treatment, was consistent with this (Table 1).

Second, sorafenib is metabolized in the liver by uridine diphosphoglucose-glucuronosyltransferase 1A9 (UGT1A9) to sorafenib glucuronide and by CYP3A4 to the active metabolite sorafenib N-oxide (*31*). Saturation of these enzymes could add to the non-linearity. ^{11}C-sorafenib accumulated predominantly in the liver, however metabolite release to the bloodstream was very low (< 5%) as a result of rapid biliary excretion (*31*). Although therapeutic administration of sorafenib significantly reduced tracer uptake in the liver (P = 0.018) and increased available ^{11}C-sorafenib in the blood pool (P = 0.018), this did not result in increased tumor accumulation of ^{11}C-sorafenib after 14 days. In fact, tracer uptake decreased in most tumor lesions at day 14 (P = 0.007), most probably caused by competition of the microdose with the much higher concentrations of unlabeled sorafenib after therapeutic dosing.

Finally, another potential cause for the different results between tracer uptake and sorafenib concentrations after therapy may consist of the complex drug-target binding characteristics of this multikinase inhibitor with fast reversible as well as slow (ir)reversible target binding sites. Previously, the target binding kinetics of sorafenib have shown to be slower than for sunitinib and lenvatinib for example and therefore the 1 hour scanning time may have been too short to reflect drug-target occupation after 14 days of continuous sorafenib treatment (*32,33*). Overall, sorafenib showed low accumulation in tumors. A recent study in mice also demonstrated that sorafenib had significantly less intratumoral drug accumulation in comparison with other anti-angiogenic drugs (*8*), which may in part be attributed to sorafenib 's higher protein bound fraction in blood

(> 99%) and its strong binding affinity for albumin, as it is assumed that only the free (unbound) drug can induce a pharmacologic effect (*34,35*). In only 3 of the 8 patients ^{11}C-sorafenib accumulation was higher in tumors than in plasma, which was correlated with increased perfusion of the tumor rim (for the whole tumor this was only borderline significant, presumably a result of central tumor necrosis).

Higher ^{11}C-sorafenib accumulation in tumors at baseline or after 14 days of sorafenib treatment was not related with treatment benefit. On the contrary, clinical benefit was associated with lower ^{11}C-sorafenib uptake in tumors, which may be a result of the lower tumor perfusion observed in these patients. This is a prognostic rather than a predictive imaging finding and in line with previous studies showing that higher expression of pro-angiogenic factors such as VEGF and VEGFR 1-3 and increased tumor vascularity were associated with poorer prognosis in patients with hepatocellular carcinoma, renal cell carcinoma and follicular thyroid carcinoma (*36-39*). Some other microdose drug tracers, such as ^{11}C-erlotinib and ^{11}C-docetaxel, showed that higher tracer accumulation in tumors was in fact correlated with treatment benefit (*9,40*). The tracer signal of ^{11}C-sorafenib is more complex as it binds to multiple pharmacological targets with different affinity and the signal may be dominated by some targets, while other targets with less affinity may lead to stronger anti-tumor effects and these target effects may also differ between different tumor types (*41,42*). In addition, neither LC-MS/MS measured sorafenib concentrations in plasma nor tumor biopsies during therapy were useful predictors of clinical response in this exploratory study. Possibly, because the current tumor concentrations achieved with sorafenib therapy already induce sufficient protein kinase inhibition (*42*). However, another explanation may be that tumor concentrations reached with the current therapeutic schedule are in fact too low, resulting in overall marginal clinical activity. Consequently, even higher tumor concentrations may be necessary to improve the anti-cancer effects of sorafenib. Preclinical and clinical studies have indeed shown that higher levels of sorafenib exposure, in comparison with the levels reached with standard sorafenib dosing, are associated with improved anti-tumor activity, but dose escalation is limited by the toxicity of sorafenib (*43-45*).

The current exploratory study showed preliminary evidence for the value of ^{15}O-H_2O PET in early response prediction to sorafenib treatment. After only 2 weeks of treatment, tumor blood flow decreased more in patients with clinical benefit as compared with patients with progressive disease (56 versus 18%). Although these results are limited by the small cohort size of this study, it is in line with other angiogenesis inhibitors. For example, early reduction in tumor perfusion as shown with ^{15}O-H_2O PET was also associated with clinical benefit in

patients treated with bevacizumab and sunitinib (*46,47*). Thus, early decrease in tumor perfusion may have predictive value for outcome of sorafenib treatment. Given the potential benefit for patients of early response prediction, this finding warrants further investigation.

CONCLUSION

In conclusion, microdose ^{11}C-sorafenib PET was not useful for the prediction of intratumoral sorafenib concentrations during treatment measured with LC-MS/MS. However, there was preliminary evidence for an association between a decrease in tumor perfusion after only 2 weeks of sorafenib therapy and clinical benefit. This warrants further investigation to assess its value as an early biomarker for sorafenib efficacy.

Acknowledgements
We thank the patients who participated in this study and their families.

Financial support
Roche Innovation Fund (WP28389).

Disclosure
no potential conflicts of interest relevant to this article exist.

SUPPLEMENTAL MATERIAL

Supplement table S1. In- and exclusion criteria

Inclusion Criteria	Exclusion Criteria
- Eastern Cooperative Oncology Group performance status 0-2 - One or more extrahepatic tumor lesion(s) measurable according to RECIST version 1.1 (19) - Hemoglobin > 6.0 mmol/L - Absolute neutrophil count (ANC) > 1.5 x 10*9/L - Platelet count ≥ 100 x 10*9/L - Total bilirubin < 2 times the upper limit of normal (ULN) - Alanine aminotransferase (ALT) and aspartate aminotransferase (AST) < 2.5 x ULN or < 5x ULN in case of liver metastases (except for patients with hepatocellular carcinoma, then Child Pugh classification A-B) - Serum creatinine eGFR ≥ 50 mL/min	- Evidence of serious uncontrolled concomitant disease (such as infections, cardiovascular, pulmonary, skin and central nervous system diseases) - Major surgery < 28 - Thromboembolic events < 3 months

Supplement table S2. Method to measure blood ^{11}C-sorafenib concentrations and metabolites

Method
- For ^{11}C-sorafenib, whole blood (0.5 mL) was weighed in duplicate and after centrifuging (5 minutes; 7°C; 4000 rpm) - Plasma was collected and 0.5 mL was weighed in duplicate - Solid phase extraction and high performance liquid chromatography (HPLC) were used to separate parent compound and radiolabeled metabolites and determine their fractions in the samples. Therefore, 1 mL plasma was diluted with 2 mL 0.15M HCl and transferred to a Waters Sep-Pak tC18 SPE column. The cartridge was washed with 5 mL of water and eluted with 1.5 mL of methanol - This eluate was injected onto a Phenomenex Luna C18 5 µm 250 x 10 mm with a flow of 4 mL·min-1. The gradient system was a mixture of acetonitrile (A) and 0.1% trifluoroacetic acid (B) and was programmed as follows: t = 0 min 90% B, t = 9 min 20% B, t = 12 min 20% B, t = 15 min 90% B - Fractions were collected and measured for radioactivity with a gamma-counter to generate an HPLC profile for ^{11}C-sorafenib and its labeled metabolites, respectively

Supplement figure S1. Correlation between tumor V_T values of ^{11}C-sorafenib derived from the arterial blood sampler input function (BSIF) and those obtained using the less invasive image derived input function (IDIF). A VOI of 12 voxels in 3 planes was drawn in the left ventricle of the heart to measure ^{11}C-sorafenib concentrations in the blood pool to serve as IDIF. IDIFs were corrected for calibration, plasma to whole blood ratios and metabolites using the manual venous samples similarly to BSIF with arterial samples as described above. The non-invasive IDIF showed excellent correlation with the arterial BSIF, therefore IDIF can be used as a non-invasive alternative of BSIF to measure ^{11}C-sorafenib V_T in tumor lesions.

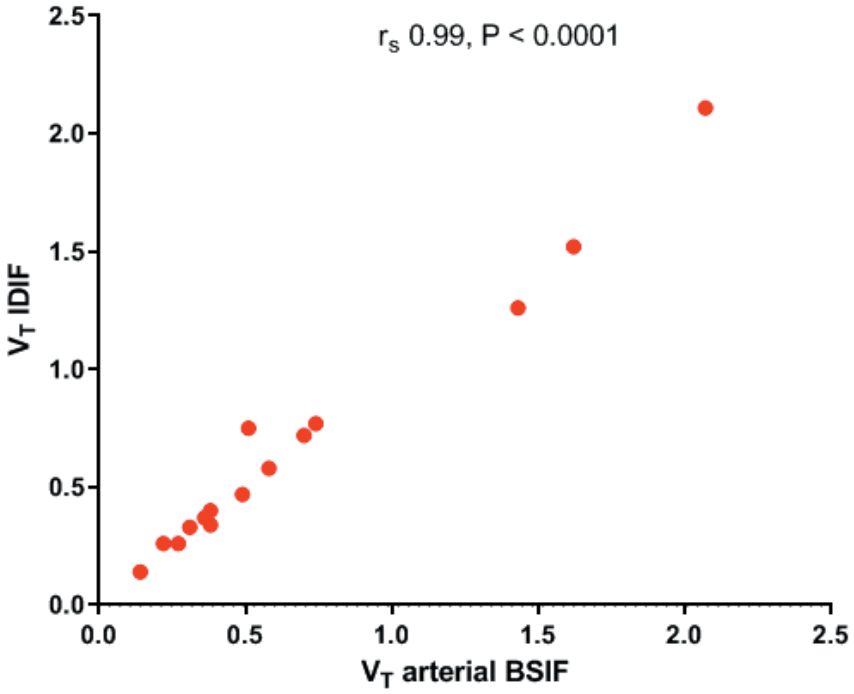

Supplement figure S2. Schematic diagram of the most frequently used compartment models: the single tissue compartment model (A), the irreversible two tissue compartment model (B) and the reversible two tissue compartment model (C). K_1 represents transport from plasma to tissue and k_2 from tissue to plasma and; k_3 and k_4 describe the exchange between free and bound tissue fractions. Typical ^{11}C-sorafenib tumor time-activity curves (blue circles) are fitted to plasma input (red line) according to these three models (green lines) and are shown for the peaks (0-8 minutes) and the complete time-activity curves (0-60 minutes). Akaike and Schwartz criteria showed preference for the reversible two tissue compartment model in 68% of the tumor lesions, as compared with 25% for the 1-tissue model and 7% for the irreversible 2-tissue model.

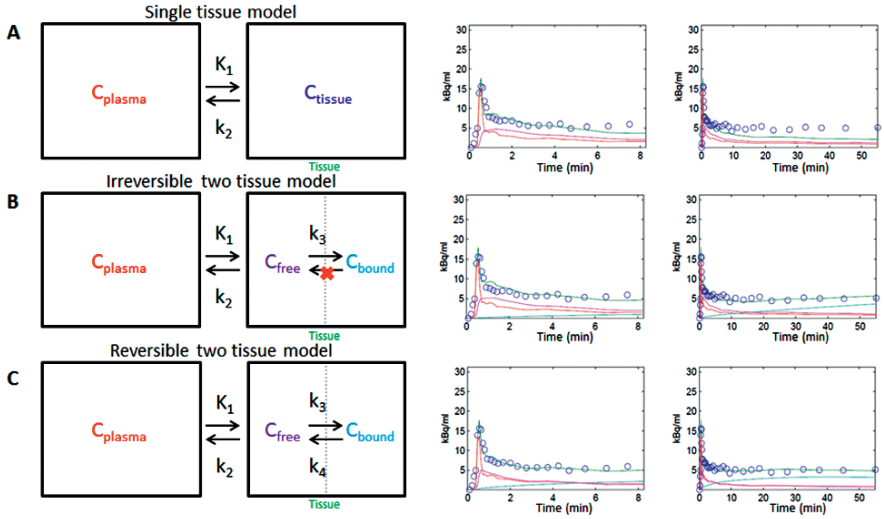

REFERENCES

1. Rapp UR, Goldsborough MD, Mark GE, et al. Structure and biological activity of v-raf, a unique oncogene transduced by a retrovirus. *Proc Natl Acad Sci U S A*. 1983;80:4218-4222.
2. Wilhelm S, Carter C, Lynch M, et al. Discovery and development of sorafenib: a multikinase inhibitor for treating cancer. *Nat Rev Drug Discov*. 2006;5:835-844.
3. Gotink KJ, Verheul HM. Anti-angiogenic tyrosine kinase inhibitors: what is their mechanism of action? *Angiogenesis*. 2010;13:1-14.
4. Wilhelm SM, Adnane L, Newell P, Villanueva A, Llovet JM, Lynch M. Preclinical overview of sorafenib, a multikinase inhibitor that targets both Raf and VEGF and PDGF receptor tyrosine kinase signaling. *Mol Cancer Ther*. 2008;7:3129-3140.
5. Escudier B, Eisen T, Stadler WM, et al. Sorafenib for treatment of renal cell carcinoma: Final efficacy and safety results of the phase III treatment approaches in renal cancer global evaluation trial. *J Clin Oncol*. 2009;27:3312-3318.
6. Llovet JM, Ricci S, Mazzaferro V, et al. Sorafenib in advanced hepatocellular carcinoma. *N Engl J Med*. 2008;359:378-390.
7. Brose MS, Nutting CM, Jarzab B, et al. Sorafenib in radioactive iodine-refractory, locally advanced or metastatic differentiated thyroid cancer: a randomised, double-blind, phase 3 trial. *Lancet*. 2014;384:319-328.
8. Torok S, Rezeli M, Kelemen O, et al. Limited Tumor Tissue Drug Penetration Contributes to Primary Resistance against Angiogenesis Inhibitors. *Theranostics*. 2017;7:400-412.
9. Bahce I, Smit EF, Lubberink M, et al. Development of [(11)C]erlotinib positron emission tomography for in vivo evaluation of EGF receptor mutational status. *Clin Cancer Res*. 2013;19:183-193.
10. Cunningham VJ, Pike VW, Bailey D, et al. A method of studying pharmacokinetics in man at picomolar drug concentrations. *Br J Clin Pharmacol*. 1991;32:167-172.
11. Mammatas LH, Verheul HM, Hendrikse NH, Yaqub M, Lammertsma AA, Menke-van der Houven van Oordt CW. Molecular imaging of targeted therapies with positron emission tomography: the visualization of personalized cancer care. *Cell Oncol (Dordr)*. 2015;38:49-64.
12. Poot AJ, van der Wildt B, Stigter-van Walsum M, et al. [(1)(1)C]Sorafenib: radiosynthesis and preclinical evaluation in tumor-bearing mice of a new TKI-PET tracer. *Nucl Med Biol*. 2013;40:488-497.
13. Strumberg D, Clark JW, Awada A, et al. Safety, pharmacokinetics, and preliminary antitumor activity of sorafenib: a review of four phase I trials in patients with advanced refractory solid tumors. *Oncologist*. 2007;12:426-437.
14. Jackson JR, Dembowski BS, Ehrenkaufer RL, McIntyre E, Reivich M. [15O]H2O, [15O]O2 and [15O]CO gas production, monitoring and quality control system. *Appl Radiat Isot*. 1993;44:631-634.
15. Boellaard R, van Lingen A, van Balen SC, Hoving BG, Lammertsma AA. Characteristics of a new fully programmable blood sampling device for monitoring blood radioactivity during PET. *Eur J Nucl Med*. 2001;28:81-89.
16. Jansen BHE, Kramer GM, Cysouw MCF, et al. Healthy Tissue Uptake of (68)Ga-Prostate-Specific Membrane Antigen, (18)F-DCFPyL, (18)F-Fluoromethylcholine, and (18)F-Dihydrotestosterone. *J Nucl Med*. 2019;60:1111-1117.

17. de Langen AJ, Lubberink M, Boellaard R, et al. Reproducibility of tumor perfusion measurements using 15O-labeled water and PET. *J Nucl Med.* 2008;49:1763-1768.
18. Ilhan H, Lindner S, Todica A, et al. Biodistribution and first clinical results of (18) F-SiFAlin-TATE PET: a novel (18)F-labeled somatostatin analog for imaging of neuroendocrine tumors. *Eur J Nucl Med Mol Imaging.* 2020;47:870-880.
19. Akaike H. A new look at the statistical model identification. *IEEE transactions on automatic control.* 1974;19:716-723.
20. Schwarz G. Estimating the dimension of a model. *The annals of statistics.* 1978;6:461-464.
21. Honeywell R, Yarzadah K, Giovannetti E, et al. Simple and selective method for the determination of various tyrosine kinase inhibitors used in the clinical setting by liquid chromatography tandem mass spectrometry. *J Chromatogr B Analyt Technol Biomed Life Sci.* 2010;878:1059-1068.
22. Eisenhauer EA, Therasse P, Bogaerts J, et al. New response evaluation criteria in solid tumours: revised RECIST guideline (version 1.1). *Eur J Cancer.* 2009;45:228-247.
23. Widmer N, Bardin C, Chatelut E, et al. Review of therapeutic drug monitoring of anticancer drugs part two--targeted therapies. *Eur J Cancer.* 2014;50:2020-2036.
24. Lammertsma AA. Forward to the Past: The Case for Quantitative PET Imaging. *J Nucl Med.* 2017;58:1019-1024.
25. Bergstrom M. The Use of Microdosing in the Development of Small Organic and Protein Therapeutics. *J Nucl Med.* 2017;58:1188-1195.
26. Bosgra S, Vlaming ML, Vaes WH. To Apply Microdosing or Not? Recommendations to Single Out Compounds with Non-Linear Pharmacokinetics. *Clin Pharmacokinet.* 2016;55:1-15.
27. Hu S, Chen Z, Franke R, et al. Interaction of the multikinase inhibitors sorafenib and sunitinib with solute carriers and ATP-binding cassette transporters. *Clin Cancer Res.* 2009;15:6062-6069.
28. Honeywell R, Hitzerd S, Kathmann I, J Peters G. Transport of six tyrosine kinase inhibitors: active or passive? *ADMET and DMPK.* 2016;4:23-34.
29. Wei Y, Ma Y, Zhao Q, et al. New use for an old drug: inhibiting ABCG2 with sorafenib. *Mol Cancer Ther.* 2012;11:1693-1702.
30. Gnoth MJ, Sandmann S, Engel K, Radtke M. In vitro to in vivo comparison of the substrate characteristics of sorafenib tosylate toward P-glycoprotein. *Drug Metab Dispos.* 2010;38:1341-1346.
31. Vasilyeva A, Durmus S, Li L, et al. Hepatocellular Shuttling and Recirculation of Sorafenib-Glucuronide Is Dependent on Abcc2, Abcc3, and Oatp1a/1b. *Cancer Res.* 2015;75:2729-2736.
32. Okamoto K, Ikemori-Kawada M, Jestel A, et al. Distinct binding mode of multikinase inhibitor lenvatinib revealed by biochemical characterization. *ACS Med Chem Lett.* 2015;6:89-94.
33. Neumann L, von Konig K, Ullmann D. HTS reporter displacement assay for fragment screening and fragment evolution toward leads with optimized binding kinetics, binding selectivity, and thermodynamic signature. *Methods Enzymol.* 2011;493:299-320.
34. Villarroel MC, Pratz KW, Xu L, Wright JJ, Smith BD, Rudek MA. Plasma protein binding of sorafenib, a multi kinase inhibitor: in vitro and in cancer patients. *Invest New Drugs.* 2012;30:2096-2102.

35. Zhang D, Hop C, Patilea-Vrana G, et al. Drug Concentration Asymmetry in Tissues and Plasma for Small Molecule-Related Therapeutic Modalities. *Drug Metab Dispos.* 2019;47:1122-1135.
36. Toyoda H, Kumuda T, Nakano S, et al. Significance of tumor vascularity as a predictor of long-term prognosis in patients with small hepatocellular carcinoma treated by percutaneous ethanol injection therapy. *J Hepatol.* 1997;26:1055-1062.
37. Iakovlev VV, Gabril M, Dubinski W, et al. Microvascular density as an independent predictor of clinical outcome in renal cell carcinoma: an automated image analysis study. *Lab Invest.* 2012;92:46-56.
38. Wong NA, Willott J, Kendall MJ, Sheffield EA. Measurement of vascularity as a diagnostic and prognostic tool for well differentiated thyroid tumours: comparison of different methods of assessing vascularity. *J Clin Pathol.* 1999;52:593-597.
39. Rini BI, Michaelson MD, Rosenberg JE, et al. Antitumor activity and biomarker analysis of sunitinib in patients with bevacizumab-refractory metastatic renal cell carcinoma. *J Clin Oncol.* 2008;26:3743-3748.
40. van der Veldt AA, Lubberink M, Mathijssen RH, et al. Toward prediction of efficacy of chemotherapy: a proof of concept study in lung cancer patients using [(1)(1)C] docetaxel and positron emission tomography. *Clin Cancer Res.* 2013;19:4163-4173.
41. Karaman MW, Herrgard S, Treiber DK, et al. A quantitative analysis of kinase inhibitor selectivity. *Nat Biotechnol.* 2008;26:127-132.
42. Labots M, Pham TV, Honeywell RJ, et al. Kinase Inhibitor Treatment of Patients with Advanced Cancer Results in High Tumor Drug Concentrations and in Specific Alterations of the Tumor Phosphoproteome. *Cancers (Basel).* 2020;12.
43. Escudier B, Szczylik C, Hutson TE, et al. Randomized phase II trial of first-line treatment with sorafenib versus interferon Alfa-2a in patients with metastatic renal cell carcinoma. *J Clin Oncol.* 2009;27:1280-1289.
44. Wang X, Zhang L, Goldberg SN, et al. High dose intermittent sorafenib shows improved efficacy over conventional continuous dose in renal cell carcinoma. *J Transl Med.* 2011;9:220.
45. Mammatas LH, Zandvliet AS, Rovithi M, et al. Sorafenib administered using a high-dose, pulsatile regimen in patients with advanced solid malignancies: a phase I exposure escalation study. *Cancer Chemother Pharmacol.* 2020.
46. de Langen AJ, van den Boogaart V, Lubberink M, et al. Monitoring response to antiangiogenic therapy in non-small cell lung cancer using imaging markers derived from PET and dynamic contrast-enhanced MRI. *J Nucl Med.* 2011;52:48-55.
47. Scott AM, Mitchell PL, O'Keefe G, et al. Pharmacodynamic analysis of tumour perfusion assessed by 15O-water-PET imaging during treatment with sunitinib malate in patients with advanced malignancies. *EJNMMI Res.* 2012;2:31.

CHAPTER 5

Sorafenib administered using a high-dose, pulsatile regimen in patients with advanced solid malignancies: *a phase I exposure escalation study*

Lemonitsa H. Mammatas, Anthe S. Zandvliet, Maria Rovithi, Richard J. Honeywell, Eleonora L. Swart, Godefridus J. Peters, C. Willemien Menke-van der Houven van Oordt, Henk M.W. Verheul

Published in: Cancer Chemother Pharmacol. 2020;85:931-40

ABSTRACT

Background: (Pre)clinical evidence is accumulating that intermittent exposure to increased doses of protein kinase inhibitors may improve their treatment benefit. In this phase I trial, the safety of high-dose, pulsatile sorafenib was studied.

Patients and Methods: High-dose sorafenib was administered once weekly in exposure escalation cohorts according to a 3+3 design. Drug monitoring was performed in weeks 1-3 and doses were adjusted to achieve a predefined target plasma Area Under the Curve (AUC)(0-12h). The effect of low gastric pH on improving sorafenib exposure was investigated by intake of the acidic beverage cola.

Results: Seventeen patients with advanced malignancies without standard treatment options were included. Once weekly, high-dose sorafenib exposure was escalated up to a target AUC(0-12h) of 125-150 mg/L/h, achieving a ~2-fold higher C_{max} compared to standard continuous dosing. Dose limiting toxicity was observed in 3 patients: grade 3 duodenal perforation (2800 mg sorafenib), grade 5 multiorgan failure (2800 mg sorafenib) and grade 5 biliary tract perforation (3600 mg sorafenib). The mean difference between observed and target AUC(0-12h) was 45% (SD±56%) in week 1 using a fixed starting dose of sorafenib compared to 2% (SD±32%) in week 3 as a result of drug monitoring (P=0.06). Dissolving sorafenib in cola, instead of water, did not improve sorafenib exposure. Clinical benefit with stable disease as best response was observed in two patients.

Conclusion: Treatment with high-dose, once weekly sorafenib administration resulted in dose limiting toxicity precluding dose escalation above the exposure cohort of 125-150 mg/L/h. Drug monitoring was a successful strategy to pursue a target exposure.

INTRODUCTION

Sorafenib is an oral multikinase inhibitor, originally developed as an inhibitor of RAF kinases [1]. Besides activity against C-RAF, B-RAF and mutant B-RAF, it also inhibits vascular endothelial growth factor receptors 1, 2 and 3, platelet derived growth factor receptor β, FMS-like tyrosine kinase 3, c-Kit protein and RET receptor tyrosine kinase at low concentrations [2]. At high intracellular concentrations, sorafenib has affinity for multiple other kinases [3]. Sorafenib is currently approved for the treatment of renal cell carcinoma, hepatocellular carcinoma and iodine refractory thyroid cancer at a standard fixed dose of 400 mg twice daily in a continuous schedule [4-7]. However, at this standard fixed dose large interpatient variability in drug exposure was demonstrated after both single and multiple doses [8].

Increased sorafenib exposure is associated with improved efficacy [9, 10]. Dose-escalation of sorafenib to 600 mg twice daily after failure of standard dosing in patients with progressive renal cell carcinoma resulted in tumor reduction in 42% of the patients [9]. In addition, intrapatient dose-escalation in patients without substantial toxicity showed that a higher area under the concentration-time curve (AUCmax > 100 mg/L/h) of sorafenib was associated with longer progression free survival (PFS) [10]. Unfortunately, toxicity limits further dose escalation of the continuous schedule [8].

An alternative approach to achieve high exposure, with less toxicity, may be high-dose, pulsatile administration of protein kinase inhibitors [11, 12]. Recently we showed promising preclinical and clinical benefit of an alternative high-dose treatment regimen of sunitinib [13]. Also, promising preclinical results for high-dose sorafenib were reported. In mice bearing 789-O renal cell carcinoma xenografts such a schedule exhibited increased reduction of tumor perfusion and microvessel density as well as slower tumor growth in comparison to continuous conventional dosing [14].

An important challenge for optimizing high-dose sorafenib administration is the amount of drug absorption in the gastro-intestinal tract. Sorafenib absorption is saturable > 800 mg/day in a daily continuous schedule. However, a moderate fat meal (in comparison to a high fat meal of ≥ 50% fat) and multiple divided doses per day have shown to improve the absorption of sorafenib by 30% and 50%, respectively [15, 16]. The influence of gastric pH on the absorption of sorafenib is less clear, although the solubility of sorafenib increases with decreasing pH and ranges from 0.034 mg/100 mL at pH 1.0 to 0.013 mg/100 mL at pH 4.5 [17-19]. Thus, the administration of an acidic beverage such as classic cola, with a pH of 2.5, could potentially improve sorafenib absorption and bioavailability [20, 21].

Based on these considerations we initiated a clinical phase I study with high-dose, pulsatile sorafenib. Weekly pulses of high sorafenib exposure over a 12 hour window (AUC(0-12h) were pursued in an attempt to improve clinical efficacy. To overcome saturation of absorption we applied dose fractioning (portions of 200-400 mg administered at 2 hour intervals), a standardized moderate fat diet, and investigated the effect of cola on sorafenib bioavailability. Sorafenib exposure was determined during 12 hours following ingestion of the last dose fraction. Finally, administration of the same dose was anticipated to result in large variability in sorafenib plasma AUC(0-12h) per patient [8]. Therefore, drug monitoring was performed during week 1-3 to titrate the patients individual dose based on the sorafenib plasma AUC(0-12h) according to exposure escalation cohorts [22].

PATIENTS AND METHODS

Patient Selection

Eligible were patients with a pathologically confirmed solid malignancy refractory to standard therapy or for whom no standard therapy existed. Patients had to be ≥ 18 years of age with an Eastern Cooperative Oncology Group Performance of ≤ 1. Required laboratory values at entry included hemoglobin ≥ 5.6 mmol/L, absolute neutrophil count ≥ 1.5 x 10*9/l, platelet count ≥ 100 x 10*9/l, total bilirubin ≤ 1.5 times the upper limit of normal (ULN), ALT and AST ≤ 2.5 x ULN (in case of liver metastases: ≤ 5 times ULN), serum creatinine ≤ 1.5 x ULN or creatinine clearance ≥ 50 ml/min (based on MDRD), albumin > 25 g/L, PT-INR/PTT < 1.5 x ULN (unless coumarin derivatives were used), activated partial thromboplastin time < 1.25 x ULN.

The main exclusion criteria were other anticancer therapies within 4 weeks (6 weeks for nitrosoureas and mitomycin C); evidence of serious uncontrolled concomitant disease (such as cardiovascular disease, nervous system disease, pulmonary disease, gastrointestinal disorders or active bacterial, viral, fungal or mycobacterial infections); uncontrollable hypertension (> 160/95 mmHg), prior radiotherapy on the abdominal or thoracic area or on > 3 vertebrae; major surgery within 4 weeks; pregnancy or breast feeding. If applicable, patients were required to take contraceptive precautions while on the trial and for 6 months afterwards.

All patients gave written informed consent before study entry and the local medical ethics committee of the Amsterdam UMC, location VUmc (Medisch Ethische Toetsingscommissie VUmc), approved the study. The study (NCT02636426) was conducted in accordance with the Declaration of Helsinki and Good Clinical Practice guidelines.

Study design and treatment plan
This single center phase I study was conducted at the Amsterdam UMC, location VUmc, the Netherlands. High-dose sorafenib was administered once weekly in exposure escalation cohorts that consisted of 3-6 patients using a standard 3 + 3 design. Drug monitoring was performed in weeks 1-3 and doses were adjusted a maximum of 2 times if necessary, to achieve the predefined target plasma AUC(0-12h) of the cohort. The starting exposure level was 25-50 mg/L/h, analogous to the continuous schedule [23], and was escalated in subsequent cohorts with increments of 25 mg/L/h.

The primary objective was to investigate the maximum tolerated plasma AUC(0-12h) of high-dose, pulsatile sorafenib and its safety and tolerability. Secondary objectives were (1) the pharmacokinetic behavior, (2) the influence of cola on sorafenib exposure, (3) the feasibility of drug monitoring to achieve the target plasma AUC(0-12h) and (4) preliminary evidence of improved anticancer activity with high-dose pulsatile sorafenib treatment of this alternative sorafenib treatment strategy.

The total weekly dose sorafenib was divided in portions of 200-400 mg and given every 2 hours to prevent saturation of absorption and to result in a high plasma peak concentration at the end of all ingested portions. Each dose was dissolved in either a large glass of water or classic Coca-Cola (the Coca-Cola Company, Atlanta GA) (~240 ml). Furthermore, patients used a standard low-fat diet (± 14 g fats, 100 g proteins, 1800 kcal) with as well as between doses on the day of administration to optimize the absorption and bioavailability of sorafenib.

Patients continued study treatment until unacceptable toxicity, disease progression or the patient's request to stop. Evaluable patients had to be treated for a minimum of 2 weeks or would otherwise be replaced by an additional patient.

Safety assessment
Safety and tolerability assessments, including physical examination, ECG and blood hematology and chemistry, were performed weekly during the first 8 weeks and once every 4 weeks thereafter. Adverse events (AEs) were graded according to the National Cancer Institute Common Terminology Criteria for Adverse Events version 4.0.

Dose (/exposure) limiting toxicity (DLT) was defined as any grade 3 toxicity that occurred within the first 6 weeks of treatment and possibly related to the

study drug. The maximum tolerated exposure (MTE) was defined at the highest exposure level at which ≤ 33% of patients experienced DLTs.

Tumor response measurements
Tumor response was assessed by computed tomography or magnetic resonance imaging at baseline and every 8 weeks thereafter using RECIST version 1.1 [24].

Pharmacokinetic analysis
During the first 3 weeks of study treatment, blood samples for measurement of sorafenib and its active metabolite sorafenib N-oxide were taken prior to each dose (i.e. prior to each portion of the total weekly dose given every 2 hours) and 1, 2, 3, 4, 8, 12 and 60-96 hours after the last dose.

The plasma concentrations of sorafenib and sorafenib N-oxide were determined using a validated liquid chromatography-tandem mass spectrometry method [25]. The sorafenib and sorafenib N-oxide plasma AUC(0-12h) were determined from the time of the last sorafenib tablet ingestion until 12 hours afterwards with a non-compartmental method. Within 72 hours after ingestion, the sorafenib AUC(0-12h) was established by our department of Clinical Pharmacology and Pharmacy and if necessary, the dose was adjusted accordingly to achieve the target AUC(0-12h) of the exposure cohort. Per patient a maximum of 2 dose adjustments were permitted. In addition, the maximum concentration (C_{max}) and time of maximum concentration (T_{max}) were determined.

Statistical considerations
Descriptive statistics were used to describe patient characteristics, treatment administration, safety, efficacy and pharmacokinetic data. Progression-free survival (PFS) was defined as the time from first treatment until progression of disease or death as a result of any cause. Fisher's exact tests were used to assess correlations between exposure level or dose and frequency of AEs. A paired t-test was used to investigate the effect of personalized dose titration on achieving the target sorafenib AUC(0-12h). Last, a Mann Whitney test was used to investigate the effect of cola on dose normalized (to a standard dose of 800 mg sorafenib) plasma sorafenib C_{max} and AUC(0-12h) levels. Data were considered significant at $P < 0.05$.

RESULTS

Patients and treatment
Seventeen patients with progressive metastatic malignancies were enrolled between November 2015 and December 2017. Patient characteristics are shown in Table 1. A total number of 114 weekly cycles sorafenib were administered with a median of 7 cycles per patient (range 1-24).

Table 1. Patient Characteristics

Characteristic	Number of patients, *N* = 17
Age (years)	
Median (range)	61 (26-74)
Gender	
Males/females	7/10
ECOG performance status	
0/1	2/15
Tumor type	
Pancreas	2
Bile duct	2
Head and neck	2
Esophagus	2
Colorectal	2
Kidney	1
Liver (HCC)	1
Melanoma	1
Uterus	1
Breast	1
Sarcoma	1
Metaplastic carcinoma	1
Prior treatment	
Surgery	8
Radiotherapy	6
Chemotherapy	13
Protein kinase inhibitor	3 (1 patient prior used standard dose sorafenib)
Number of prior systemic regimens	
Median (range)	2 (0-6)

Patients were treated at target AUC(0-12h) levels from 25-50 to 125-150 mg/L/h. Because the first exposure cohort (AUC(0-12h) 25-50 mg/L/h) already resulted in higher sorafenib exposure than expected (median AUC(0-12h) 71, range 61-103 mg/L/h), the second exposure cohort was set at 75-100 mg/L/h. In subsequent cohorts, target exposure levels were increased with steps of 25 mg/L/h (Table 2).

Reasons for treatment discontinuation were disease progression (*N* = 11), treatment related toxicity (*N* = 3), completion of the study protocol i.e. treatment discontinuation because ≥ 33% of patients experienced DLTs in that cohort (*N* = 1), patient withdrawal (*N* = 1) and a pathological bone fracture (*N* = 1). The latter two patients were considered non-evaluable as described in the protocol because they had only received one week of study treatment and were replaced.

Table 2. Treatment related adverse events

Toxicity	Grade	All cohorts (*N* = 15)	Cohort 1 (*N* = 3)	Cohort 2 (*N* = 6)	Cohort 3 (*N* = 3)	Cohort 4 (*N* = 3)	Dose < 2400 mg (*N* = 11)	Dose ≥ 2400 mg (*N* = 9)	Observed AUC < 100 mg/L/h (*N*= 14)	Observed AUC ≥ 100 mg/L/h (*N* = 11)
Fatigue	All	10 (67%)	1 (33%)	5 (83%)	3 (100%)	1 (33%)	4 (36%)	6 (67%)	3 (21%)	7 (64%)
	Grade ≥ 3	0	0	0	0	0	0	0	0	0
Nausea	All	10 (67%)	2 (67%)	4 (67%)	2 (67%)	2 (67%)	5 (45%)	5 (56%)	5 (36%)	5 (45%)
	Grade ≥ 3	0	0	0	0	0	0	0	0	0
Vomiting	All	8 (53%)	2 (67%)	3 (50%)	1 (33%)	2 (67%)	5 (45%)	3 (33%)	7 (50%)	1 (9%)
	Grade ≥ 3	0	0	0	0	0	0	0	0	0
Diarrhea	All	4 (27%)	1 (33%)	1 (17%)	1 (33%)	1 (33%)	2 (18%)	2 (22%)	2 (14%)	2 (18%)
	Grade ≥ 3	0	0	0	0	0	0	0	0	0
Anorexia	All	3 (20%)	0	2 (33%)	1 (33%)	0	0	3 (33%)	1 (7%)	2 (18%)
	Grade ≥ 3	0	0	0	0	0	0	0	0	0
Bloating	All	2 (13%)	0	1 (17%	0	1 (33%)	1 (9%)	1 (11%)	1 (7%)	1 (9%)
	Grade ≥ 3	0	0	0	0	0	0	0	0	0
Stomatitis	All	2 (13%)	0	1 (17%)	1 (33%)	0	0	2 (22%)	0	2 (18%)
	Grade ≥ 3	0	0	0	0	0	0	0	0	0
Perforation	All	2 (13%)	0	1 (17%)	0	1 (33%)	0	2 (22%)	1 (7%)	1 (11%)
	Grade ≥ 3	2 (13%)	0	1 (17%)	0	1 (33%)	0	2 (22%)	1 (7%)	1 (11%)
Multiorgan failure	All	1 (7%)	0	0	0	1 (33%)	0	1 (11%)	1 (7%)	0
	Grade ≥ 3	1 (7%)	0	0	0	1 (33%)	0	1 (11%)	1 (7%)	0

Table 2. Continued.

Toxicity	Grade	All cohorts (*N* = 15)	Cohort 1 (*N* = 3)	Cohort 2 (*N* = 6)	Cohort 3 (*N* = 3)	Cohort 4 (*N* = 3)	Dose < 2400 mg (*N* = 11)	Dose ≥ 2400 mg (*N* = 9)	Observed AUC < 100 mg/L/h (*N*= 14)	Observed AUC ≥ 100 mg/L/h (*N* = 11)
ALP increased	All	3 (20%)	0	0	1 (33%)	2 (67%)	0	3 (33%)	1 (7%)	2 (18%)
	Grade ≥ 3	2 (13%)	0	0	0	2 (67%)	0	2 (22%)	1 (7%)	1 (9%)
Bilirubin increased	All	2 (13%)	0	0	0	2 (67%)	0	2 (22%)	1 (7%)	1 (9%)
	Grade ≥ 3	0	0	0	0	0	0	0	0	0
GGT increased	All	1 (7%)	0	0	0	1 (33%)	0	1 (11%)	1 (7%)	0
	Grade ≥ 3	1 (7%)	0	0	0	1 (33%)	0	1 (11%)	1 (7%)	0

Table 3. Pharmacokinetic results for high-dose, pulsatile sorafenib

Cohort	No of patients	Target AUC(12h) (mg/L/h)	Fixed dose week 1 (mg)	PK-guided dose week 3 (mg), mean (± SD)	Observed AUC(12h) week 1 (mg/L/h), mean (± SD)	Observed AUC(12h) week 3 (mg/L/h), mean (± SD)	C_{max} week 1 (µg/L), mean (± SD)	C_{max} week 3 (µg/L), mean (± SD)
1	3	25-50	1000	533 (± 306)	78 (± 22)	31 (± 13)	9089 (± 3281)	4385 (± 1312)
2	8	75-100	2000	1867 (± 993)	125 (± 59)	102 (± 49)	13696 (± 5866)	11098 (± 6115)
3	3	100-125	2400	2333 (± 219)	204 (± 113)	96 (± 40)	20829 (± 11234)	13280 (± 5310)
4	3	125-150	2800	NA*	120 (± 13)	NA*	15200 (± 1266)	NA*

Safety
Adverse events which were at least possibly related to high-dose sorafenib are summarized in Table 3. Most common clinical toxicities were fatigue (67%), nausea (67%), vomiting (53%) and diarrhea (27%). These grades 1-2 toxicities typically started 1-2 days after sorafenib administration and were manageable with standard supportive care measures.

Serious adverse events were predominantly observed in the gastro-intestinal tract. At the target exposure level of 75-100 mg/L/h, 1 patient developed grade 5 biliary tract perforation after 3 cycles of treatment (sorafenib dose was 3600 mg with an observed AUC(0-12h) of 182 mg/L/h). The cohort was expanded to 6 evaluable patients, but no further DLT occurred. At the subsequent 100-125 mg/L/h target exposure level, 3 patients were treated without DLT. However, a DLT occurred in 2 out of 3 patients in the 125-150 mg/L/h cohort. One patient developed grade 3 duodenal perforation after 2 cycles of treatment (sorafenib dose was 2800 mg with an observed AUC(0-12h) of 54 mg/L/h). The other patient suffered from grade 5 multiorgan failure after 2 cycles of treatment (sorafenib dose was 2800 mg with an observed AUC(0-12h) of 47 mg/L/h) and died. At that point the phase I study was preliminary terminated because these serious toxicities precluded further dose escalation and investigation of a potential benefit of a high-dose, pulsatile approach.

Overall, the frequency and rate of grade ≥ 3 AEs increased with a higher dose of sorafenib (P = 0.003 and P = 0.008, respectively) but did not increase with higher exposure (P = 0.43 and P = 0.70, respectively). Grade ≥ 3 AEs developed from doses ≥ 2800 mg/week. Dose interruptions were required in 5 (33%) patients, of which 3 (20%) were due to the previously reported DLTs leading to permanent study discontinuation.

Pharmacokinetics
Plasma samples for pharmacokinetic analyses were available from all 17 included patients and results are summarized in Table 3. Mean exposure increased with higher sorafenib doses up to 2400 mg per week, after which no additional increases were seen. This is possibly related to a saturation of uptake in the gastro-intestinal tract. The increases were similar for AUC(0-12h) as well as C_{max} throughout the escalating exposure cohorts. In the current phase I study, highest exposure levels were up to 204 mg/L/h (SD ± 113 mg/L/h) with a C_{max} up to 21.0 mg/L (SD ± 11 mg/L), reached at median 7 hours after ingestion (range 1-12 hours). The plasma concentration time curves of sorafenib showed a biphasic pattern, which has been described previously, and is most likely caused by biliary excretion and the enterohepatic cycle (Figure 1). No accumulation of sorafenib was seen a week after each ingestion. The major

metabolite of sorafenib, sorafenib N-oxide, comprised approximately 4% of the parent drug and showed similar C_{max} and AUC(0-12h) patterns compared to sorafenib (Supplementary Figure S1).

Figure 1. **A** High-dose, pulsatile sorafenib plasma concentrations (mean ± SD) in week 1 using a standard fixed dose for each cohort (*N* = 17, black dots are time points of sorafenib ingestion) and **B** shows the effect of drug monitoring (*N* = 12, each colored symbol represents an individual patient followed in weeks 1-3).

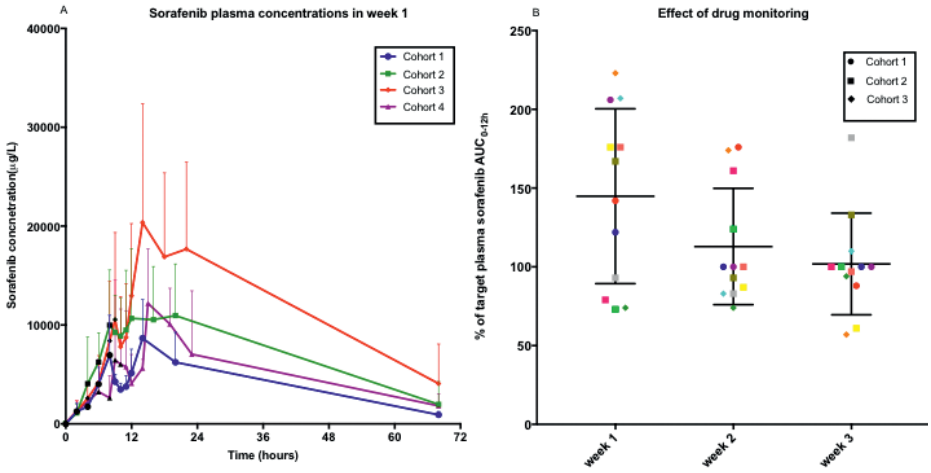

At start of treatment, with a pulsatile fixed high-dose, sorafenib exposure showed large interpatient variability with a mean difference between observed and target AUC(0-12h) of 45% (SD ± 56%) in week 1 (Figure 1). Personalized dose titration resulted in a mean difference between observed and target AUC(0-12h) of 2% (SD ± 32%) in week 3. The difference between week 1 and week 3 showed a trend towards an improved prediction of exposure (*P* = 0.06).

All patients in this phase I study used proton pump inhibitors (PPI) for various reasons, which could decrease sorafenib absorption as a result of an increasing gastric pH. In order to lower the pH, sorafenib was dissolved in cola, but this did not lead to an increase in sorafenib AUC(0-12h) or C_{max} compared to patients treated with sorafenib dissolved in water (*P* = 0.24 and 0.33, respectively) (Figure 2).

Figure 2. Effect of cola on sorafenib absorption. Cola did not affect sorafenib AUC(0-12h) (**A**) or C_{max} (**B**) Black and red dots represent sorafenib dissolved in water and cola, respectively.

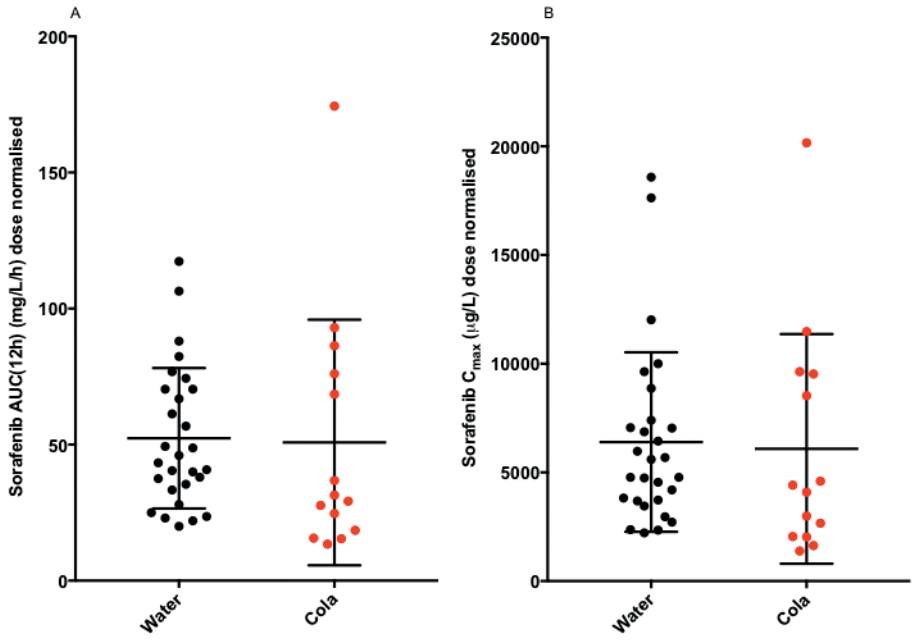

Treatment efficacy

Thirteen patients were evaluable for response. As best response, 2 patients (15%) had stable disease: a patient with cholangiocarcinoma for a duration of 3 months and treated at the target exposure level of 75-100 mg/L/h (sorafenib dose was 2400 mg/week and observed AUC(0-12h) was 100 mg/L/h in week 3) and another patient with hepatocellular carcinoma for a duration of 5.5 months, who was treated at the target exposure level of 100-125 mg/L/h (sorafenib dose was 4800 mg/week and observed AUC(0-12h) was 94 mg/L/h in week 3). The latter patient was previously progressive during treatment with sorafenib at the standard continuously dosed schedule. Eleven patients (85%) had progressive disease. No complete or partial responses were observed.

Discussion

In this phase 1 study, a high-dose, intermittent sorafenib schedule was investigated and dose escalation was performed according to a novel concept, i.e. based on escalating sorafenib plasma AUC(0-12h) levels, instead of conventional dose escalating cohorts. The aim was to reach the highest

tolerable plasma sorafenib peak concentration supposed necessary for the highest intratumoral concentration to improve blockade of tumor kinase targets. With the standard continuous sorafenib schedule of 400 mg twice daily, mean sorafenib exposure varied from 21.8-107 mg/L/h on day 1 and 47.8-71.7 mg/L/h at steady state, while mean C_{max} values ranged from 2.9-3-4 mg/L on day 1 to 5.4-9.4 mg/L at steady state, which was reached approximately 3 hours after ingestion (range 0-24 hours) [8, 26]. High-dose pulsatile sorafenib resulted in a C_{max} up to 21.0 mg/L (SD ± 11 mg/L), i.e. approximately 7-fold and 2-fold higher in comparison to a single dose and continuous standard dosing, respectively.

A few other protein kinase inhibitors have been investigated in a high-dose, pulsatile schedule. High-dose erlotinib administered at a dose of 2000 mg per week in NSCLC patients was well tolerated and resulted in a mean overall survival (OS) of 9.5 months [27]. Another phase II study investigated high-dose erlotinib 450 mg every three days or the EGFR-inhibitor gefitinib 1000 mg every four days in patients with known EGFR-mutations and disease progression after treatment with conventional dose erlotinib or gefitinib [28]. Treatment was well tolerated and resulted in a median PFS of 6 months in both groups and response rates of 15 and 21%, respectively. In addition, a phase I study escalating the HER2-inhibitor lapatinib in heavily pre-treated patients with HER2-positive breast cancer to 7000 mg on days 1-5 of repeating 14-day cycles showed an objective response rate in 15% of the patients [29]. We recently investigated the multikinase inhibitor sunitinib in a high-dose, pulsatile phase I study in more than 70 heavily pre-treated patients with advanced solid malignancies [13]. The study showed that a high-pulsatile schedule of 14 times the conventional dose of sunitinib was well tolerated and led to an 18-fold higher C_{max}. In addition, the drug showed promising preliminary efficacy with clinical benefit in 63% of the patients, including a PFS of ≥ 5 months in 30% of the patients and is currently being investigated in two phase II trials (NCT03909724 and NCT03025893). Unfortunately, high-dose, pulsatile sorafenib exposure did not achieve sufficiently increased peak concentration levels, which were considered necessary for improved efficacy. With only ~3.5 times its conventional dose tolerated in a pulsatile schedule, a peak concentration of only 2 times the standard C_{max} was attained in this study. Drug exposure is influenced by its absorption in the stomach which is dependent of factors such as diet and pH. The patients ingested sorafenib with a moderate fat meal and multiple divided doses of 200-400 mg every 2 hours, to maximize absorption. This resulted in increased exposure up to sorafenib doses of 2400 once per week, which is 3 times higher than the previously reported saturation > 800 mg sorafenib per day using the standard continuous schedule [15]. Regarding the stomach pH, there have been contradicting results on the effects of PPI on

sorafenib absorption, varying from no effects to 1/3 reduction of sorafenib absorption [17, 18]. We observed that an acidic beverage such as cola did not improve sorafenib exposure in patients using a PPI. Previously it was shown that erlotinib bioavailability did improve by cola intake in patients using omeprazole [20]. However, erlotinib is poorly soluble in water, while the maximal aqueous solubility of 0.4 mg/mL, occurs at pH ~2.0 [19]. Thus, the absolute differences in solubility for erlotinib dependent on stomach pH are much higher than for sorafenib, which ranges from 0.013 mg/100 mL at pH 4.5 to 0.034 mg/100 mL at pH 1.0 [17-19].

In this phase 1 study, dose escalation was performed in exposure escalation cohorts, instead of conventional dose escalation cohorts, because sorafenib exposure has large interpatient variability using a fixed dose [8]. Drug monitoring of sorafenib, with a maximum of 2 dose adjustments, resulted in a difference of 2% between observed and target AUC(0-12h) compared to 45% at the start of treatment using a fixed dose. Although this was only borderline significant (P = 0.06) in this small patient group, the feasibility of sorafenib drug monitoring to achieve a target exposure, supports this strategy to improve controlled drug exposure. Further research is necessary to investigate whether dose titration based on exposure will lead to improved efficacy.

Unfortunately, we observed considerable toxicity in this phase 1 study with high-dose, intermittent sorafenib. Grade 5 biliary tract perforation was observed in a patient treated at the target exposure level of 75-100 mg/L/h, and grade 3 duodenal perforation and grade 5 multiorgan failure in 2 separate patients treated at target exposure level of 100-125 mg/L/h. We found that ≥ grade 3 toxicity was associated with increased ingested sorafenib dose (doses ≥ 2800 mg/week), but not with plasma sorafenib AUC(0-12h). Because sorafenib is a multikinase inhibitor, including inhibition of angiogenesis, perforation of the gastro-intestinal tract is a well-known side effect, but occurs at a low incidence in < 1% of the patients treated at the standard continuous schedule [30, 31]. We therefore took precautions to prevent perforations by excluding patients with previous radiotherapy of the thoracic/bowel region as other studies showed this was a risk factor for gastro-intestinal perforation in combination with VEGF-inhibitors [13, 32, 33]. Several phase I studies have investigated the safety and pharmacokinetics of standard dose sorafenib and the most important DLTs were skin toxicity, diarrhea and fatigue [23]. However, this was the first study to investigate the safety and pharmacokinetics of sorafenib in a high-dose, pulsatile schedule, which showed a different DLT profile. The incidence of perforation was 13%. The frequency and type of serious toxicities (perforation and multiorgan failure) observed at only ~3.5 times the conventional sorafenib dose in a weekly schedule, were unexpected and reason for preliminary study

termination. This was in contrast to the example of high-dose, pulsatile sunitinib, which is also an anti-angiogenic drug and showed tolerability comparable to daily administration up to 14 times the conventional dose [13]. A possible explanation may be the enterohepatic circulation of sorafenib. This encompasses the hepatobiliary excretion of sorafenib and a second round of exposure of the intestinal tract to sorafenib with subsequent partial reabsorption. Enterohepatic circulation has been observed in animal models for sorafenib, but not for sunitinib, and is also an explanation for the biphasic plasma concentration time curve typical for sorafenib and observed in the current study [16, 34-37]. In addition, in this pulsatile weekly regimen, sorafenib doses were divided over consecutive 2-hourly dose administrations. For instance, a 3600 mg dose was administered as 9 consecutive doses of 400 mg, which was done to circumvent the saturable absorption of sorafenib. As a result, local drug concentrations in the GI-tract were high during prolonged periods of time and may have caused local anti-angiogenic effects in the GI-tract, inducing DLT. The sorafenib dose administered is a better measure of local GI-tract sorafenib exposure as opposed to the observed plasma concentrations of sorafenib. This also explains why adverse events were not associated with sorafenib exposure, but rather with sorafenib dose. In contrast to the observed DLT in this study, we only observed mild diarrhea (< grade 3) in 27% of the patients. This may indicate that the anti-angiogenic effects of high-dose pulsatile sorafenib were more pronounced than other cytotoxic effects responsible for diarrhea, such as inhibition of the MAPK signaling pathway that can lead to increased chloride secretion by the normal GI-mucosa and subsequent secretory diarrhea [38, 39]. While the pulsatile regimen was targeting high exposure (irrespective of dose), the study was discontinued early due to the occurrence of unexpected, serious DLT (despite relatively low plasma exposure). These results may help to guide the future selection of protein kinase inhibitors suitable for an alternative, pulsatile, high-dosing schedule.

In conclusion, we have shown the feasibility of drug monitoring to achieve exposure based treatment cohorts for high-dose, pulsatile sorafenib. Unfortunately, potentially effective high peak concentrations could not be reached due to early toxicity at already lower concentrations than anticipated. Dose escalation above the exposure cohort of 125-150 mg/L/h was impossible, so the potential benefit of this alternative approach could not be investigated further.

NOTES

Acknowledgements
we thank the patients who participated in this trial and their families.

In addition, we thank Bram Wilhelm of the department of Clinical Pharmacology & Pharmacy for his contribution to the study.

Funding
none declared.

COMPLIANCE WITH ETHICAL STANDARDS

Conflict of interest statement
the authors declare that they have no conflict of interest.

Ethical approval
all procedures performed in studies involving human participants were in accordance with the ethical standards of the institutional committee of the Amsterdam UMC, location VUmc (Medisch Ethische Toetsingscommissie VUmc) and with the 1964 Helsinki declaration and its later amendments or comparable ethical standards.

Informed consent
informed consent was obtained from all individual participants included in the study.

Supplementary Figure S1. Sorafenib versus sorafenib N-oxide AUC(0-12h) (**A**) and C_{max} (**B**).

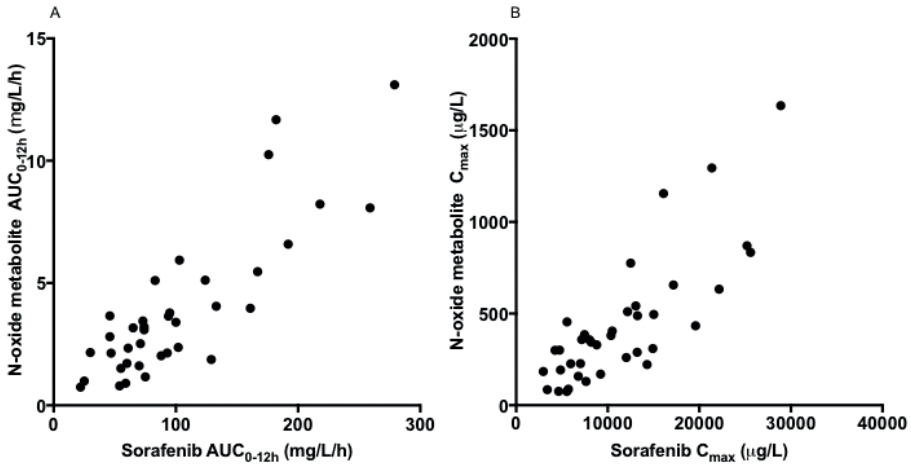

REFERENCES

1. Wilhelm S, Carter C, Lynch M, Lowinger T, Dumas J, Smith RA, et al. Discovery and development of sorafenib: a multikinase inhibitor for treating cancer. Nat Rev Drug Discov. 2006;5(10):835-44. doi: 10.1038/nrd2130. PubMed PMID: 17016424.
2. Wilhelm SM, Adnane L, Newell P, Villanueva A, Llovet JM, Lynch M. Preclinical overview of sorafenib, a multikinase inhibitor that targets both Raf and VEGF and PDGF receptor tyrosine kinase signaling. Mol Cancer Ther. 2008;7(10):3129-40. doi: 10.1158/1535-7163.MCT-08-0013. PubMed PMID: 18852116.
3. Karaman MW, Herrgard S, Treiber DK, Gallant P, Atteridge CE, Campbell BT, et al. A quantitative analysis of kinase inhibitor selectivity. Nat Biotechnol. 2008;26(1):127-32. Epub 2008/01/10. doi: 10.1038/nbt1358. PubMed PMID: 18183025.
4. Escudier B, Eisen T, Stadler WM, Szczylik C, Oudard S, Staehler M, et al. Sorafenib for treatment of renal cell carcinoma: Final efficacy and safety results of the phase III treatment approaches in renal cancer global evaluation trial. J Clin Oncol. 2009;27(20):3312-8. doi: 10.1200/JCO.2008.19.5511. PubMed PMID: 19451442.
5. Llovet JM, Ricci S, Mazzaferro V, Hilgard P, Gane E, Blanc JF, et al. Sorafenib in advanced hepatocellular carcinoma. N Engl J Med. 2008;359(4):378-90. doi: 10.1056/NEJMoa0708857. PubMed PMID: 18650514.
6. Brose MS, Nutting CM, Jarzab B, Elisei R, Siena S, Bastholt L, et al. Sorafenib in radioactive iodine-refractory, locally advanced or metastatic differentiated thyroid cancer: a randomised, double-blind, phase 3 trial. Lancet. 2014;384(9940):319-28. doi: 10.1016/S0140-6736(14)60421-9. PubMed PMID: 24768112; PubMed Central PMCID: PMCPMC4366116.
7. Kim JE, Ryoo BY, Ryu MH, Chang HM, Suh DJ, Lee HC, et al. Sorafenib for hepatocellular carcinoma according to Child-Pugh class of liver function. Cancer Chemother Pharmacol. 2011;68(5):1285-90. Epub 2011/03/30. doi: 10.1007/s00280-011-1616-x. PubMed PMID: 21445543.
8. Strumberg D, Richly H, Hilger RA, Schleucher N, Korfee S, Tewes M, et al. Phase I clinical and pharmacokinetic study of the Novel Raf kinase and vascular endothelial growth factor receptor inhibitor BAY 43-9006 in patients with advanced refractory solid tumors. J Clin Oncol. 2005;23(5):965-72. doi: 10.1200/JCO.2005.06.124. PubMed PMID: 15613696.
9. Escudier B, Szczylik C, Hutson TE, Demkow T, Staehler M, Rolland F, et al. Randomized phase II trial of first-line treatment with sorafenib versus interferon Alfa-2a in patients with metastatic renal cell carcinoma. J Clin Oncol. 2009;27(8):1280-9. doi: 10.1200/JCO.2008.19.3342. PubMed PMID: 19171708.
10. Pecuchet N, Lebbe C, Mir O, Billemont B, Blanchet B, Franck N, et al. Sorafenib in advanced melanoma: a critical role for pharmacokinetics? Br J Cancer. 2012;107(3):455-61. doi: 10.1038/bjc.2012.287. PubMed PMID: 22767146; PubMed Central PMCID: PMCPMC3405224.
11. Rovithi M, Verheul HMW. Pulsatile high-dose treatment with antiangiogenic tyrosine kinase inhibitors improves clinical antitumor activity. Angiogenesis. 2017;20(3):287-9. doi: 10.1007/s10456-017-9555-8. PubMed PMID: 28421290; PubMed Central PMCID: PMCPMC5511614.

12. Rovithi M, de Haas RR, Honeywell RJ, Poel D, Peters GJ, Griffioen AW, et al. Alternative scheduling of pulsatile, high dose sunitinib efficiently suppresses tumor growth. J Exp Clin Cancer Res. 2016;35(1):138. doi: 10.1186/s13046-016-0411-2. PubMed PMID: 27604186; PubMed Central PMCID: PMCPMC5013589.
13. Rovithi M, Gerritse SL, Honeywell RJ, Ten Tije AJ, Ruijter R, Peters GJ, et al. Phase I Dose-Escalation Study of Once Weekly or Once Every Two Weeks Administration of High-Dose Sunitinib in Patients With Refractory Solid Tumors. J Clin Oncol. 2018:JCO1800725. doi: 10.1200/JCO.18.00725. PubMed PMID: 30586316.
14. Wang X, Zhang L, Goldberg SN, Bhasin M, Brown V, Alsop DC, et al. High dose intermittent sorafenib shows improved efficacy over conventional continuous dose in renal cell carcinoma. J Transl Med. 2011;9:220. doi: 10.1186/1479-5876-9-220. PubMed PMID: 22188900; PubMed Central PMCID: PMCPMC3258225.
15. Hornecker M, Blanchet B, Billemont B, Sassi H, Ropert S, Taieb F, et al. Saturable absorption of sorafenib in patients with solid tumors: a population model. Invest New Drugs. 2012;30(5):1991-2000. doi: 10.1007/s10637-011-9760-z. PubMed PMID: 22006162.
16. (Nexavar) UFaDAS. Clinical Pharmacology and Biopharmaceutics Review. 2005.
17. Lalani AA, McKay RR, Lin X, Simantov R, Kaymakcalan MD, Choueiri TK. Proton Pump Inhibitors and Survival Outcomes in Patients With Metastatic Renal Cell Carcinoma. Clin Genitourin Cancer. 2017;15(6):724-32. doi: 10.1016/j.clgc.2017.05.019. PubMed PMID: 28645482.
18. Lind JS, Dingemans AM, Groen HJ, Thunnissen FB, Bekers O, Heideman DA, et al. A multicenter phase II study of erlotinib and sorafenib in chemotherapy-naive patients with advanced non-small cell lung cancer. Clin Cancer Res. 2010;16(11):3078-87. doi: 10.1158/1078-0432.CCR-09-3033. PubMed PMID: 20395213.
19. Budha NR, Frymoyer A, Smelick GS, Jin JY, Yago MR, Dresser MJ, et al. Drug absorption interactions between oral targeted anticancer agents and PPIs: is pH-dependent solubility the Achilles heel of targeted therapy? Clin Pharmacol Ther. 2012;92(2):203-13. doi: 10.1038/clpt.2012.73. PubMed PMID: 22739140.
20. van Leeuwen RW, Peric R, Hussaarts KG, Kienhuis E, NS IJ, de Bruijn P, et al. Influence of the Acidic Beverage Cola on the Absorption of Erlotinib in Patients With Non-Small-Cell Lung Cancer. J Clin Oncol. 2016;34(12):1309-14. Epub 2016/02/10. doi: 10.1200/JCO.2015.65.2560. PubMed PMID: 26858332.
21. Retamero A, Conde-Estevez D. Erlotinib and acid suppressive agents: is it worth to take a coke? Ann Oncol. 2017;28(1):192-3. Epub 2017/02/09. doi: 10.1093/annonc/mdw530. PubMed PMID: 28177427.
22. Widmer N, Bardin C, Chatelut E, Paci A, Beijnen J, Leveque D, et al. Review of therapeutic drug monitoring of anticancer drugs part two--targeted therapies. Eur J Cancer. 2014;50(12):2020-36. Epub 2014/06/15. doi: 10.1016/j.ejca.2014.04.015. PubMed PMID: 24928190.
23. Strumberg D, Clark JW, Awada A, Moore MJ, Richly H, Hendlisz A, et al. Safety, pharmacokinetics, and preliminary antitumor activity of sorafenib: a review of four phase I trials in patients with advanced refractory solid tumors. Oncologist. 2007;12(4):426-37. doi: 10.1634/theoncologist.12-4-426. PubMed PMID: 17470685.

24. Schwartz LH, Seymour L, Litiere S, Ford R, Gwyther S, Mandrekar S, et al. RECIST 1.1 - Standardisation and disease-specific adaptations: Perspectives from the RECIST Working Group. Eur J Cancer. 2016;62:138-45. doi: 10.1016/j.ejca.2016.03.082. PubMed PMID: 27237360; PubMed Central PMCID: PMCPMC5737786.
25. Honeywell R, Yarzadah K, Giovannetti E, Losekoot N, Smit EF, Walraven M, et al. Simple and selective method for the determination of various tyrosine kinase inhibitors used in the clinical setting by liquid chromatography tandem mass spectrometry. J Chromatogr B Analyt Technol Biomed Life Sci. 2010;878(15-16):1059-68. doi: 10.1016/j.jchromb.2010.03.010. PubMed PMID: 20382575.
26. European Medicines Agency (EMA). Nexavar: European Public Assessment Reports (EPAR)-Scientific Discussion, 2006, [cited 2019, June 2]. Available from: https://www.ema.europa.eu/en/documents/scientific-discussion/nexavar-epar-scientific-discussion_en.pdf.
27. Milton DT, Azzoli CG, Heelan RT, Venkatraman E, Gomez JE, Kris MG, et al. A phase I/II study of weekly high-dose erlotinib in previously treated patients with nonsmall cell lung cancer. Cancer. 2006;107(5):1034-41. doi: 10.1002/cncr.22088. PubMed PMID: 16878326.
28. Zhu Y, Du Y, Liu H, Ma T, Shen Y, Pan Y. Study of efficacy and safety of pulsatile administration of high-dose gefitinib or erlotinib for advanced non-small cell lung cancer patients with secondary drug resistance: A single center, single arm, phase II clinical trial. Thorac Cancer. 2016;7(6):663-9. doi: 10.1111/1759-7714.12384. PubMed PMID: 27755796; PubMed Central PMCID: PMCPMC5093174.
29. Chien AJ, Munster PN, Melisko ME, Rugo HS, Park JW, Goga A, et al. Phase I dose-escalation study of 5-day intermittent oral lapatinib therapy in patients with human epidermal growth factor receptor 2-overexpressing breast cancer. J Clin Oncol. 2014;32(14):1472-9. doi: 10.1200/JCO.2013.52.1161. PubMed PMID: 24711549; PubMed Central PMCID: PMCPMC4017711.
30. EMA. European Public Assessment Report - Product Information. NEXAVAR® sorafenib. London: EMA; [updated July 26, 2018]. Available from: https://www.ema.europa.eu/documents/product-information/nexavar-epar-product-information_en.pdf
31. Gyawali B, Shimokata T, Ando M, Honda K, Ando Y. Risk of serious adverse events and fatal adverse events with sorafenib in patients with solid cancer: a meta-analysis of phase 3 randomized controlled trialsdagger. Ann Oncol. 2017;28(2):246-53. Epub 2016/10/25. doi: 10.1093/annonc/mdw549. PubMed PMID: 27771613.
32. Murray L, Longo J, Wan J, Chung C, Wang L, Dawson L, et al. Phase I dose escalation study of concurrent palliative radiation therapy with sorafenib in three anatomical cohorts (Thorax, Abdomen, Pelvis): The TAP study. Radiother Oncol. 2017;124(1):74-9. doi: 10.1016/j.radonc.2017.06.007. PubMed PMID: 28668472.
33. Lee MO, Song SH, Jung S, Hur S, Asahara T, Kim H, et al. Effect of ionizing radiation induced damage of endothelial progenitor cells in vascular regeneration. Arterioscler Thromb Vasc Biol. 2012;32(2):343-52. doi: 10.1161/ATVBAHA.111.237651. PubMed PMID: 22075244.
34. Abbiati RA, Manca D. Enterohepatic Circulation Effect in Physiologically Based Pharmacokinetic Models: The Sorafenib Case. Industrial & Engineering Chemistry Research. 2017;56(12):3156-66. doi: 10.1021/acs.iecr.6b03686.

35. Abbiati RA, Manca D. Innovations and Improvements in Pharmacokinetic Models Based on Physiology. Curr Drug Deliv. 2017;14(2):190-202. doi: 10.2174/1567201813666160524142031. PubMed PMID: 27216546.
36. Haznedar JÖ, Patyna S, Bello CL, Peng GW, Speed W, Yu X, et al. Single- and multiple-dose disposition kinetics of sunitinib malate, a multitargeted receptor tyrosine kinase inhibitor: comparative plasma kinetics in non-clinical species. Cancer Chemotherapy and Pharmacology. 2009;64(4):691-706. doi: 10.1007/s00280-008-0917-1.
37. Edginton AN, Zimmerman EI, Vasilyeva A, Baker SD, Panetta JC. Sorafenib metabolism, transport, and enterohepatic recycling: physiologically based modeling and simulation in mice. Cancer Chemother Pharmacol. 2016;77(5):1039-52. Epub 2016/04/08. doi: 10.1007/s00280-016-3018-6. PubMed PMID: 27053087; PubMed Central PMCID: PMCPMC4846505.
38. Keely SJ, Barrett KE. p38 mitogen-activated protein kinase inhibits calcium-dependent chloride secretion in T84 colonic epithelial cells. Am J Physiol Cell Physiol. 2003;284(2):C339-48. Epub 2002/10/22. doi: 10.1152/ajpcell.00144.2002. PubMed PMID: 12388102.
39. Heinzerling L, Eigentler TK, Fluck M, Hassel JC, Heller-Schenck D, Leipe J, et al. Tolerability of BRAF/MEK inhibitor combinations: adverse event evaluation and management. ESMO Open. 2019;4(3):e000491. Epub 2019/06/25. doi: 10.1136/esmoopen-2019-000491. PubMed PMID: 31231568; PubMed Central PMCID: PMCPMC6555610.

CHAPTER 6

Summary, discussion and future perspectives

This thesis focused on the value of different positron emission tomography (PET) imaging techniques visualizing targets and targeted anticancer therapies for future treatment tailoring.

In **chapter 1,** a literature overview showed the possible applications of molecular imaging with PET for the improvement of personalized cancer care. In PET, a radiotracer consisting of a positron emitting radionuclide attached to the biologically active molecule of interest is administrated to the patient and its biodistribution throughout the body is detected by the PET-scan. Several approaches have been undertaken for direct visualization of the drug biodistribution in vivo, for example radiolabeled ligands have been developed for target/receptor identification and radiolabeled drugs have been developed to investigate intratumoral uptake. Although only a limited number of clinical studies with radiolabeled targeted anticancer drugs are available, the results indicate that PET imaging of targets and targeted therapies offers opportunities for response prediction, early response evaluation and optimization of dosing schedules.

Part I visualizing targets: hormone receptor imaging

Part I of this thesis concerned PET imaging of targets: estrogen receptor (ER) and androgen receptor (AR) imaging in patients with breast cancer. Correct identification of tumor receptor status is important for treatment decisions in breast cancer. About 75% of all breast cancers have ER expression, which means they can grow in response to the binding of estrogen and it is the main predictor of potential response to anti-estrogen therapies.[1,2] Recently, also AR expression emerged as a possible target for therapy, whilst it is present in 70-80% of the patients with breast cancer.[3] AR antagonists are currently under investigation in multiple breast cancer trials. A tumor biopsy is the gold standard to determine receptor expression. However, this is an invasive procedure, only gives information about a single lesion, is not always feasible in case of inaccessible tumor sites, and is subject to sampling errors.[4-6] The imaging techniques 16α-[^{18}F]fluoro-17β-estradiol ([^{18}F]FES) PET and 16β-[^{18}F]fluoro-5α-dihydrotestosterone ([^{18}F]FDHT) PET have been developed to non-invasively visualize the ER and AR status respectively, in tumor lesions within a patient. In this thesis essential steps were taken in the clinical application process of hormone receptor imaging.

In **chapter 2**, we evaluated whether [^{18}F]FES and [^{18}F]FDHT PET correlated with levels of ER and AR expression, respectively, in biopsies of corresponding metastases. In this prospective study, a total of 13 patients with metastatic breast cancer were analyzed. The amount of [^{18}F]FES and [^{18}F]FDHT uptake, respectively, correlated strongly with ER (R^2 = 0.78, P = 0.01) and moderately

with AR expression levels (R^2 = 0.47, P = 0.01) in representative tumor biopsies. For [^{18}F]FES PET, the optimal maximum standardized uptake value (SUV_{max}) cut-off for ER-positive lesions (more than 1% nuclear staining) was 1.54, resulting in a sensitivity and specificity of 100%. For [^{18}F]FDHT, an optimal SUV_{max} cut-off of 1.94 was found for AR-positivity (more than 10% nuclear staining), resulting in a sensitivity of 91% and specificity of 100%. There was substantial intrapatient heterogeneity in tracer uptake, with the majority of patients having both lesions with and without uptake of [^{18}F]FES and [^{18}F]FDHT, respectively. In addition, hormone receptor conversion in metastases, when compared with biopsies of the primary tumor, occurred in 23% of the patients. These results indicate that [^{18}F]FES and [^{18}F]FDHT PET have the potential to serve as a surrogate for tumor biopsies and have the advantage of being non-invasive techniques that can visualize heterogeneous receptor expression of different tumor lesions within a patient.

In **chapter 3**, the visual and quantitative interobserver variability of [^{18}F]FES PET and [^{18}F]FDHT PET interpretation were determined in patients with metastatic breast cancer. This is an important validation step in the clinical application of these new diagnostic tools. Here, we showed that visual and quantitative evaluation of [^{18}F]FES PET was highly reproducible between independent observers at separate centers using different scanners and software. Visual positive and negative absolute agreement was > 80%, with a kappa of 0.67 (95% CI 0.48-0.87). Intraclass correlation coefficients (ICC) for quantification of SUV_{max}, SUV_{peak} and SUV_{mean} were 0.98 (95% CI 0.96-0.98), 0.97 (95% CI 0.96-0.98) and 0.89 (95% CI 0.83-0.92). [^{18}F]FDHT PET showed relatively low visual agreement (positive and negative absolute agreement of 49% and 74%, respectively and kappa = 0.23, 95% CI -0.04-0.49), presumably a result of the lower tumor to background ratios of [^{18}F]FDHT in comparison to [^{18}F]FES. However, there was good quantitative agreement between observers (ICCs ≥ 0.75). This study demonstrated high interobserver agreement of [^{18}F]FES PET assessments that support the use of this imaging technique in clinical practice, while for [^{18}F]FDHT PET the lower visual agreement underscores the relevance of quantitative PET analysis in future breast cancer studies.

The role of [^{18}F]FES and [^{18}F]FDHT PET in addition to conventional diagnostic modalities in daily clinical practice needs to be defined further. The non-invasive visualization of receptor status in different tumor lesions with PET offers a number of potential clinical advantages. In patients with metastatic breast cancer for example, it can help to establish a final diagnosis in case conventional diagnostics cannot, e.g. as a result of inaccessible biopsy sites or repeated biopsy sampling errors.

In addition, in patients with breast cancer amenable for curative treatment accurate staging is of great importance. Currently, the staging methods comprise of physical examination, mammography, ultrasound of the breast and axilla, magnetic resonance imaging (MRI) and, in case of stage IIB, III or recurrent disease also 2-[^{18}F]-2-deoxy-D-glucose ([^{18}F]FDG) PET/CT scanning to improve lymph node detection and to rule out the presence of distant metastases.[7-9] [^{18}F]FDG PET detects lymph node involvement and distant metastases with a sensitivity of 63-100% and 98-100%, respectively.[8,10] However, in case of biological factors such as low-grade breast cancer or lobular breast cancer, the detection accuracy of [^{18}F]FDG PET decreases, leading to inadequate staging.[11-13] In these ER-positive breast cancer subtypes, [^{18}F]FES PET may be of additional value to conventional staging.[14] We are currently investigating the use of [^{18}F]FES PET for staging patients with low grade, ER-positive locally advanced or recurrent breast cancer in comparison to [^{18}F]FDG PET (NCT03726931).

Furthermore, in metastatic breast cancer PET imaging may help to determine the hormone receptor status of different tumor sites within one patient, which may guide treatment decisions. Discordant ER expression between the different breast cancer lesions within a patient has previously been described in 15 to 40% of the patients, and was also observed in our studies.[5,6] A single biopsy may therefore not be representative for the ER expression in other metastases throughout the body and may lead to suboptimal treatment choices for an individual patient. Hormone receptor imaging may help to select personalized, multimodality treatment strategies for heterogeneous tumor sites of breast cancer, such as endocrine therapy for [^{18}F]FES positive lesions combined with a local modality such as radiotherapy for concurrent [^{18}F]FES negative lesions. Recently, an exploratory study suggested that the extent of [^{18}F]FES PET heterogeneity may potentially identify the subset of ER positive, metastatic breast cancer patients who will benefit from endocrine therapy combined with cyclin-dependent kinase inhibitors.[15] The more heterogeneity in intrapatient [^{18}F]FES uptake (i.e. more [^{18}F]FES negative lesions), the shorter the progression-free survival (PFS) and higher risk of progression during endocrine therapy alone.[16] This is currently being investigated further in the SONImage study that aims to develop a [^{18}F]FES/[^{18}F]FDG PET prediction model based on the extent of heterogeneity to select patients for endocrine therapy alone or in combination with a cyclin-dependent kinase inhibitor (NCT04125277).

Hormone receptor imaging may also help to guide dosing strategies. Inadequate reduction of the [^{18}F]FES PET signal (< 75%) by fulvestrant treatment, a selective ER downregulator (SERD), has shown to be associated with early progression.[17] Future studies should investigate the role of hormone receptor imaging in drug monitoring, for example to establish the effect of higher fulvestrant dosing

on patient outcome in the case of incomplete reduction of [^{18}F]FES uptake after standard therapy. In addition, hormone receptor imaging has proven useful during drug development. For example, in patients with prostate cancer [^{18}F]FDHT PET was used to determine the optimal dose of the AR blocker enzalutamide in a phase 1 trial.[18] In phase I studies involving novel estrogen receptor antagonists, such as the oral SERD G1T48 (NCT03455270) and the selective estrogen receptor modulator (SERM) GDC0810, [^{18}F]FES PET provided information about ER occupancy and helped to select the optimal dosage for phase II trials.[19]

Although the value of ER-blocking therapies for ER-positive breast cancer is well established, the exact role of AR and AR-blocking therapies in breast cancer is still subject of investigation. Between hormone receptors a level of promiscuous DNA binding occurs and practically every binding site of AR in the DNA of breast cancer is shared with the ER.[20] Both AR agonists and antagonists have shown clinical efficacy in the treatment of breast cancer.[21-24] Distinct signatures of ER and/or AR positivity may be indicative of treatment effects.[25] Hormone receptor imaging with [^{18}F]FDHT PET may help to guide for which patient with breast cancer AR-blocking therapies may be suitable and to visualize the effects of androgen blocking therapies in clinical trials (NCT02697032).

However, before clinical implementation of hormone receptor imaging can be finalized, some issues need to be addressed. We have shown that visual and quantitative [^{18}F]FES uptake correlates well with ER expression levels in representative breast cancer biopsies. Although the study had a small sample size of 10 patients, these results have recently been confirmed in a larger study with 93 patients that showed an excellent positive predictive value of [^{18}F]FES PET of 100% and a negative predicative value of 76.6% (CI 66.0-84.6%) compared to estrogen receptor status by immunohistochemical assay.[26] Of particular importance in the latter study is the very high specificity of [^{18}F]FES PET, with no false-positives, as well as the good concordance with immunohistochemical ER assays (ρ = 0·83; p < 0·0001) endorsing it to be an alternative to tissue biopsies.[26] Currently, in a prospective Dutch multicenter trial, the value of [^{18}F]FES PET and [^{89}Zr]trastuzumab PET is being investigated for the selection of first line treatment in patients with metastatic breast cancer and the optimal SUV_{max} cut-off point correlating with ER and HER2 positivity in tumor biopsies is validated further (NCT01957332).

In this thesis, we presented the first study investigating [^{18}F]FDHT PET in patients with metastatic breast cancer. Larger confirmatory studies are necessary to validate the cut-off value for [^{18}F]FDHT uptake corresponding with AR positivity and with response to AR targeted therapies. Another issue concerns

the physiological background uptake: for [^{18}F]FES in the liver, gallbladder, intestine and bladder and for [^{18}F]FDHT also in the blood pool. This hinders the evaluation of adjacent tumor lesions. A trial is in progress which examines the sensitivity of parametric [^{18}F]FES PET imaging to distinguish background activity in healthy liver tissue from uptake in ER positive liver metastases using a compartmental approach to estimate the spatial distribution of the kinetic parameters governing tracer flow (NCT04150731).

A last issue to light out is that future widespread availability of these new imaging techniques in hospitals requires adequate tracer production and distribution within the half-life of the tracer (109.8 minutes), standardized scanning processes comparable to [^{18}F]FDG PET, and finally training of nuclear physicians in the interpretation.[27]

Part II visualizing targeted anticancer therapies and effects: sorafenib imaging

Part II of this thesis focused on PET imaging of the targeted anti-cancer drug sorafenib. Sorafenib is an oral multikinase inhibitor with activity against multiple targets involved in the growth, angiogenesis and spread of cancer, such as C-RAF, B-RAF, mutant B-RAF, vascular endothelial growth factor receptors 1, 2 and 3, platelet-derived growth factor receptor β, FMS-like tyrosine kinase 3, c-Kit protein and RET receptor tyrosine kinase.[28] Sorafenib has been approved for treatment of locally advanced and metastatic hepatocellular carcinoma, renal cell carcinoma and iodine-refractory differentiated thyroid carcinoma at a standard fixed dose of 400 mg twice daily in a continuous schedule.[29-31] Recently, its indication has been extended to also include advanced or refractory desmoid tumors at a standard fixed dose of 400 mg once daily.[32] However, responses to sorafenib are variable resulting in clinical benefit for only a subgroup of patients, while all are exposed to potential toxicity.[29-32] Most common side effects include gastrointestinal symptoms, fatigue, and (hand-foot) skin reactions.[29-32] Currently, no biomarkers are available to identify which patients are likely to benefit from sorafenib.

In **chapter 4**, we investigated whether [^{11}C]sorafenib PET and [^{15}O]H_2O PET have the potential to act as predictive/early biomarkers of sorafenib efficacy. A response to sorafenib is thought to be directly related to drug concentrations achieved in tumor tissue, therefore the primary objective of this study was to assess whether microdose [^{11}C]sorafenib PET at baseline or a change in uptake after 14 days of treatment (steady state), could predict sorafenib concentrations at therapeutic dosing as measured in corresponding tumor biopsies using liquid chromatography tandem mass spectrometry (LC-MS/MS) as a reference method.[33-36] Secondary objectives included the association of [^{11}C]sorafenib

uptake, perfusion [^{15}O]H_2O PET and sorafenib concentrations after therapeutic dosing, with response. In this prospective exploratory study, 8 patients with advanced solid malignancies and an indication for sorafenib treatment were included. [^{11}C]Sorafenib uptake, measured as the total distribution volume (V_T), did not predict sorafenib concentrations in tumors during therapy as measured in corresponding tumor biopsies with LC-MS/MS. Although sorafenib plasma and tumor concentrations, measured with LC-MS/MS, were not associated with clinical outcome in this exploratory study, higher [^{11}C]sorafenib accumulation in tumors at baseline (0.92 ± 0.61 versus 0.34 ± 0.08) and day 14 of treatment (0.37 ± 0.18 versus 0.13 ± 0.05) was associated with worse prognosis and was correlated with the perfusion of the tumor (r_s = 0.671, P = 0.020). Interestingly, [^{15}O]H_2O PET demonstrated that patients with stable disease had a greater percentage decrease in tumor perfusion (56% ± 23%) after only 14 days of sorafenib treatment compared to patients with progressive disease (18% ± 32%).

To the best of our knowledge, this was the first clinical study directly comparing uptake of a tracer with drug concentrations after therapeutic dosing measured with LC-MS/MS in corresponding tumor biopsies. For sorafenib, concentrations in tumors during treatment could not be predicted by microdose [^{11}C]sorafenib PET studies. There are multiple factors that can help to explain these findings, such as intratumoral heterogeneity causing differences in outcome depending on the exact location of the tumor biopsy, partial saturation of drug transporting systems leading to differences in tumor accumulation between microdose and therapeutic dose, and slow drug-target binding kinetics after intra-tumor drug delivery for which 1 hour scanning time may have been too short to reflect drug-target occupation after 14 days of continuous sorafenib treatment. In addition, the tracer signal of [^{11}C]sorafenib is presumably complex as it binds to multiple pharmacological targets and the signal may be dominated by some targets, while other targets with less signal may lead to stronger antitumor effects. In contrast, there was preliminary evidence that early decrease in tumor perfusion as shown with [^{15}O]H_2O PET after only 2 weeks of treatment, may be associated with response to sorafenib treatment. This is in line with early perfusion reduction seen in patients with clinical benefit of other angiogenesis inhibitors, such as sunitinib and bevacizumab.[37,38] The amount of decrease in tumor perfusion may have early predictive value and may guide treatment choices before effects on conventional CT can be evaluated. Given the potential benefit for patients, this finding warrants further investigation in larger clinical trials. In addition to PET, other promising techniques currently under investigation as predictive biomarkers for sorafenib response include molecular subtyping, phosphoproteomics and liquid biopsies (NCT03956940).[39-44]

For future PET-studies that aim to investigate a dose-response relationship between tracer uptake and anti-cancer efficacy, we suggest to start by selecting drug tracers with strong affinity for one or a limited number of targets and linear, dose proportional pharmacokinetics, so that the microdose represents the behavior of the therapeutic dose. For some small molecule protein kinase inhibitors, this has already proven successful. A study in ten patients with non-small cell lung cancer (NSCLC) investigated the uptake of the endothelial growth factor receptor (EGFR) inhibitor [^{11}C]erlotinib in relation to EGFR mutations such as exon 19 deletion and exon 21 point mutations, which are positively correlated with the anti-tumor activity of erlotinib.[45] Compared with wild type EGFR, these mutations resulted in a 2-3 fold higher tumor binding activity of [^{11}C]erlotinib, p = 0.009, and tumor uptake of this tracer correlated well with treatment effects.[45] In addition, [^{11}C]afatinib PET has similar potential in patients with NSCLC, and showed significantly higher uptake in tumors harboring EGFR mutations in comparison to wild type tumours.[46] Other clinical studies are underway, including [^{18}F]dabrafenib PET in patients with BRAF-mutant metastatic melanoma (NCT02700763), [^{11}C]osimertinib PET in patients with metastatic EGFR mutated NSCLC (NCT03463525) and recently a study investigated [^{11}C]lapatinib PET which showed uptake in brain metastases in patients with HER2-positive breast cancer, but not in the normal brain, indicative of HER2 targeting across the blood brain barrier.[47] In addition to small molecule kinase inhibitors, PET imaging with labeled monoclonal antibodies has made rapid progress. For example, [^{89}Zr]trastuzumab PET showed to support clinical decision making when HER2 status could not be determined by standard work-up.[48] In addition, [^{89}Zr]rituximab PET in patients with diffuse large B cell lymphoma demonstrated a positive correlation between tumor uptake and CD20 expression in tumor biopsies.[49] Finally, [^{89}Zr]atezolizumab uptake in tumors appeared to be a strong predictor of response (including progression-free and overall survival) to the anti-PD-L1 monoclonal antibody atezolizumab in patients with various solid malignancies.[50]

Chapter 5 was performed to evaluate an alternative dosing schedule of sorafenib. In chapter 4 we already showed that in several patients sorafenib accumulation in tumors was lower in comparison to plasma. There is growing evidence that tumor concentrations reached with the current therapeutic sorafenib schedule of 400 mg twice daily are too low, resulting in overall marginal clinical activity, and that higher sorafenib exposure may be necessary.[51-53] In chapter 5, we performed a phase 1 study with high-dose, intermittent sorafenib. The aim was to reach the highest tolerable plasma sorafenib peak concentration supposed necessary for the highest intratumoral concentration to improve blockade of tumor kinase targets and increase sorafenib efficacy based on accumulating (pre)clinical literature.[51,53-55] Dose escalation was performed

according to a novel concept, i.e. based on exposure escalating cohorts, instead of conventional dose escalating cohorts, because administration of a fixed dose has previously shown to result in large variability in sorafenib plasma area under the curve (AUC)(0–12 h) per patient.[56] Drug monitoring was performed in weeks 1-3 and doses were adjusted to achieve a predefined target plasma AUC(0-12h). An important challenge for optimizing high-dose sorafenib administration is the amount of drug absorption in the gastrointestinal tract. Sorafenib absorption is saturable > 800 mg/day.[57] To overcome saturation of absorption, we applied dose fractioning, a standardized moderate fat diet, and investigated the effect of cola on sorafenib bioavailability.[57,58] A total of 17 patients with various advanced malignancies without standard treatment options were included. Once weekly, high-dose sorafenib exposure was escalated from a target AUC(0–12 h) of 25-50 mg/L/h up to 125–150 mg/L/h, achieving a twofold higher maximum plasma concentration (C_{max}) compared to standard continuous dosing. Dissolving sorafenib in cola, instead of water, did not improve sorafenib exposure. Dose-limiting toxicity (DLT) was observed in three patients: at the target AUC(0-12h) level of 75-100 mg/L/h 1 out of 6 patients suffered from grade 5 biliary tract perforation (3600 mg sorafenib) and at the target level of 125-150 mg/L/h 2 out of 3 patients developed grade 3 duodenal perforation (2800 mg sorafenib) and grade 5 multiorgan failure (2800 mg sorafenib), respectively. Clinical benefit with stable disease as the best response was observed in 2 patients. The mean difference between observed and target AUC(0–12 h) was 45% (SD ± 56%) in week 1 using a fixed starting dose of sorafenib compared to 2% (SD ± 32%) in week 3 as a result of drug monitoring (P = 0.06). The study showed the feasibility of drug monitoring to achieve a target sorafenib AUC(0-12h). Unfortunately, potentially effective high peak concentrations could not be reached due to early toxicity of this sorafenib schedule at lower dosing than anticipated; from doses of 2800 mg per day and higher, i.e. 3.5 times the conventional dose.

In contrast, a phase I study with high-dose, intermittent sunitinib, another inhibitor of angiogenesis, showed tolerability comparable to daily administration up to 14 times the conventional dose and promising preliminary efficacy with clinical benefit in 63% of the patients, including a PFS of ≥ 5 months in 30% of the patients and is therefore currently being investigated in two phase II trials (NCT03909724 and NCT03025893).[55] Possible explanations for this difference in tolerability between high-dose, pulsatile schedules of sorafenib and sunitinib may be the enterohepatic circulation of sorafenib, leading to a second round of exposure of the intestinal tract, and dose fractioning with multiple doses per day once a week, instead of one single dose per day once a week as was the case for sunitinib, resulting in high local sorafenib concentrations in the GI tract over a prolonged period of time inducing DLT. These results can

help select future targeted therapies suitable for alternative, pulsatile, high-dosing schedules. Other protein kinase inhibitors have also been subject of investigation, including the EGFR inhibitors erlotinib and gefitinib. Erlotinib administered at a pulsatile, high-dose of 2000 mg per week in NSCLC patients, was well tolerated and resulted in a mean overall survival (OS) of 9.5 months.[59] Another phase II study investigated high-dose erlotinib 450 mg every 3 days or the EGFR inhibitor gefitinib 1000 mg every 4 days in patients with known EGFR mutations and disease progression after treatment with conventional dose erlotinib or gefitinib.[60] Treatment was tolerated well and resulted in a median PFS of 6 months in both groups and response rates of 15 and 21%, respectively. Finally, a phase I study escalating the HER2 inhibitor lapatinib in heavily pre-treated patients with HER2-positive breast cancer to 7000 mg on days 1–5 of repeating 14-day cycles showed an objective response rate in 15% of the patients.[61] In addition, a preclinical study has demonstrated improved anti-tumor efficacy, including prolonged T-cell activity, of high-dose pulsatile MEK-inhibitors.[62] Further investigation of these alternative dosing strategies is necessary in an attempt to improve the activity of protein kinase inhibitors, preferably guided by techniques that can monitor the effects of these dose optimizing strategies, such as PET.

Conclusion

To conclude, PET imaging of targets and targeted anticancer therapies leads to better understanding of target expression in different tumor lesions within one patient and visualization of the tumor accumulation and effects of therapy. Although the development of each tracer has challenges, such as its target affinity, physiological background uptake and metabolism, concordance between tracer uptake and target expression/drug accumulation in tumors, physical half-life, scanning logistics, and reliable observer-independent evaluation, PET imaging has the potential to lead to progress in personalized treatment strategies, which includes dose optimizing strategies and treatment (combination) choices for an individual patient with cancer.

References

1. Blamey RW, Hornmark-Stenstam B, Ball G, et al: ONCOPOOL - a European database for 16,944 cases of breast cancer. Eur J Cancer 46:56-71, 2010
2. Yamashita H, Yando Y, Nishio M, et al: Immunohistochemical evaluation of hormone receptor status for predicting response to endocrine therapy in metastatic breast cancer. Breast Cancer 13:74-83, 2006
3. Collins LC, Cole KS, Marotti JD, et al: Androgen receptor expression in breast cancer in relation to molecular phenotype: results from the Nurses' Health Study. Mod Pathol 24:924-31, 2011
4. Youk JH, Kim EK, Kim MJ, et al: Missed breast cancers at US-guided core needle biopsy: how to reduce them. Radiographics 27:79-94, 2007
5. Chung GG, Zerkowski MP, Ghosh S, et al: Quantitative analysis of estrogen receptor heterogeneity in breast cancer. Lab Invest 87:662-9, 2007
6. Layfield LJ, Saria E, Mooney EE, et al: Tissue heterogeneity of immunohistochemically detected estrogen receptor. Implications for image analysis quantification. Am J Clin Pathol 110:758-64, 1998
7. Whitman GJ, Strom EA: Workup and staging of locally advanced breast cancer. Semin Radiat Oncol 19:211-21, 2009
8. Segaert I, Mottaghy F, Ceyssens S, et al: Additional value of PET-CT in staging of clinical stage IIB and III breast cancer. Breast J 16:617-24, 2010
9. Cardoso F, Senkus E, Costa A, et al: 4th ESO-ESMO International Consensus Guidelines for Advanced Breast Cancer (ABC 4)dagger. Ann Oncol 29:1634-1657, 2018
10. Brennan ME, Houssami N: Evaluation of the evidence on staging imaging for detection of asymptomatic distant metastases in newly diagnosed breast cancer. Breast 21:112-23, 2012
11. Groheux D, Giacchetti S, Moretti JL, et al: Correlation of high 18F-FDG uptake to clinical, pathological and biological prognostic factors in breast cancer. Eur J Nucl Med Mol Imaging 38:426-35, 2011
12. Bos R, van Der Hoeven JJ, van Der Wall E, et al: Biologic correlates of (18) fluorodeoxyglucose uptake in human breast cancer measured by positron emission tomography. J Clin Oncol 20:379-87, 2002
13. Iqbal R, Aras T, Mammatas L, et al: Staging with [18F]FDG PET/CT. Cancer Research 79, 2019
14. Venema C, de Vries E, Glaudemans A, et al: 18F-FES PET Has Added Value in Staging and Therapy Decision Making in Patients With Disseminated Lobular Breast Cancer. Clin Nucl Med 42:612-614, 2017
15. Boers J, Venema CM, de Vries EFJ, et al: Molecular imaging to identify patients with metastatic breast cancer who benefit from endocrine treatment combined with cyclin-dependent kinase inhibition. Eur J Cancer 126:11-20, 2020
16. Gennari A, Brain E, Nanni O, et al: 114PMolecular imaging with 18F-fluoroestradiol (18F-FES) to assess intra-patient heterogeneity in metastatic breast cancer (MBC): A European TRANSCAN program. Annals of Oncology 28, 2017
17. van Kruchten M, de Vries EG, Glaudemans AW, et al: Measuring residual estrogen receptor availability during fulvestrant therapy in patients with metastatic breast cancer. Cancer Discov 5:72-81, 2015

18. Scher HI, Beer TM, Higano CS, et al: Antitumour activity of MDV3100 in castration-resistant prostate cancer: a phase 1-2 study. Lancet 375:1437-46, 2010
19. Wang Y, Ayres KL, Goldman DA, et al: (18)F-Fluoroestradiol PET/CT Measurement of Estrogen Receptor Suppression during a Phase I Trial of the Novel Estrogen Receptor-Targeted Therapeutic GDC-0810: Using an Imaging Biomarker to Guide Drug Dosage in Subsequent Trials. Clin Cancer Res 23:3053-3060, 2017
20. Severson TM, Kim Y, Joosten SEP, et al: Characterizing steroid hormone receptor chromatin binding landscapes in male and female breast cancer. Nat Commun 9:482, 2018
21. Kennedy BJ: Fluoxymesterone therapy in advanced breast cancer. N Engl J Med 259:673-5, 1958
22. Goldenberg IS: Testosterone Propionate Therapy in Breast Cancer. JAMA 188:1069-72, 1964
23. Traina TA, Miller K, Yardley DA, et al: Enzalutamide for the Treatment of Androgen Receptor-Expressing Triple-Negative Breast Cancer. J Clin Oncol 36:884-890, 2018
24. Schwartzberg LS, Yardley DA, Elias AD, et al: A Phase I/Ib Study of Enzalutamide Alone and in Combination with Endocrine Therapies in Women with Advanced Breast Cancer. Clin Cancer Res 23:4046-4054, 2017
25. Venema CM, Bense RD, Steenbruggen TG, et al: Consideration of breast cancer subtype in targeting the androgen receptor. Pharmacology & Therapeutics 200:135-147, 2019
26. Chae SY, Ahn SH, Kim SB, et al: Diagnostic accuracy and safety of 16alpha-[(18)F] fluoro-17beta-oestradiol PET-CT for the assessment of oestrogen receptor status in recurrent or metastatic lesions in patients with breast cancer: a prospective cohort study. Lancet Oncol 20:546-555, 2019
27. Venema CM, Apollonio G, Hospers GA, et al: Recommendations and Technical Aspects of 16alpha-[18F]Fluoro-17beta-Estradiol PET to Image the Estrogen Receptor In Vivo: The Groningen Experience. Clin Nucl Med 41:844-851, 2016
28. Wilhelm SM, Adnane L, Newell P, et al: Preclinical overview of sorafenib, a multikinase inhibitor that targets both Raf and VEGF and PDGF receptor tyrosine kinase signaling. Mol Cancer Ther 7:3129-40, 2008
29. Escudier B, Eisen T, Stadler WM, et al: Sorafenib for treatment of renal cell carcinoma: Final efficacy and safety results of the phase III treatment approaches in renal cancer global evaluation trial. J Clin Oncol 27:3312-8, 2009
30. Llovet JM, Ricci S, Mazzaferro V, et al: Sorafenib in advanced hepatocellular carcinoma. N Engl J Med 359:378-90, 2008
31. Brose MS, Nutting CM, Jarzab B, et al: Sorafenib in radioactive iodine-refractory, locally advanced or metastatic differentiated thyroid cancer: a randomised, double-blind, phase 3 trial. Lancet 384:319-28, 2014
32. Gounder MM, Mahoney MR, Van Tine BA, et al: Sorafenib for Advanced and Refractory Desmoid Tumors. N Engl J Med 379:2417-2428, 2018
33. Strumberg D, Clark JW, Awada A, et al: Safety, pharmacokinetics, and preliminary antitumor activity of sorafenib: a review of four phase I trials in patients with advanced refractory solid tumors. Oncologist 12:426-37, 2007
34. Widmer N, Bardin C, Chatelut E, et al: Review of therapeutic drug monitoring of anticancer drugs part two--targeted therapies. Eur J Cancer 50:2020-36, 2014

35. Honeywell R, Yarzadah K, Giovannetti E, et al: Simple and selective method for the determination of various tyrosine kinase inhibitors used in the clinical setting by liquid chromatography tandem mass spectrometry. J Chromatogr B Analyt Technol Biomed Life Sci 878:1059-68, 2010
36. Torok S, Rezeli M, Kelemen O, et al: Limited Tumor Tissue Drug Penetration Contributes to Primary Resistance against Angiogenesis Inhibitors. Theranostics 7:400-412, 2017
37. de Langen AJ, van den Boogaart V, Lubberink M, et al: Monitoring response to antiangiogenic therapy in non-small cell lung cancer using imaging markers derived from PET and dynamic contrast-enhanced MRI. J Nucl Med 52:48-55, 2011
38. Scott AM, Mitchell PL, O'Keefe G, et al: Pharmacodynamic analysis of tumour perfusion assessed by 15O-water-PET imaging during treatment with sunitinib malate in patients with advanced malignancies. EJNMMI Res 2:31, 2012
39. Horwitz E, Stein I, Andreozzi M, et al: Human and mouse VEGFA-amplified hepatocellular carcinomas are highly sensitive to sorafenib treatment. Cancer Discov 4:730-43, 2014
40. Arao T, Ueshima K, Matsumoto K, et al: FGF3/FGF4 amplification and multiple lung metastases in responders to sorafenib in hepatocellular carcinoma. Hepatology 57:1407-15, 2013
41. Miyahara K, Nouso K, Morimoto Y, et al: Pro-angiogenic cytokines for prediction of outcomes in patients with advanced hepatocellular carcinoma. Br J Cancer 109:2072-8, 2013
42. Sun W, Li S, Xu L, et al: High FLT3 Levels May Predict Sorafenib Benefit in Hepatocellular Carcinoma. Clin Cancer Res, 2020
43. Wirbel J, Cutillas P, Saez-Rodriguez J: Phosphoproteomics-Based Profiling of Kinase Activities in Cancer Cells. Methods Mol Biol 1711:103-132, 2018
44. Labots M, Pham TV, Honeywell RJ, et al: Kinase Inhibitor Treatment of Patients with Advanced Cancer Results in High Tumor Drug Concentrations and in Specific Alterations of the Tumor Phosphoproteome. Cancers (Basel) 12, 2020
45. Bahce I, Smit EF, Lubberink M, et al: Development of [(11)C]erlotinib positron emission tomography for in vivo evaluation of EGF receptor mutational status. Clin Cancer Res 19:183-93, 2013
46. van de Stadt E, Yaqub M, Poot A, et al: Can [18F] afatinib PET/CT be used in identifying NSCLC patients with different EGFR mutational status: tracer quantification and assessment of tumor uptake. Journal of Nuclear Medicine 60:522-522, 2019
47. Saleem A, Searle GE, Kenny LM, et al: Lapatinib access into normal brain and brain metastases in patients with Her-2 overexpressing breast cancer. EJNMMI research 5:1-10, 2015
48. Bensch F, Brouwers AH, Lub-de Hooge MN, et al: (89)Zr-trastuzumab PET supports clinical decision making in breast cancer patients, when HER2 status cannot be determined by standard work up. Eur J Nucl Med Mol Imaging 45:2300-2306, 2018
49. Jauw YW, Zijlstra JM, de Jong D, et al: Performance of 89Zr-Labeled-Rituximab-PET as an Imaging Biomarker to Assess CD20 Targeting: A Pilot Study in Patients with Relapsed/Refractory Diffuse Large B Cell Lymphoma. PLoS One 12:e0169828, 2017

50. Bensch F, van der Veen EL, Lub-de Hooge MN, et al: (89)Zr-atezolizumab imaging as a non-invasive approach to assess clinical response to PD-L1 blockade in cancer. Nat Med 24:1852-1858, 2018
51. Escudier B, Szczylik C, Hutson TE, et al: Randomized phase II trial of first-line treatment with sorafenib versus interferon Alfa-2a in patients with metastatic renal cell carcinoma. J Clin Oncol 27:1280-9, 2009
52. Pecuchet N, Lebbe C, Mir O, et al: Sorafenib in advanced melanoma: a critical role for pharmacokinetics? Br J Cancer 107:455-61, 2012
53. Wang X, Zhang L, Goldberg SN, et al: High dose intermittent sorafenib shows improved efficacy over conventional continuous dose in renal cell carcinoma. J Transl Med 9:220, 2011
54. Rovithi M, Verheul HMW: Pulsatile high-dose treatment with antiangiogenic tyrosine kinase inhibitors improves clinical antitumor activity. Angiogenesis 20:287-289, 2017
55. Rovithi M, Gerritse SL, Honeywell RJ, et al: Phase I Dose-Escalation Study of Once Weekly or Once Every Two Weeks Administration of High-Dose Sunitinib in Patients With Refractory Solid Tumors. J Clin Oncol 37:411-418, 2019
56. Strumberg D, Richly H, Hilger RA, et al: Phase I clinical and pharmacokinetic study of the Novel Raf kinase and vascular endothelial growth factor receptor inhibitor BAY 43-9006 in patients with advanced refractory solid tumors. J Clin Oncol 23:965-72, 2005
57. Hornecker M, Blanchet B, Billemont B, et al: Saturable absorption of sorafenib in patients with solid tumors: a population model. Invest New Drugs 30:1991-2000, 2012
58. van Leeuwen RW, Peric R, Hussaarts KG, et al: Influence of the Acidic Beverage Cola on the Absorption of Erlotinib in Patients With Non-Small-Cell Lung Cancer. J Clin Oncol 34:1309-14, 2016
59. Milton DT, Azzoli CG, Heelan RT, et al: A phase I/II study of weekly high-dose erlotinib in previously treated patients with nonsmall cell lung cancer. Cancer 107:1034-41, 2006
60. Zhu Y, Du Y, Liu H, et al: Study of efficacy and safety of pulsatile administration of high-dose gefitinib or erlotinib for advanced non-small cell lung cancer patients with secondary drug resistance: A single center, single arm, phase II clinical trial. Thoracic cancer 7:663-669, 2016
61. Chien AJ, Munster PN, Melisko ME, et al: Phase I dose-escalation study of 5-day intermittent oral lapatinib therapy in patients with human epidermal growth factor receptor 2-overexpressing breast cancer. J Clin Oncol 32:1472-9, 2014
62. Choi H, Deng J, Li S, et al: Pulsatile MEK inhibition improves anti-tumor immunity and T cell function in murine Kras mutant lung cancer. Cell reports 27:806-819. e5, 2019

CHAPTER 7

Appendices

Dutch summary
Acknowledgements
Curriculum Vitae
List of publications

Nederlandse Samenvatting

Kanker is de belangrijkste doodsoorzaak na hart- en vaatziekten in Europa en heeft zeer grote impact op patiënten, hun dierbaren en de maatschappij: ieder jaar krijgen meer dan 3 miljoen patiënten deze diagnose en sterven 1.7 miljoen mensen als gevolg hiervan. Er zijn de laatste jaren vele nieuwe antikankerbehandelingen ontwikkeld, zoals nieuwe zogenaamde doelgerichte therapieën ("targeted therapieën"), medicijnen die de groei en deling van kankercellen blokkeren doordat ze de werking tegengaan van specifieke moleculen ("targets") die de kankercellen nodig hebben voor hun groei en overleving. Bij targeted therapieën wordt gebruik gemaakt van het verschil tussen normale lichaamscellen en kankercellen, waar deze targets bijvoorbeeld tot (over)expressie komen of in een gemuteerde vorm aanwezig zijn.

Hormoontherapie kan worden beschouwd als de oudste vorm van targeted therapie omdat het tegengaat dat een hormoon groei-impulsen kan geven aan een hormoonreceptor gedreven tumor, zoals bijvoorbeeld een oestrogeenreceptor-positieve borstkanker (mammacarcinoom). De ontdekking van nieuwe tumortargets heeft geleid tot de ontwikkeling van diverse andere targeted therapieën die bijvoorbeeld groeisignaalroutes blokkeren of bloedvatnieuwvorming (angiogenese) van tumoren tegengaan.

Slechts bij de helft van de in de praktijk toegepaste targeted therapieën zijn er testen beschikbaar om te voorspellen welke patiënten wel of niet zullen reageren op een antikankerbehandeling (predictieve biomarkers). Voorbeelden hiervan zijn HER2-receptor overexpressie of een PIC_3CA mutatie die aanwezig moeten zijn bij patiënten met mammacarcinoom om een potentieel effect te kunnen verwachten van respectievelijk HER2-antilichamen of $PI_3K\alpha$-remmers. Echter, ook als dergelijke predictieve biomarkers beschikbaar zijn, bestaan er beperkingen bij de toepasbaarheid voor de patiënt. Dergelijke testen worden namelijk vooral bepaald in tumorweefsel waarvoor invasieve biopten nodig zijn, iets wat niet altijd mogelijk of veilig is door de locatie van de tumor, noch patiëntvriendelijk. Soms kan er net naast de tumor, in normaal weefsel, worden geprikt (sample errors), waardoor de procedure opnieuw moet plaatsvinden. Daarbij kan de expressie van een biomarker veranderen in de loop der tijd en verschillen tussen de verschillende tumorlocaties binnen één patiënt. Als gevolg hiervan kan één enkel tumorbiopt inadequate informatie geven voor een persoonlijk behandelplan. Het is daarom van belang om nieuwe methoden te ontwikkelen die het effect van een antikankerbehandeling kunnen voorspellen.

Positron emissie tomografie (PET) is een onderzoek waarbij een radioactieve stof (tracer) kan worden afgebeeld in het lichaam. De manier waarop tumoren

en normale lichaamsweefsels de tracer opnemen kan hiermee zichtbaar worden gemaakt, gemeten en informatie geven over de stof. Deze techniek heeft als voordeel dat het in één keer informatie geeft over de verschillende tumorlocaties binnen één patiënt op een weinig belastende manier. PET imaging kan bijvoorbeeld inzicht geven over de mate van targetexpressie op/in tumoren en de mate waarin een doelgerichte therapie die gekoppeld is aan een radioactieve stof de tumorlocaties in het lichaam bereikt. Dit zou kunnen helpen bij het voorspellen van de effecten van een targeted therapie bij een individuele patiënt.

Dit proefschrift beschrijft onderzoek naar de waarde van verschillende PET-technieken om tumortargets en targeted therapieën af te kunnen beelden met als doel te beoordelen of deze technieken al dan niet in de toekomst gebruikt kunnen worden om de juiste antikankerbehandeling voor een individuele patiënt te selecteren.

In **Hoofdstuk 1** wordt een introductie en overzicht gegeven van de ontwikkelingen op het gebied van PET imaging om antikankerbehandelingen te visualiseren en personaliseren. Er zijn tracers in ontwikkeling die tumortargets afbeelden, maar ook radioactief gelabelde targeted therapieën zoals proteïne/tyrosine kinase remmers (TKI-PET), of grote monoclonale antilichamen (immuno-PET). Hoewel er nu nog een beperkt aantal patiëntgebonden onderzoeken gepubliceerd zijn over dit onderwerp, tonen deze de mogelijkheden die geboden worden als potentiele predictieve biomarker, bij vroege evaluatie van behandeleffecten en om doseerstrategieën voor een individuele patiënt te kunnen optimaliseren.

Deel 1 Het visualiseren van tumortargets: hormoonreceptor imaging

Deel 1 van het proefschrift richt zich op PET imaging van tumortargets: de oestrogeen receptor (ER) en androgeen receptor (AR) bij patiënten met mammacarcinoom. Correcte identificatie van de hormoonreceptorexpressie van borstkanker is van belang voor behandelbeslissingen. Bij ongeveer 75% van de patiënten met mammacarcinoom is er sprake van ER-expressie. De tumorcellen groeien als oestrogeen aan deze receptor bindt en het is de belangrijkste voorspeller voor een potentiële respons op hormoontherapie. Recent is ook de AR onder de aandacht gekomen als een mogelijke target voor therapie bij mammacarcinoom, welke aanwezig is op 70-80% van de borstkankers. Verschillende studies onderzoeken op dit moment de waarde van AR-blokkerende medicijnen bij de behandeling van mammacarcinoom. Een tumor biopsie is de gouden standaard om hormoonreceptorexpressie te bepalen. De PET-technieken [^{18}F]fluor-17β-oestradiol ([^{18}F]FES) PET en 16β-[^{18}F]fluor-5α-dihydrotestosteron ([^{18}F]FDHT) PET zijn ontwikkeld om op non-invasieve manier ER- en AR-expressie van verschillende tumorlaesies binnen een

patiënt te kunnen bepalen. Dit proefschrift levert een bijdrage aan de validatie van hormoonreceptor PET, wat nodig is voor toekomstige toepassing hiervan in de dagelijkse praktijk.

In **Hoofdstuk 2** staat beschreven in hoeverre [^{18}F]FES en [^{18}F]FDHT PET opname overeenkomt met de mate van ER- en AR-expressie gemeten in een biopt van eenzelfde tumor laesie bij 13 patiënten met uitgezaaid (gemetastaseerd) mammacarcinoom. De mate van [^{18}F]FES en [^{18}F]FDHT opname (maximale Standardized Uptake Value, SUV_{max}) in tumoren, was respectievelijk sterk geassocieerd met ER-expressie (R^2 = 0.78, P = 0.01) en redelijk geassocieerd met AR-expressie (R^2 = 0.47, P = 0.01). De optimale [^{18}F]FES afkapwaarde voor ER-expressie (gedefinieerd als > 1% kernaankleuring) was een SUV_{max} van 1.54, resulterend in een sensitiviteit en specificiteit van 100%. De optimale [^{18}F]FDHT afkapwaarde voor AR-expressie (gedefinieerd als > 10% kernaankleuring) was een SUV_{max} van 1.94, resulterend in een sensitiviteit van 91% en specificiteit van 100%. Er was heterogeniteit in traceropname tussen de tumorlaesies binnen een patiënt, waarbij het merendeel van de patiënten zowel tumorlaesies met als zonder traceropname van respectievelijk [^{18}F]FES en [^{18}F]FDHT hadden. Ook was er bij 23% van de patiënten receptorconversie aantoonbaar tussen biopten van metastasen vergeleken met de primaire tumor. Deze resultaten tonen aan dat [^{18}F]FES en [^{18}F]FDHT PET als een non-invasieve surrogaat zouden kunnen dienen van invasieve tumorbiopten om de receptorstatus te bepalen in de verschillende tumorlaesies binnen een patiënt met borstkanker. Grotere vervolgstudies zijn nodig om deze resultaten te bevestigen.

Hoofdstuk 3 beschrijft onderzoek naar de mate van visuele en kwantitatieve variabiliteit tussen beoordelaars van [^{18}F]FES en [^{18}F]FDHT PET scans bij patiënten met gemetastaseerd mammacarcinoom. Bij visuele beoordeling wordt er met het oog gekeken of tumorweefsel meer tracer opneemt dan de achtergrondaankleuring in normaal weefsel. Bij kwantitatieve beoordeling wordt de hoeveelheid traceropname in (tumor)weefsel daadwerkelijk gemeten en uitgedrukt als SUV: de gemeten radioactiviteit in de tumor gecorrigeerd voor de hoeveelheid geïnjecteerde radioactiviteit en het lichaamsgewicht. Hiervoor werden de volgende SUV-maten gebruikt: SUV_{max} (de voxel in de tumor met de hoogste waarde), SUV_{peak} (de gemiddelde waarde in een gebied van 1 cm^3 rondom de heetste voxel van de tumor) en SUV_{mean} met isocontour 50% (de gemiddelde waarde van alle voxels in de tumor waarbij de uptake ≥ 50% van de SUV_{max} is). We toonden aan dat er een hoge mate van reproduceerbaarheid is tussen onafhankelijke beoordelaars van [^{18}F]FES PET scans in verschillende ziekenhuizen waar andere PET-scanners en analyse software wordt gebruikt. Het absolute aantal visueel positieve en negatieve consistente waarnemingen (positive/negative absolute interobserver agreement) tussen beoordelaars van

[^{18}F]FES PET scans was > 80%. Cohen's kappa (visuele interobserver agreement met correctie voor toevalsovereenstemming) was 0.67 (95% CI 0.48-0.87). Intraclass correlatiecoëfficiënten (ICC) voor de mate van overeenstemming tussen beoordelaars met betrekking tot de kwantificatie van SUV_{max}, SUV_{peak} and SUV_{mean} waren 0.98 (95% CI 0.96-0.98), 0.97 (95% CI 0.96-0.98) en 0.89 (95% CI 0.83-0.92). Voor [^{18}F]FDHT PET werd een relatief lage mate van consistentie tussen beoordelaars getoond met betrekking tot visuele waarnemingen. Het absolute aantal visuele positieve en negatieve consistente waarnemingen was respectievelijk 49% en 74%, waarbij Cohen's kappa 0.23 was (95% CI -0.04-0.49). Dit is waarschijnlijk het gevolg van de lagere tumor/achtergrond ratio voor de opname van [^{18}F]FDHT ten opzichte van [^{18}F]FES. Echter, er was goede overeenkomst tussen beoordelaars met betrekking tot de kwantificatie van [^{18}F]FDHT opname (ICC ≥ 0.75). Dit benadrukt het belang van kwantitatieve [^{18}F]FDHT beoordelingen bij toekomstig borstkankeronderzoek, terwijl voor [^{18}F]FES PET zowel visuele als kwantitatieve beoordelingen reproduceerbaar zijn in de dagelijkse praktijk.

De rol van [^{18}F]FES PET bij de behandeling van oestrogeenreceptor-positief mammacarcinoom wordt op dit moment onderzocht in verschillende (vervolg) studies o.a. bij de stadiëring (bepaling van de uitgebreidheid) van borstkanker, bij het bepalen van de optimale dosering van nieuwe vormen van hormoontherapie en om vast te stellen of de mate van heterogeniteit tussen tumorlaesies binnen één patiënt met gemetastaseerde ziekte kan helpen bij keuzes voor het starten van endocriene monotherapie, danwel combinatietherapieën.

Deel 2 Het visualiseren van targeted therapieën en effecten: sorafenib imaging

Deel 2 van het proefschrift is gewijd aan het medicijn sorafenib. Sorafenib is een orale proteïne kinase remmer met activiteit tegen verschillende targets betrokken bij de groei, angiogenese en metastasering van kanker zoals de eiwitten C-RAF, B-RAF, gemuteerd B-RAF, vasculair endotheliale groeifactor receptoren 1, 2 en 3, bloedplaatjes afgeleide groeifactor receptor β, FMS-like tyrosine kinase 3, c-Kit en RET-receptor tyrosine kinase. Sorafenib is in Nederland goedgekeurd als behandeling van lokaal gevorderd en gemetastaseerd hepatocellulair carcinoom, niercelcarcinoom en gedifferentieerd schildkliercarcinoom dat refractair is voor radioactief jodium. Hierbij krijgen patiënten standaard een vaste dosering van 400 mg tweemaal per dag continue voorgeschreven. Echter, de respons op sorafenib is variabel waarbij slechts een deel van de behandelde patiënten daadwerkelijk baat heeft van het medicijn, terwijl alle patiënten worden blootgesteld aan mogelijke toxiciteit. De meest voorkomende bijwerkingen omvatten onder andere maag-darm klachten, vermoeidheid en huidreacties (hand-voetsyndroom). Op dit moment zijn er geen methoden

beschikbaar om te voorspellen welke patiënten baat zullen hebben van een behandeling met sorafenib.

In **Hoofdstuk 4** wordt onderzoek beschreven naar de waarde van [^{11}C]sorafenib PET en [^{15}O]H_2O PET als respectievelijk predictieve en vroege biomarker van een respons op sorafenib. Voor een antitumor effect moet een adequate concentratie van het medicijn de tumor bereiken. Het primaire doel van de studie was om te onderzoeken in hoeverre een microdosis [^{11}C]sorafenib dynamische PET scan vooraf en na 14 dagen behandeling met sorafenib, de concentratie in de tumor kon voorspellen tijdens therapie zoals werd gemeten in corresponderende tumorbiopten met zogenaamde vloeibare chromatografie in combinatie met tandem massaspectrometrie (LC-MS/MS). In deze prospectieve exploratieve studie werden 8 patiënten met verschillende gemetastaseerde tumoren geïncludeerd die in aanmerking kwamen voor een behandeling met sorafenib. De [^{11}C]sorafenib opname in tumorweefsel vanuit het bloed, gemeten als het totale distributievolume (V_T), was niet voorspellend (baseline, noch na 14 dagen behandeling) voor de concentraties sorafenib gemeten in tumorbiopten met LC-MS/MS. Bij een minderheid van de patiënten kwam de [^{11}C]sorafenib opname en de concentratie sorafenib in de tumor boven die van het plasma uit. In deze exploratieve studie waren de concentraties sorafenib die met LC-MS/MS in plasma en tumorweefsel werden gemeten ook niet voorspellend voor de respons op therapie. Echter, hogere [^{11}C]sorafenib opname in tumoren werd gemeten bij patiënten met een slechtere uitkomst (V_T voor patiënten met progressieve ziekte versus patiënten die klinisch baat hadden van de behandeling: baseline 0.92 ± 0.61 versus 0.34 ± 0.08 en na 14 behandeling 0.37 ± 0.18 versus 0.13 ± 0.05). De [^{11}C]sorafenib V_T was geassocieerd met de perfusie van de tumor (r_s = 0.671, P = 0.020). Eerdere studies toonden een associatie tussen een hogere mate van tumorangiogenese en een slechtere prognose, wat een verklaring kan zijn voor deze bevindingen. Bij patiënten met stabiele ziekte op de CT-scan toonde [^{15}O]H_2O PET al na 14 dagen therapie een grotere percentuele daling in tumorperfusie (56% ± 23%) vergeleken met patiënten die progressieve ziekte hadden (18% ± 32%). Huidige responsevaluatie met conventionele CT-scans vindt na gemiddeld 12 weken behandeling plaats, het is dus van belang dat toekomstige studies de rol van [^{15}O]H_2O PET verder onderzoeken bij het vroegtijdig (na 2 weken) identificeren van patiënten die baat hebben van een behandeling met angiogeneseremmers zoals sorafenib.

In **Hoofdstuk 5** wordt een alternatief doseringsschema van sorafenib onderzocht. In het vorige hoofdstuk toonden we dat bij de meerderheid van de patiënten de sorafenib concentratie in tumoren lager was vergeleken met de concentratie in plasma. Ook in eerder dierproefonderzoek is aangetoond dat sorafenib een duidelijk lagere tumoraccumulatie toont vergeleken met

andere angiogeneseremmers. Een hoge, intermitterende dosering sorafenib toonden in muizen een verbetering van de antikankereffecten vergeleken met conventionele continue dosering. In dit hoofdstuk wordt een fase I studie beschreven waarbij 17 patiënten tabletten sorafenib wekelijks intermitterend in een hoge dosering innamen. De hypothese was dat een hogere piekdosering zou kunnen resulteren in hogere tumorconcentraties sorafenib en dat dit de blokkade van tumor kinase targets en de effectiviteit van sorafenib zou kunnen verbeteren. Het hoofddoel was om de hoogst tolereerbare blootstelling aan wekelijks sorafenib vast te stellen. Dosisescalatie werd volgens een nieuw concept uitgevoerd: door middel van exposure-escalatie cohorten op geleide van een na te streven plasmaconcentratie (area under the curve, AUC (0-12h)) in plaats van conventionele dosisescalatie cohorten. Eerder onderzoek toonde namelijk dat een vaste dosis sorafenib resulteert in een hoge mate van AUC(0-12h) variabiliteit tussen patiënten. Wij pasten drug monitoring toe in week 1 t/m 3 waarbij de doseringen werden aangepast per patiënt om de streef AUC(0-12h) van het cohort te bereiken. Een belangrijke uitdaging was de absorptie van sorafenib in het maagdarmkanaal. Sorafenib absorptie neemt namelijk sterk af bij doseringen > 800 mg per dag. Om de verminderde absorptie bij hogere doseringen te kunnen voorkomen werden de wekelijkse doseringen gesplitst in meerdere porties die dag (dosis fractionering), werd een gestandaardiseerd matig vet dieet gegeven om sorafenib opname te verbeteren en werd het effect van klassieke Coca Cola, een zure drank met een pH van 2.5, onderzocht op de biologische beschikbaarheid van sorafenib. Totaal werden 17 patiënten geïncludeerd met diverse gemetastaseerde maligniteiten voor wie er geen reguliere behandelingen meer beschikbaar waren. Wekelijks, hoge dosis sorafenib exposure kon in stappen worden opgehoogd van streef AUC(0–12 h) 25-50 mg/L/h tot maximaal 125–150 mg/L/h en dit resulteerde in een maximale plasmaconcentratie (C_{max}) die tweemaal hoger was vergeleken met standaard continue dosering. De biologische beschikbaarheid van sorafenib verbeterde niet door dit op te lossen in cola in plaats van water. Dosis limiterende toxiciteit (DLT) werd geobserveerd bij 3 patiënten: in het cohort met streef AUC(0-12h) 75-100 mg/L/h kreeg 1 van de 6 patiënten een graad 5 galwegperforatie (3600 mg wekelijks sorafenib) en in het cohort met streef AUC(0-12h) 125-150 mg/L/h kregen 2 van de 3 patiënten respectievelijk een graad 3 duodenumperforatie (2800 mg wekelijks sorafenib) en graad 5 multiorgaanfalen (2800 mg wekelijks sorafenib. Stabiele ziekte was de beste behandelrespons in deze studie en werd geobserveerd bij 2 patiënten. Het gemiddelde verschil tussen de gemeten en nagestreefde AUC(0–12 h) was 45% (SD ± 56%) in week 1 met een vaste startdosering vergeleken met 2% (SD ± 32%) in week 3 als gevolg van drug monitoring (P = 0.06). De studie toont de uitvoerbaarheid aan van drug monitoring om een sorafenib AUC(0-12h) na te streven. Helaas konden er geen potentieel effectieve hoge piek concentraties worden bereikt door vroege

toxiciteit bij lagere doseringen sorafenib dan geanticipeerd: vanaf een wekelijkse doses van 2800 mg en hoger, dus slechts 3.5 maal de conventionele dagelijkse dosering sorafenib. Mogelijke verklaringen hiervoor zijn dosisfractionering en de enterohepatische kringloop van sorafenib, waarbij na opname en vervolgens uitscheiding door de galwegen, de darmen langere tijd worden blootgesteld aan sorafenib leidend tot DLT. Deze bevindingen kunnen helpen om toekomstige targeted therapieën te selecteren die wel/niet geschikt zijn voor onderzoek met alternatieve hoge, intermitterende doseringsschema's.

Conclusie

PET imaging van targets en targeted antikankertherapieën leidt tot een beter inzicht in de targetexpressie van de verschillende tumorlaesies binnen één patiënt en maakt het mogelijk om behandelingen en behandeleffecten in het lichaam te visualiseren en kwantificeren. De ontwikkeling van iedere nieuwe PET tracer heeft diverse uitdagingen, zoals het vaststellen van de affiniteit van een tracer voor de target van interesse, de fysiologische achtergrondopname en het metabolisme van een tracer in het lichaam, concordantie tussen de microdose traceropname en de daadwerkelijke medicijnconcentratie in de tumor tijdens behandeling, de logistiek van productie tot aan distributie van een tracer rekening houdend met de halfwaardetijd door radioactief verval, gestandaardiseerde scanmethoden en betrouwbare, reproduceerbare beoordelingen van de scans. Maar, als deze uitdagingen zijn overwonnen kan PET imaging tot vooruitgang leiden in behandelstrategieën toegespitst op een individuele patiënt met kanker, dit omvat bijvoorbeeld de selectie van een (gecombineerde) tumorbehandeling of dosisoptimalisatie strategieën.

Dankwoord

Dit proefschrift is mogelijk geworden door de inzet van vele mensen. Hierbij wil ik eenieder bedanken voor alle hulp en betrokkenheid in de afgelopen jaren. Een aantal personen wil ik daarbij in het bijzonder bedanken.

Op de eerste plaats is mijn dank groot aan alle patiënten die, ondanks hun ernstige ziekte en alle onzekerheid die dit met zich meebrengt, aan het onderzoek hebben willen deelnemen. Zij ondergingen biopten, scans en ziekenhuisopnames voor de wetenschap. Zo vaak hoorde ik: 'ook al heb ik er zelf niks aan, dan hebben jullie hopelijk wat kunnen leren voor de patiënten na mij'. Dit getuigt van grote onbaatzuchtigheid en moed. Graag had ik sommige uitkomsten van deze thesis anders gezien, grotere stappen voor u willen zetten, maar kanker is zo complex.

Natuurlijk wil ik ook mijn (co)promotoren bedanken. Prof. dr. H.M.W. Verheul, beste Henk, een hoogleraar die marathons rent in het weekend… Ik herinner me nog het eerste gesprek dat we hadden ingeroosterd om te bespreken dat ik graag translationeel oncologisch onderzoek wilde doen. Wat binnensmonds en voorzien van een lichte frons vertelde je mij dat dit niet gemakkelijk zou zijn naast de opleiding, dat hiervoor meerdere jaren moest worden uitgetrokken en dit ook in de vrije tijd de nodige investering zou vergen, en dat hier natuurlijk ook financiering voor geregeld zou moeten worden. Dankbaar ben ik dat ik de kans hiervoor gekregen heb, en de frons was terecht, want een promotietraject opzetten en uitvoeren naast een opleiding tot medisch oncoloog is geen sinecure, maar deze marathon is nu ten einde. Wat mij verder zal bijblijven is jouw manier van "contra-denken": steevast de compleet tegenovergestelde invalshoek kiezen dan die van de onderzoeker. Dit houdt de discussie scherp en kan leiden tot verrassende resultaten.

Prof. dr. A.A. Lammertsma, beste Adriaan, zo veel kennis wat betreft kwantitatieve PET-studies om de kinetiek van tracers in de mens te bestuderen! Meer dan 500 wetenschappelijke artikelen dragen jouw naam als (co)auteur in de loop der jaren, maar toch was ook jij verbaasd over het gedrag van de tracer [^{11}C]sorafenib. Jouw expertise, waarbij steeds nieuwe fysische analyses werden bedacht om deze tracer beter te kunnen doorgronden, zijn van groot belang geweest.

Prof. dr. E. Boven, beste Epie, bij jou is mijn eerste onderzoek ooit begonnen, een wetenschappelijke stage tijdens de studie geneeskunde. Een grande dame binnen de oncologie, direct, nauwgezet en gedreven. Je hebt de oncologie zien ontwikkelen en hier ook een belangrijke bijdrage aan geleverd ("al in 1985

publiceerden Tore Lindmo en ik een eerste artikel over het berekenen van de immunofractie na labelen van een monoclonaal antilichaam"), dank voor jouw interesse in dit onderzoek ook na het pensioen.

Dr. C.W. Menke-van der Houven van Oordt, beste Willemien, toen wij begonnen met dit onderzoek was PET imaging voor ons beiden nog relatief nieuwe materie. Je bijtte je erin vast en wist van de verschillende afdelingen en centra de juiste mensen samen te brengen. Daarbij wilde je van ieder dat de onderste steen boven kwam. Dat leidde bijvoorbeeld tot een uitgebreide lijst aan vragen in de kanttekening van mijn manuscripten. Dit alles heeft zijn vruchten afgeworpen, want inmiddels is er een lijst met mooie imaging publicaties tot stand gekomen binnen de afdeling medische oncologie en interessante vervolgonderzoeken door nieuwe promovendi zijn gaande. Ik herinner me nog jouw verjaardag tijdens ons laatste congres in Wenen, waarbij wij je als verrassing meenamen naar de staatsopera. Ondanks dat we maar een deel van het podium konden zien klonk "una furtiva lagrima" prachtig, een toepasselijke afsluiting van de SOPRANO studie. Veel dank!

Leden van de leescommissie, Prof. dr. J.M. Zijlstra-Baalbergen, Prof. dr. R.J. Bennink, Prof. dr. G.S. Sonke, Dr. W. Vogel, Dr. N. van Erp, Dr. I. Bahce, Dr. S. Oosting, Dr. N. Bijker, veel dank voor de aandacht waarmee u dit proefschrift heeft bestudeerd en de tijd die u genomen heeft voor het voeren van de oppositie.

Verder was dit proefschrift niet mogelijk geweest zonder de volgende personen. Dr. M. Yaqub, beste Maqsood, jouw rol bij dit proefschrift was essentieel. Als de dynamische PET-onderzoeken gedaan zijn, begint het echte analytische werk namelijk pas. Achter de computer VOI's tekenen en dan 'modellen', 'fitten' en kijken naar de uitkomsten zoals V_T en delta K1. Een taal apart om klinisch relevante data te krijgen, veel dank ook voor jouw rol als tolk hierbij.

Prof. dr. O.S. Hoekstra, beste Otto, als nucleair geneeskundige met veel onderzoekservaring was jouw bijdrage van grote waarde. Een nuchtere blik, altijd pragmatisch en je voorziet ons in supersnelle mails van nuttige respons. Dank dat je me de PET-scans leerde beoordelen, hier heb ik in de dagelijkse praktijk nog heel veel profijt van.

Prof. dr. G.J. Peters, beste Frits, wij werkten al samen tijdens mijn allereerste fase-1-onderzoek bij de afdeling medische oncologie als geneeskundestudent. Nu dus ook een fijne samenwerking bij dit proefschrift, dank voor al het meedenken en jouw scherpzinnige commentaar.

Dr. R. Honeywell en Dr. R. Schuit, beste Richard en Robert, beide de mannen van de sorafenib metingen in bloed, de ene van de 'koude' en de andere van de 'hete' variant. De kleinste hoeveelheden werden door jullie zorgvuldig gemeten en het was daarom ook een lastige kwestie dat koud zich niet door heet liet voorspellen. Dank voor jullie input om dit beter te kunnen begrijpen.

Dr. A. Zandvliet, beste Anthe, dank voor jouw farmacologische bijdrage, je bent creatief en strategisch, precies wat nodig is om het maximale uit een studie te kunnen halen.

Oncologisch onderzoekers: Liesbeth, Suzanne, Maria, Madelon, Dennis, Robin, Elske, Esther, Joeri, Hanneke, Lisanne, Henk, Richard, Tineke, Mariette en Kathelijn, veel dank voor de fijne sfeer, interessante voordrachten en mooie discussies die zeer waardevol waren voor de voortgang van de onderzoeken.

Imagers uit het UMC Groningen, veel dank voor de fijne samenwerking tijdens het onderzoek met [^{18}F]FES en [^{18}F]FDHT PET. Dergelijke samenwerkingen zijn van groot belang om sneller vooruitgang te kunnen boeken binnen de oncologie.

Researchverpleegkundigen van de afdeling Medische Oncologie, Medisch Nucleair Werkers en verpleegkundigen van afdeling 4A, veel dank voor al jullie hulp bij het uitvoeren van deze onderzoeken, jullie altijd lieve bejegening en verzorging van de deelnemende patiënten en jullie interesse naar de resultaten.

Collega's uit het VU medisch centrum, Antoni van Leeuwenhoek, College ter Beoordeling van Geneesmiddelen en Reinier de Graaf Gasthuis, veel dank voor jullie interesse in dit proefschrift. Addy, Annelie, Arjan en Marlies, wat heb ik het getroffen met jullie als collega-oncologen in het Reinier de Graaf Gasthuis!

Behalve de opgedane kennis, houd ik ook een aantal vrienden over aan dit proefschrift. Lieve Ludo's (deze vreemde naam is te danken aan een concert van Ludovico Einaudi). Totaal 7 onderzoekers die op de te kleine kamer van 3A17 al snel vriendschap sloten. Compleet verschillende karakters, met ieder zo zijn/haar eigen kracht (en eigenaardigheden) en bovenal doorzetters die hun einddoel weten te bereiken en tussendoor het gemoed hooghouden met veel humor. Dinja Kruger, powervrouw, direct, niet bang voor confrontaties, maar ook beschermend en dat gaat veel verder dan de toegewijde zorg voor de kamerplanten op kantoor. Sophie Gerritse, ongelooflijk sociaal, gedreven en nooit een tekort aan gesprekstof, wat een verdienste is, want met je vrolijke verhalen tover je een lach op de gezichten van al je toehoorders. Claudia Schuurhuizen: heeft flair, is 'too blessed to ever be stressed', en kan daarbij heel veel ballen tegelijk hooghouden in de lucht. Anne van der Werf, achter deze

vegetarische hipster schuilt een ware bèta-vrouw met een indrukwekkende wiskundeknobbel die met precisie werkt volgens planning. En dan de heren, mijn twee paranimfen en inmiddels beiden experts op het gebied van imaging binnen de oncologie. Erik van Helden, onze onderzoekprojecten liepen vrijwel parallel, en dat was een feest. We konden veel kennis uitwisselen, droomden over de resultaten, raakten dan weer ontnuchterd, en dan weer vierden we kleine overwinningen, want zo gaat dat met translationeel oncologisch onderzoek. Jouw positiviteit, humor, spontaniteit en verantwoordelijkheidsgevoel werken ontwapenend bij patiënten en collega's. Cyrillo Brahm, je hebt evenzoveel humor en verantwoordelijkheidsgevoel en weet inmiddels heel veel over muizen. Je weet overigens ook heel veel over mensen en kunt hen feilloos aanvoelen, waarbij je hen probeert te geven wat ze nodig hebben. Patiënten en de mensen direct om je heen hebben het daarom ook altijd goed bij jou en dat alles doe je op je eigen bruisende wijze. Ik ben blij dat jullie mijn paranimfen zijn!

Lieve vrienden en families Bokelman, Droog, van Hattum, Huys, Kitzen, Mammatas, Rietveld en Semotok, veel dank voor jullie steun en interesse in dit proefschrift! Ευχαριστώ πολύ για την υποστήριξη και το ενδιαφέρον σας σε αυτή τη διατριβή! Ondanks dat sommigen van ons in verschillende landen verblijven, voelt het altijd dichtbij.

Liefste mama en Hans, jullie hebben er altijd alles aan gedaan zodat ik het goed zou hebben in het leven. Rekening houden met elkaar en met plezier hard werken waren vanzelfsprekend binnen onze familie. Lieve mama, jij werkte > 25 jaar als verpleegkundige op de intensive care in het Antoni van Leeuwenhoek. Je bent uiterst zorgzaam, intelligent en we genieten groots van de kleine, mooie dingen in het leven tijdens het drinken van een kopje thee. Mijn vader kan dit proefschrift niet meer meemaken, maar had anders trots 'το νέο μου κοστούμι' aangetrokken. Hij genoot van de natuur, van het eiland Ikaria en de zee waarover hij als kapitein grote schepen van continent naar continent voer. Door mijn vaders verblijf in het buitenland en mijn moeders werk was het daarom fijn om altijd ondersteuning te hebben van mijn oma, opa en oom Hans. Zij werkten hard in familiebedrijf 'Het Tapijthuis Droog', mijn opa en oma zelfs tot na hun 80e levensjaar. In de weekenden ging ik vaak mee en studeerde bij opa op kantoor. Zij stimuleerden mij altijd liefdevol, vele mooie boeken en mijn eerste torso van het menselijk lichaam heb ik van hen gekregen. Hans, je bent mijn oom, ouder en maatje. Staat altijd voor mij klaar, zo creatief, eerlijk, beschermend en jij geeft mijn leven een betoverende glans. Ik houd zo veel van jullie!

Liefste Marco, jij hebt mij gevonden en daar ben ik iedere dag weer dankbaar voor. Vanaf de eerste dag dat ik je leerde kennen was ik onder de indruk van je: lief, zorgzaam, observerend, ad rem, evenwichtig en authentiek. Jouw

nonchalante lokken die vaak de oortjes gevuld met muziek of actualiteiten verstoppen brengen een lach op mijn gezicht. Ik ben zeer gelukkig dat ik aan jouw zijde het leven mag beleven, voor alles wat komen gaat. Ik hou zo veel van je, ontelbare kussen!

Curriculum Vitae

Lemonitsa Hillegonda Mammatas was born on June 26th 1983 in Amsterdam, the Netherlands. After graduating from secondary school in 2001 (gymnasium, Keizer Karel College in Amstelveen), she studied Medicine at the VU University in Amsterdam and graduated with honors (cum laude) in 2007. She started as a resident not in training at the department Internal Medicine of the Kennemer Gasthuis in Haarlem under supervision of Prof. dr. R.W. ten Kate in 2008. This resulted in her specialization in Internal Medicine from 2009 to 2017 at Medisch Centrum Alkmaar supervised by Dr. F. Stam and the VU University Medical Center in Amsterdam headed by Prof. dr. M.H.H. Kramer. She combined her differentiation in Medical Oncology at the VU University Medical Center under supervision of Prof. dr. H.M.W. Verheul with the scientific research published in this thesis. Subsequently, she served as a medical oncologist at the Netherlands Cancer Institute/Antoni van Leeuwenhoek from 2018 to 2020 and combined this with working at the Dutch Medicines Evaluation Board Agency as an assessor of new (indications of) oncological therapies. In 2020 she was appointed medical staff member at the Reinier de Graaf Gasthuis in Delft where she continues her work as a medical oncologist combined with scientific research.

List of publications

Mammatas LH, Yaqub M, Hendrikse NH, et al. ^{11}C-sorafenib and ^{15}O-H_2O PET for early evaluation of sorafenib therapy. J Nucl Med. 2020. Online ahead of print.

Mammatas LH, Zandvliet AS, Rovithi M, et al. Sorafenib administered using a high-dose, pulsatile regimen in patients with advanced solid malignancies: a phase I exposure escalation study. Cancer Chemother Pharmacol. 2020;85:931-40.

Mammatas LH, Venema CM*, Schröder CP, et al. Visual and quantitative evaluation of [^{18}F]FES and [^{18}F]FDHT PET in patients with metastatic breast cancer: an interobserver variability study. EJNMMI Res. 2020;10:40.

Mammatas LH, van Helden EJ, Verheul HMW, Menke-van der Houven van Oordt CW. FDG PET and FES PET Predict PFS on Endocrine Therapy-Letter. Clin Cancer Res. 2018;24:248.

Venema CM, Mammatas LH*, Schröder CP, et al. Androgen and Estrogen Receptor Imaging in Metastatic Breast Cancer Patients as a Surrogate for Tissue Biopsies. J Nucl Med. 2017;58:1906-12.

Mammatas LH, Verheul HM, Hendrikse NH, et al. Molecular imaging of targeted therapies with positron emission tomography: the visualization of personalized cancer care. Cell Oncol (Dordr). 2015;38:49-64.

Mammatas LH, Regelink JC, Klein IE, Barbé E, Huijgens PC. Palmar necrosis during the treatment of acute myeloid leukaemia. Neth J Med. 2012;70:467,472.

Mammatas LH, Stam F. A nonproductive cough that would give most people a headache, but not this patient! Neth J Med. 2011;69:185,199.

van Riel JM, Peters GJ, Mammatas LH, et al. A phase I and pharmacokinetic study of gemcitabine given by 24-h hepatic arterial infusion. Eur J Cancer. 2009;45:2519-27.

*Shared co-first authorship